

**AN-NAJAH NATIONAL UNIVERSITY
FACULTY OF GRADUATE STUDIES**

**XO(X=Be, Zn) COMPOUNDS UNDER
HIGH PRESSURE**

By

Omar Mahmood A. Isleem

Supervisor

Dr. Mohammed S. Abu-Ja'far

This Thesis submitted in Partial fulfilment of the Requirements for the degree of Master of Science in Physics, faculty of Graduate studies, at An-Najah National University, Nablus, Palestine.

2008

XO(X=Be, Zn) COMPOUNDS UNDER HIGH PRESSURE

By

Omar Mahmood A. Isleem

This Thesis was defended successfully on 23/10/2008 and approved by

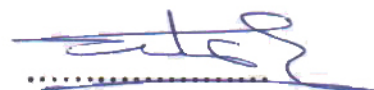
Committee Members

Signature

1- Dr. Mohammed Abu Ja'far (Supervisor)



2- Dr. Khaled Ilaiwi (External Examiner)



3- Dr. Abdel-Rahman Abu Labdeh (Internal Examiner)



Dedications

To the memory of my parents,
To my kids and to the one who supported me and Whom
I respect, to my wife.

ACKNOWLEDGEMENT

I would like to thank my teacher and supervisor Dr. Mohammed Abu-Ja'far for his support, guidance and for his help with the WIEN2K code which based on his wide experience in teaching and research. Thanks and appreciation to my committee Dr. Khaled Ilaiwi-American Arabian University as an (external examiner) and Dr. Abdel-Rahman Abu Labedeh-AN-Najah university as (an internal examiner) for their time and patient. Also I would like to thank all the physics department members who taught me and guide me to the truth. I will never forget to thank my colleagues Faruh Saleh, Naim Malak and Kamal Najie for their help and support. Special thanks and special appreciation to the one who supported me , brightened my way and encouraged me all the time, thanks to Orooba. Finally I would like to thank my family sisters, brothers especially Huda and my kid's lattifa, Aseel, Essraa and Abdel-Rahmman for their support, encouragement and patient.

إقرار

أنا الموقع أدناه مقدم الرسالة التي تحمل العنوان:

دراسة مركبي ZnO و BeO تحت تأثير ضغط مرتفع

أقر بأن ما اشتملت عليه هذه الرسالة إنما هي نتاج جهدي الخاص ، باستثناء ما تمت الإشارة إليه حيثما ورد ، وأن هذه الرسالة ككل ، أو أي جزء منها لم يقدم من قبل لنيل أية درجة أو لقب علمي أو بحثي لدى أي مؤسسة تعليمية أو بحثية أخرى.

Declaration

The work provided in this thesis, unless otherwise referenced, is the researcher's own work, and has not been submitted elsewhere for any other degree or qualification.

Student's name:

اسم الطالب :

Signature:

التوقيع :

Date:

التاريخ:

Table of contents

<i>Section</i>	<i>Subject</i>	<i>Page</i>
	Committee decision	ii
	Dedication	iii
	Acknowledgment	iv
	Declaration	v
	Table of contents	vi
	List of tables	ix
	List of figures	x
	Abstract	xii
1	INTRODUCTION	1-7
2	DESITY FUNCTIOAL THEORY	8-24
2.1	Introduction	8
2.2	Level 1: The born-Oppenheimer approximation	10
2.3	Level 2: density Functional Theory	11
2.3.1	The Theorems of Hohenberg and Kohen	11
2.3.2	The Kohen-Sham equations	13
2.3.3	The exchange-correlation functional	18
2.3.4	Level 3: solving the equations	21
2.4	The local spin Density Approximation	22
2.5	Generalized Gradient Approximation	23
3	METHODOLOGY	25-38
3.1	Introduction	25
3.2	The Augmented Plane Wave (APW) method	26
3.3	The LAPW method	29
3.3.1	The regular LAPW method	29
3.3.2	LAPW with local orbital (LAPW + LO)	31
3.4	The FLAPW method	33

<i>Section</i>	<i>Subject</i>	<i>Page</i>
3.5	The WIEN2K code	34
3.6	Computational considerations	34
3.7	Applications of WIEN2k	35
3.7.1	Systems	35
3.7.2	Band structure and density of states (DOS)	36
3.7.3	Electron Densities	37
3.7.4	Total energy and phase transition	37
3.7.5	Forces and structure optimization	38
3.7.6	Equilibrium volume and bulk modulus	38
4	COMPUTATIONAL DETAILS	39-53
4.1	Introduction	39
4.2	Crystal structure	39
4.2.1	How do atoms pack together	40
4.2.2	Unit cell	42
4.2.3	Classification of crystals by symmetry	43
4.2.4	Crystal system	44
4.2.5	The Bravais lattices	44
4.2.6	Point and space group	45
4.3	Some simple structures for oxides and ionic compounds	45
4.3.1	The rock Salt (NaCl) structure RS	46
4.3.2	The zinc-blende (ZnS) structure ZB	47
4.3.3	The wurtzite structure W	48
4.3.4	Cesium chloride structure CsCl	49
4.4	Computational details	50
5	RESULTS, DISCUSSION AND CONCLUSION	54-93
5.1	Introduction	54
5.2	BeO compound	54

<i>Section</i>	<i>Subject</i>	<i>Page</i>
5.2.1	General considerations	54
5.2.1.1	Finding $R_{k_{\max}}$	54
5.2.1.2	How to select R_{MT} radii	56
5.2.1.3	Choice of the k-point mesh	56
5.2.1.4	Optimization	60
5.2.1.4.1	Wurtzite structure (W)	61
5.2.1.4.2	Zinc-blende structure (ZB)	64
5.2.1.4.3	Rocksalt structure (RS)	65
5.2.1.5	Transition phases	66
5.2.1.6	Band structure	72
5.3	ZnO compound	75
5.3.1	Optimization	76
5.3.1.1	Wurtzite structure	76
5.3.1.2	Zinc-blende structure	76
5.3.1.3	Rock salt structure	77
5.3.1.4	Cesium-chloride structure	77
5.3.2	Transition phases	77
5.3.3	Band structure	88
5.4	Conclusion	92
	REFERENCES	94-99

LIST OF TABLES

number	name	page
Table(5.1)	Testing best Rkmax for RS& ZB structures of BeO	55
Table(5.2)	Testing best Rkmax for WZ structure of BeO	55
Table(5.3)	Choosing best K-point for ZB structure by GGA for BeO	59
Table(5.4)	Choosing best k-point for RS structure by LDA	59
Table(5.5)	Choosing best k-point for WZ structure by Wu-Cohen	60
Table(5.6)	Finding c/a by LDA for WZ structure of BeO	61
Table(5.7)	Finding c/a ratio by GGA	61
Table(5.8)	Finding c/a ratio by Wu-Cohen for WZ structure of BeO	61
Table(5.9)	Finding u by LDA for WZ structure of BeO	62
Table(5.10)	Finding u by GGA for WZ structure of BeO	62
Table(5.11)	The structural parameters of WZ for BeO	63
Table(5.12)	The structural parameters of ZB for BeO	65
Table(5.13)	The structural parameters of RS for BeO	66
Table(5.14)	The transition pressure and volume for BeO phases	70
Table(5.15)	The energy band gap of BeO structures	75
Table(5.16)	The structural parameters of WZ phase for ZnO	76
Table(5.17)	The structural parameters of ZB phase for ZnO	76
Table(5.18)	The structural parameters of RS phase for ZnO	77
Table(5.19)	The structural parameter of CsCl phase for ZnO	77
Table(5.20)	The transition pressure and volume for ZnO phases	86
Table(5.21)	The energy band gap for ZnO structures	91

LIST OF FIGURES

Number	name	page
Fig(2.1)	Flow chart for nth iteration to solve Kohn-Sham eq.	17
Fig(2.2)	Illustration the idea behind LDA	20
Fig(3.1)	Division of unit cell	27
Fig(4.1)	Hcp & fcc close package of spheres	41
Fig(4.2)	Schematic views of hcp & fcc type structures	41
Fig(4.3)	Bcc packing of spheres	42
Fig(4.4)	Sc packing of spheres	42
Fig(4.5)	NaCl structure (RS)	46
Fig(4.6)	BeO & ZnO in rocksalt structure	47
Fig(4.7)	BeO & ZnO in zinc-blende structure	48
Fig(4.8)	BeO & ZnO in wurtzite structure	49
Fig(4.9)	CsCl structure	50
Fig(5.1)	Energy vs. volume for W by GGA method	63
Fig(5.2)	Energy vs. volume for ZB by LDA	64
Fig(5.3)	Energy vs. volume for RS by Wu-Cohen	65
Fig(5.4)	Transition from W-RS under high pressure by LDA	66
Fig(5.5)	Transition from W-RS under high pressure by GGA	67
Fig(5.6)	Transition from W-RS under high pressure by Cohen	68
Fig(5.7)	Transition from ZB-RS under high pressure by LDA	68
Fig(5.8)	Transition from ZB-RS under high pressure by GGA	69
Fig(5.9)	Transition from ZB-RS under high pressure by Cohen	69
Fig(5.10)	W, ZB and RS phase together by LDA	70
Fig(5.11)	W, ZB and RS phases together by Wu-Cohen	71
Fig(5.12)	Transition from W to ZB by LDA	71
Fig(5.13)	Transition from W to ZB by Wu-Cohen	72
Fig(5.14)	Band gap for W by LDA & GGA	73

Fig(5.15)	Band gap for RS by LDA & GGA	73
Fig(5.16)	Band gap for RS by Cohen and for ZB by LDA	74
Fig(5.17)	Band gap for ZB by GGA & Wu-Cohen	74
Fig(5.18)	Transition from W-RS by LDA	78
Fig(5.19)	Transition from W- RS by GGA	79
Fig(5.20)	Transition from W-RS by Wu-Cohen	79
Fig(5.21)	Tr. from W- CsCl LDA	80
Fig(5.22)	W- CsCl by GGA	80
Fig(5.23)	W- CsCl by Wu-Cohen	81
Fig(5.24)	Transition from ZB – RS by LDA	82
Fig(5.25)	From ZB – RS by GGA	82
Fig(5.26)	From ZB – RS by Wu-Cohen	82
Fig(5.27)	From ZB – CsCl by LDA	83
Fig(5.28)	From ZB – CsCl by GGA	83
Fig(5.29)	From ZB- CsCl by Wu-Cohen	84
Fig(5.30)	From RS- CsCl by LDA	85
Fig(5.31)	From RS- CsCl by GGA	85
Fig(5.32)	From RS- CsCl by Wu-Cohen	86
Fig(5.33)	W, ZB, RS and CsCl phases by LDA	87
Fig(5.34)	W, ZB, RS and CsCl phases by GGA	87
Fig(5.35)	W, ZB, RS and CsCl phases by Wu-Cohen	88
Fig(5.36)	Band gap for W by LDA, GGA and Wu-Cohen	88
Fig(5.37)	Band gap for ZB by LDA, GGA and Wu-Cohen	89
Fig(5.38)	Band gap for RS by LDA, GGA and Wu-Cohen	89
Fig(5.39)	Band gap for CsCl by LDA, GGA and Wu-Cohen	90

XO (X=Be, Zn) compounds under high pressure**By****Omar Mahmood A. Isleem****Supervised by****Dr. Mohammed Abu Ja'far****Abstract**

The structural phase transformations of semiconductors under high pressure have recently attracted a lot of attention. Experimental studies in this field are very difficult and expensive, the computational physics programs make these studies very easy, very accurate and inexpensive. The computational approach enables us to know the atomic structures of materials, the electronic properties and give the chance to modify the bonding between atoms to create novel materials with predetermined properties. In the present study the Full-Potential Linearized Augmented Plane-Wave (FP-LAPW) (which is included in a computer code WIEN2K) method depending on the Density Functional Theory (DFT) were used to investigate the structural phase transformations of BeO and ZnO compounds under high pressure. In these calculations, the local density approximation(LDA), the gradient generalized approximation (GGA) and the modified Wu- Cohen-GGA approximation for the exchange correlation potential have been used. For BeO the equations of state (EOS's) of wurtzite(WZ), zinc-blende(ZB) and rock salt (RS) have been calculated. From these (EOS's) the transition under high pressure is occurred from wurtzite to rock salt and from zinc-blende to rock salt structures, the transition pressure and the structural properties have also been calculated. The energy band gap for all phases of BeO have been calculated and a large band gap was found to be (6 ~ 8 eV) which is indicating that BeO is a good insulator.

The same work was done for ZnO using the same method and the same approximations. A number of transition phases is predicted for ZnO, wurtzite to rock salt, wurtzite to cesium chloride, zinc-blende to rock salt, zinc-blende to cesium-chloride and rock salt to cesium-chloride. The transition pressure for each case was calculated. The structural properties have also been calculated and finally the energy band gap for each phase was investigated.

Small energy band gap (0.3 ~1.5eV) is found, which means that ZnO behaves as a semiconductor.

The most important results of this study are:

- 1- The present calculations agree very well with the available experimental data and the other theoretical calculations.
- 2- The transition from structure to another is possible under high pressure.
- 3- BeO behave as an insulator in all its structures.
- 4- Wurtzite found to be the ground state for BeO compound at zero temperature.
- 5- ZnO behave as a semiconductor in all its structures except in cesium-chloride structure it behaves as a semi-metal.

Chapter One

Introduction

The structural phase transformation of semiconductors under high pressure have recently attracted a lot of attention [1]. Recent experiments performed by using image-plate angle dispersive X-ray techniques for many II-VI, III-V and group-IV semiconductors have significantly altered the understanding of their structural systematic from the view that had been widely accepted[2] . Experimental findings as well as numerous possibilities for industrial applications initiated a number of theoretical studies of structural [3] and electronic [4] properties of II-VI compounds. II-VI, III-V and group-IV wide-gap semiconductor materials are very important because of their opto-electronic technological applications as a commercial short wavelength light-emitting diode[5], laser diode candidate by p-type doping with nitrogen, transparent conductors, solar cells, high-density optical memory, visual display [6]. This importance is due to the d-electrons in the valance band in hybridization which tends to: 1- open a gap at the band crossing; 2- make angular momentum labelling no longer suitable [7]. The large variation of fundamental band gap (0-4eV.) for these compounds yields a great flexibility for producing new II-VI and III-V compounds(superlattices, hetero structures and alloys) with the desirable properties to satisfy the increasing demand for such materials in various device applications as opto-electronic devices operating in the visible-light region [8]. The alkali oxides play a vital role as supports in catalysis [9] and the properties of insulating refractory oxides at high pressure are important in both ceramic and materials science [10]. Beryllium Oxide BeO compound is of particular importance because of its high thermal conductivity and low electrical conductivity [11].

BeO is unique for oxides as it combines excellent electrical insulating properties with high thermal conductivity. It is also corrosion resistant. The high toxicity of the beryllium oxide powders when inhaled, and the high cost of the raw material, has limited its use to applications that exploit its singular properties. BeO is extracted from the naturally occurring minerals beryl¹ and bertrandite², and produced as a powder by the thermal decomposition of Be(OH)₂. Powders are commercially available at purity levels of greater than 99%. Components can be made as near net shapes by most of the commonly used fabrication methods, for example pressing, slip casting³ or extruding⁴ the powder. Sintering⁵ is carried out in the range 1600-1800C. High density components (<5% porosity⁶) can be easily made with commercially pure powders. Near theoretical density (<1% porosity) can be achieved using high purity materials and hot pressing in graphite dies. BeO is one of the most expensive raw materials used in ceramics. The expense is linked in part to the precautions to avoid the toxic effects of the powder when handling during fabrication. Inhalation of fine particles of beryllium oxide results in respiratory disease, with the severity related to the length of

¹ **Beryl** (3BeO·Al₂O₃·6SiO₂ which is known since ancient times as the gemstones)

² **Bertrandite** is a beryllium sorosilicate hydroxide mineral with composition: Be₄Si₂O₇(OH)₂. Bertrandite is a colorless to pale yellow orthorhombic mineral with a hardness of 6-7

³ **Slip-casting** is a technique for the mass-production of pottery, especially for shapes not easily made on a wheel.[Slip in a ceramic is made by mixing clays and other minerals with water].

⁴ **Extrusion** is a manufacturing process used to create long objects of a fixed cross-sectional profile.

⁵ **Sintering** is a method for making objects from powder, by heating the material (below its melting point- solid stage sintering) until its particles adhere to each other. Sintering is traditionally used for Manufacturing ceramic objects, and has also found uses in such fields as powder metallurgy.

⁶ **Porosity** is a measure of the void spaces in a material, and is measured as a fraction, between 0–1, or as a percentage between 0–100%. The term porosity is used in multiple fields including manufacturing, earth sciences and construction

exposure. BeO has an outstanding combination of physical and chemical properties and it forms above (600 C). Apart from reactivity with water vapour at high temperature (1000 C), it is one of the most chemically stable oxides, resisting both carbon reduction and molten metal attack at high temperatures. Points worth noting about its properties include thermal conductivity is extremely high in comparison with other ceramics, particularly below 300C. For comparison the thermal conductivity of beryllium oxide at room temperature is $300 \text{ W}\cdot\text{m}^{-1}\text{K}^{-1}$, Copper $300 \text{ W}\cdot\text{m}^{-1}\text{K}^{-1}$ and Alumina is $35 \text{ W}\cdot\text{m}^{-1}\text{K}^{-1}$. Electrical resistivity is high. BeO is classed as an electrical insulator. Mechanical strength is normally lower than alumina, but can reach acceptable levels through control of the fabrication process. BeO has good thermal shock resistance if the component has good strength due to the high thermal conductivity. Beryllium oxide has lower density than Aluminium oxide; $3010 \text{ kg}\cdot\text{m}^{-3}$ and $3970 \text{ kg}\cdot\text{m}^{-3}$ respectively. The thermal expansion of BeO is similar to the other oxides [12].

As a low-Z oxide and the lightest II-VI compound, BeO is also important from a more fundamental point of view [13]. BeO crystallizes in the hexagonal wurtzite (WZ) structure with the polar space group $p63mc$. According to the Phillips-ionicity f_i argument [14], the tetrahedral compounds with $f_i > 0.35$ will transform into an ionic six-fold rock-salt (RS) structure under pressure. Since the Phillips ionicity of BeO is 0.602, a phase transition from WZ to RS is expected at high pressure [15]. During the last two decades, a few theoretical calculations and experiments have been performed to investigate the pressure induced phase transition in BeO. However a significant discrepancy exists in the magnitude of the transition pressure. Earlier first-principles pseudo potential calculation predicted the WZ-RS transition at 22 GPa. The same transition was found at 40 GPa [13] by the potential-induced-breathing

PIB method. Recently similar calculations predicted that the WZ first transformed into the zincblende ZB and then into the RS [11]. In the first work, Van Camp and Van Doren employed soft nonlocal pseudopotentials to predict the WZ-ZB-RS transitions at 74 and 137 GPa [16]. In the second work Boettger and Wills found the corresponding transitions at 63-76 and 95 GPa, respectively by an all-electron and full-potential electronic-structure calculation [17]. In the last work Park et al. obtained 91 GPa and 147 GPa for the transient pressure using a first-principles soft nonlocal pseudo potential method within the generalized-gradient approximation [18]. In order to explore whether the phase transition sequence is WZ-ZB-RS, not only the free energy of these phases but also the transitional barriers should be investigated. A large transitional barrier might impede a transition at the equilibrium pressure, leading to a hysteresis between the forward and backward transforms even preventing a transition [19]. BeO is special in this class of materials in that it crystallizes in the hexagonal wurtzite structure while the other earth alkali oxides crystallize in the cubic sodium chloride structure. This indicates that the BeO chemical bond is not exclusively ionic but has also some covalent character [10]. BeO is of technological importance, e.g., as catalyst, for semiconductor devices and as moderator in nuclear reactors. For semiconductor device applications an understanding of the geometric and electronic properties of bulk BeO and its surfaces is highly desirable. As to more complex structures, very recently graphitic BeO nano films have been shown to be useful as precursors in the growth of wurtzite films [20], and be useful as precursors in the growth of wurtzite films [20] and BeO nanotubes have been investigated [21] as well. The electronic structure of bulk BeO has been studied previously in experiment and by first-principles calculations employing the standard local density approximation LDA [22] generalized gradient approximation GGA [22], and Hartree-Fock HF [22] calculations.

While LDA and GGA calculations yield a band gap that is significantly too small, HF calculations often yield too large band gaps and valence-band widths. The structure of BeO has been studied by Chang and Cohen [15] as well as by Van Camp *et al.*, [16] employing LDA total energy minimization. Both studies show that the ground state of BeO is the wurtzite structure.

Zinc oxide is a chemical compound with the formula ZnO. It is nearly insoluble in water but soluble in acids and alkalis. It occurs as white hexagonal crystals or a white powder commonly known as zinc white. Zinc oxide occurs in nature as the mineral zincite ⁷[23]. Crystalline zinc oxide exhibits the piezoelectric⁸ effect and is thermo-chromic⁹, changing from white to yellow when heated. ZnO is a semiconductor with a direct band gap energy of 3.37 eV at room temperature. The most common applications are in laser diodes and light emitting diodes since it has an exciton and biexciton energies of 60 meV and 15 meV, respectively. It is expected that this exciton properties of ZnO will be improved further by epitaxy. Zinc oxide plays an important role in a very wide range of applications varying from tyres to ceramics, from pharmaceuticals to agriculture, and from paints to chemicals [24]. The biggest use of zinc oxide is in glass and ceramics, where the main role is as a fluxing agent in the preparation of frits and enamels for ceramic wall and floor tiles, or of enamels for sanitary and tableware ceramic objects. Thin-film solar cells, LCD and flat panel displays are typical applications of this material. Appropriately doped ZnO may be transparent and conductive, and can therefore be used as a transparent electrode. Indium tin oxide (ITO) is another transparent

⁷ *Zincite is the mineral form of zinc oxide (ZnO), It has a hexagonal crystal structure and color that depends on impurities*

⁸ *Piezoelectricity is the ability of some materials (notably crystals and certain ceramics) to generate an electric potential in response to applied mechanical stress. This may take the form of a separation of electric charge across the crystal lattice.*

⁹ *Thermo-chromism is the ability of substance to change color due to a change in temperature*

conducting oxide often used in microelectronics. ZnO has also been considered for spintronics¹⁰ applications because of theoretical predictions of room temperature ferromagnetism [23].

Unsubstantiated reports of ferromagnetism have been made, but presence of dilute magnetic semiconductors remains unanswered question in physics.

ZnO compound also found to be crystallized in the wurtzite-type where its valence bands consists of extended O 2p and Zn 4s orbital's, and rather localized Zn 3d and O 2s orbitals [25]. ZnO compound is the object of quickly growing attention in the last few years to owing to its potential application in ultraviolet opto-electronic devices technology since the material is optically transparent and can be doped with both electrons and holes . High pressure studies are very efficient tool in understanding the electronic structure of semiconductors compounds like ZnO [25].The band structure of ZnO has been studied theoretically by several investigators [26]. Density-functional theory (DFT) provides a foundation for modern electronic structure calculations, and the local-density approximation (LDA) and the generalized gradient approximation (GGA) are an efficient ways to calculate the ground-state of material [27]. Time-dependent (DFT) can in principle describe the excited state [28]. In this study we are going to use the full-potential linearized augmented plane wave (FP-LAPW),WIEN2K computer code [29],within the (LDA),(GGA) and the improved Wu–GGA, By the (FP-LAPW), program, WIEN2K, the Kohn-Sham equation can be solved, in (FP-LAPW) method, the wave function is expanded in atomic orbitals in spherical regions around the atomic positions while in the region between the spheres, it is expanded in plane waves. The wave functions and

¹⁰ *Spintronics (a neologism for "spin-based electronics"), also known as magneto electronics, is an emerging technology which exploits the quantum spin states of electrons as well as making use of their charge state*

their derivatives are made continuous at the boundary of the spheres. The FP-LAPW method places no restrictions on the form of crystalline potential and is known to yield reliable structural parameters for semiconductors, metals, and insulators. WIEN2K [29] allows us to perform electronic structure calculations of solids using (DFT) [30], and it is based on (FP-LAPW) one among the most accurate schemes for band structure calculation. The purpose of this study is to:

- 1- calculate the structural parameters of the zinc-blende(ZB), rock-salt(RS), and wurtzite (W) phases of BeO compound
- 2- calculate the structural parameters of the ZB, RS, and W phases of ZnO compound
- 3- determine the equations of state of ZB, RS, W and CsCl phases of BeO and ZnO by calculating the total energy at different volumes and fitting the calculated values to Murnaghan's EO'S [31].
- 4-determine the transition pressure of W to RS, ZB to RS and W to ZB structural phases transformations for BeO and ZnO.
- 5-determine the band structure of ZB, RS, W and CsCl phases of BeO and ZnO.

This thesis is organized as follows:

In chapter 2 we describe the Density Functional Theory, chapter 3 contains the method we used in the calculations. In chapter 4 , we display the computational details. Finally, in chapter 5 we report and discuss our results and we give a summery of our main results and conclusion.

Chapter Two

Density Functional Theory (DFT)

2.1 Introduction

As a result of recent successes in describing and predicting properties of materials, atomistic simulations in general and electronic structure calculations in particular have become increasingly important in the fields of physics and chemistry over the past decade, especially with the advent of present-day, high-performance computers. Assuming knowledge of the types of atoms comprising any given material, a computational approach enables us to answer two basic questions:

- What is the atomic structure of the material?
- What are its electronic properties?

Besides this, it would be nice to get the answer to another question:

- How can we modify the bonding between atoms or the material chemical content to create novel materials with predetermined properties [32]?

A number of methods have been developed to derive answers to these questions. These methods for computing the structure and properties of materials can conditionally be divided into two classes: those that do not use any empirically or experimentally derived quantities, and those that do. The former are often called ab-initio, or first principles methods like density functional theory (DFT), while the latter are called empirical or semi-empirical like empirical tight binding (ETB). The ab-initio methods are particularly useful in predicting the properties of new materials and for predicting trends across a wide range of materials.

The calculation of the energy levels of electrons in solids, that is the determination of the energy bands, is a central theoretical problem of solid state

physics. Knowledge of these energies and of electron wave function is required, in principle, for any calculation of more directly observable properties including electrical and thermal conductivities, optical dielectric function, vibrational spectra and soon. In practice, phenomenological models are often employed which apparently do not require such specific information; however, it means a task for fundamental theory to account for the values obtained for the parameters of such a model. The parameters of the considered models are the functions of the crystal potential which can, in principle, be determined from the results of a sufficiently complete energy band calculation. In the present work, the sufficiently complete energy band structure and structural properties (lattice parameters, cohesive energy, bulk modulus, transition volume, etc.) of compounds, such as BeO, and ZnO have been obtained by the combination of first principle and empirical calculations based on density functional and tight binding theories, respectively, this chapter will start outlining the aspects of the density functional theory in details [34].

A solid is a collection of heavy, positively charged particles (nuclei) and lighter, negatively charged particles (electrons) [35]. If we have N nuclei and each has Z electrons, then we are dealing with a problem of $N+ZN$ electromagnetically interacting particles. This is a many-body problem, and because the particles are so light, quantum mechanics is needed: a quantum many body problem. In principle, to study the materials and their properties, the theorist has to solve the time independent Schrödinger equation.

$$\hat{H}\Psi = E\Psi \quad (2.1)$$

Here, Ψ is the wave function of all participating particles and \hat{H} is the exact many-particle Hamiltonian for this system:

$$\begin{aligned} \hat{H} = & -\frac{\hbar^2}{2} \sum_i \frac{\nabla_{\vec{R}_i}^2}{M_i} - \frac{\hbar^2}{2} \sum_i \frac{\nabla_{\vec{r}_i}^2}{m_i} - \frac{1}{4\pi\epsilon_0} \sum_{i,j} \frac{e^2 Z_i}{|\vec{R}_i - \vec{r}_j|} + \frac{1}{8\pi\epsilon_0} \sum_{i \neq j} \frac{e^2}{|\vec{r}_i - \vec{r}_j|} \\ & + \frac{1}{8\pi\epsilon_0} \sum_{i \neq j} \frac{e^2 Z_i Z_j}{|\vec{R}_i - \vec{R}_j|} \end{aligned} \quad (2.2)$$

The mass of the nucleus at R_i is M_i , the electrons have mass m_e and are at r_i . The first term is the kinetic energy operator for the nuclei (T_n), the second for the electrons (T_e). The last three terms describe the Coulomb interaction between electrons and nuclei (V_{en}), between electrons and other electrons (V_{ee}), and between nuclei and other nuclei (V_{nn}). It is out of question to solve this problem exactly. In order to find acceptable approximate eigen states, we will need to make approximations at 3 different levels [36].

2.2 Level 1: The Born-Oppenheimer approximation

The nuclei are much heavier and therefore much slower than the electrons. We can hence ‘freeze’ them at fixed positions and assume the electrons to be in instantaneous equilibrium with them. In other words: only the electrons are kept as players in our many body problem [36].

The nuclei are deprived from this status, and reduced to a given source of positive charge, they become ‘external’ to the electron cloud. After having applied this approximation, we are left with a collection of NZ interacting negative particles, moving in the (now external or given) potential of the nuclei.

What are the consequences of the Born-Oppenheimer approximation on the Hamiltonian (equation 2.2)? The nuclei do not move any more, their kinetic energy is zero and the first term disappears. The last term reduces to a

constant. We are left with the kinetic energy of the electron gas, the potential energy due to electron-electron interactions and the potential energy of the electrons in the (now external) potential of the nuclei. We write this formally as:

$$H = \hat{T} + \hat{V} + \hat{V}_{ext} \quad (2.3)$$

It is interesting to note here that the kinetic and electron-electron terms of 2.3 depend only on the fact that we are dealing with a many-electron system (and not with a many-proton system for instance, where the strong nuclear force would play a role). They are independent of the particular kind of many-electron system [35]. This part is universal System-specific information (which nuclei, and on which positions) is given entirely by \hat{V}_{ext} .

2.3 Level 2: Density Functional Theory

The quantum many body problem obtained after the first level approximation (Born-Oppenheimer) is much simpler than the original one, but still far too difficult to solve. Several methods exist to reduce equation 2.2 to an approximate but tractable form. A historically very important one is the Hartree-Fock method (HF), described in many condensed matter textbooks. It performs very well for atoms and molecules, and is therefore used a lot in quantum chemistry. For solids it is less accurate, however. We will not treat HF, but explain a more modern and probably also more powerful method: Density Functional Theory (DFT)[37]. Although its history goes back to the early thirties of the 20th century, DFT has been formally established in 1964 by two theorems due to Hohenberg and Kohn.

2.3.1 The Theorems of Hohenberg and Kohn

The traditional formulation of the two theorems of Hohenberg and Kohn is as follows:

First theorem: There is a **one-to-one** correspondence between the ground-state density $\rho(r)$ of a many-electron system (atom, molecule, solid) and the external potential V_{ext} . An immediate consequence is that the ground-state expectation value of any observable \hat{O} is a unique functional of the exact ground-state electron density:

$$\langle \Psi | \hat{O} | \Psi \rangle = O[\rho] \quad (2.4)$$

Second theorem: For \hat{O} being the Hamiltonian \hat{H} , the ground state total energy functional $H[\rho] \equiv E_{\text{Vext}}[\rho]$ is of the form

$$E_{\text{Vext}}[\rho] = \underbrace{\langle \Psi | \hat{T} + \hat{V} | \Psi \rangle}_{F_{\text{HK}}[\rho]} + \langle \Psi | \hat{V}_{\text{ext}} | \Psi \rangle \quad (2.5)$$

$$= F_{\text{HK}}[\rho] + \int \rho(\vec{r}) V_{\text{ext}}(\vec{r}) d\vec{r} \quad (2.6)$$

where the Hohenberg-Kohn density functional $F_{\text{HK}}[\rho]$ is universal for any many-electron system. $E_{\text{Vext}}[\rho]$ reaches its minimal value (equal to the ground-state total energy) for the ground state density corresponding to V_{ext} .

We do not prove these theorems here, but ponder a few implications of the three keywords invariability (one-to-one correspondence $\rho \leftrightarrow V_{\text{ext}}$) [38], universality and variational access (minimal value).

Invariability: the one-to-one correspondence between ground-state density and external potential is intriguing. It is obvious that a given many-electron system has a unique external potential, which by the Hamiltonian (Eq. 2.3) and the Schrödinger equation yields a unique ground-state many particle wave function. From this wave function, the corresponding electron density is easily found. An external potential hence leads in a well-defined way to a unique ground-state density corresponding to it. But intuitively it looks

like the density contains less information than the wave function. If this would be true, it would not be possible to find a unique external potential if only a ground-state density is given. The first theorem of Hohenberg and Kohn tells exactly that this is possible. The density contains as much information as the wave function does (i.e. everything you could possibly know about an atom, molecule or solid). All observable quantities can be retrieved therefore in a unique way from the density only (i.e. they can be written as functionals of the density).

Universality (the universality of $F_{\text{HK}}[\rho]$): Equation (2.6) is easily written down by using the density operator, and supposing the ground-state density is known, the contribution to the total energy from the external potential can be exactly calculated. An explicit expression for the Hohenberg-Kohn functional, F_{HK} , is not known. But anyway, because F_{HK} does not contain information on the nuclei and their position, it is a universal functional for any many-electron system. This means that in principle an expression for $F_{\text{HK}}[\rho]$ exists which can be used for every atom, molecule or solid which can be imagined.

Variational access: the second theorem makes it possible to use the variational principle of Rayleigh-Ritz in order to find the ground-state density. Out of the infinite number of possible densities, the one which minimizes $E_{\text{Vext}}[\rho]$ is the ground-state density corresponding to the external potential $V_{\text{ext}}(\mathbf{r})$. Of course, this can be done only if (an approximation to) $F_{\text{HK}}[\rho]$ is known. But having found ρ , all knowledge about the system is within reach [35]. It is useful to stress the meaning of the energy functional $E_{\text{Vext}}[\rho]$ once more. When it is evaluated for the density ρ corresponding to the particular V_{ext} for this solid, it gives the ground state energy. When it is evaluated for any other density

however, the resulting number has no physical meaning [40]!

2.3.2 The Kohn-Sham equations

The equations of Kohn and Sham, published in 1965[3], turn DFT into a practical tool [5]. They are a practical procedure to obtain the ground state density. Let us first rewrite the Hohenberg-Kohn theorem. The correlation energy is defined as this part of the total energy which is present in the exact solution, but absent in the Hartree-Fock solution [38]. The total energy functional $E_e[\rho]$ and $E_{HF}[\rho]$ corresponding to the exact and Hartree-Fock Hamiltonians respectively, are:

$$E_e = T + V \quad (2.7)$$

$$E_{HK} = T_0 + \underbrace{(V_H + V_x)}_V \quad (2.8)$$

Here T and V are the exact kinetic and electron-electron potential energy functionals, T_0 is the functional for the kinetic energy of a non-interacting electron gas, V_H stands for the Hartree contribution and V_x for the exchange contribution. By subtracting 2.7 from 2.8, the functional for the correlation contribution appears to be:

$$V_e = T - T_0 \quad (2.9)$$

The exchange contribution to the total energy is defined as the part which is present in the Hartree-Fock solution, but absent in the Hartree solution. Obviously, with the Hartree functional given by

$$E_H = T_0 + V_H \quad (2.10)$$

it can be defined as

$$V_x = V - V_H \quad (2.11)$$

With this knowledge, we can rewrite the Hohenberg-Kohn functional in the following way:

$$\begin{aligned}
F_{\text{HK}} &= T + V + T_0 - T_0 \\
&= T_0 + V + \underbrace{(T - T_0)}_{V_0} \\
&= T_0 + V + V_c + V_H - V_H \\
&= T_0 + V_H + V_c + \underbrace{(V - V_H)}_{V_x} \\
&= T_0 + V_H + \underbrace{(V_x + V_c)}_{V_{xc}}
\end{aligned}$$

Here V_{xc} is the exchange-correlation energy functional. We don't know it formally, as it contains the difficult exchange and correlation contributions only. If we assume for a while that we do know V_{xc} [41], we can write explicitly the energy functional:

$$E_{\text{Vext}}[\rho] = T_0[\rho] + V_H[\rho] + V_{xc}[\rho] + V_{\text{ext}}[\rho] \quad (2.12)$$

One could use now the second Hohenberg-Kohn theorem to find the ground state density, but then we would have won nothing by our transformation. Instead, you can interpret the above expression also as the energy functional of a non-interacting classical electron gas, subject to two external potentials: one due to the nuclei, and one due to exchange and correlation effects. The corresponding Hamiltonian - called the Kohn-Sham Hamiltonian - is

$$\hat{H}_{\text{KS}} = T_0 + \hat{V}_H + \hat{V}_{xc} + \hat{V}_{\text{ext}} \quad (2.13)$$

$$= -\frac{\hbar^2}{2m_e} \nabla_i^2 + \frac{e^2}{4\pi\epsilon_0} \int \frac{\rho(\vec{r}')}{|\vec{r} - \vec{r}'|} d\vec{r}' + V_{xc} + V_{\text{ext}} \quad (2.14)$$

Where the exchange-correlation potential is given by the functional derivative

$$\hat{V}_{xc} = \frac{\delta V_{xc}[\rho]}{\delta \rho} \quad (2.15)$$

The theorem of Kohn and Sham can now be formulated as follows:

The exact ground-state density $\rho(\vec{r})$ of an N-electron system is

$$\rho(\vec{r}) = \sum_{i=1}^N \phi_i(\vec{r})^* \phi_i(\vec{r}) \quad (2.16)$$

where the single-particle wave functions $\phi_i(\vec{r})$ are the N lowest-energy solutions of the Kohn Sham equation

$$\hat{H}_{KS} \phi_i = \epsilon_i \phi_i \quad (2.17)$$

And now we did win a lot. To find the ground-state density, we don't need to use the second Hohenberg-Kohn theorem any more, but we can rely on solving familiar Schrödinger-like non-interacting single-particle equations. The alternative of using the regular Schrödinger equation, would have led to a far more difficult system of coupled differential equations [42], because of the electron-electron interaction.

Be aware that the single-particle wave functions ϕ_i are not the wave functions of electrons! They describe mathematical quasi-particles, without a direct physical meaning. Only the overall density of these quasi-particles is guaranteed to be equal to the true electron density. Also the single-particle energies ϵ_i are not single-electron energies.

Both the Hartree operator V_H and the exchange-correlation operator V_{xc} depend on the density $\rho(\vec{r})$, which in turn depends on the ϕ_i which are being searched. This means we are dealing with a self-consistency problem: *the solutions (ϕ_i) determine the original equation (V_H and V_{xc} in H_{KS}), and the equation cannot be written down and solved before its solution is known.* An iterative procedure is needed to escape from this paradox (see fig. 2.1). Some starting density ρ_0 is guessed, and a Hamiltonian H_{KS1} [43] is constructed with it. The eigen value problem is solved, and results in a set of ϕ_1 from which a density ρ_1 can be derived. Most probably ρ_0 will differ from ρ_1 . Now ρ_1 is used to construct H_{KS2} , which will yield a ρ_2 , etc. The procedure can be set up in such a way that this series will converge to a density ρ_f which generates a H_{KSf} which yields as solution again ρ_f : this final density is then consistent with the Hamiltonian.

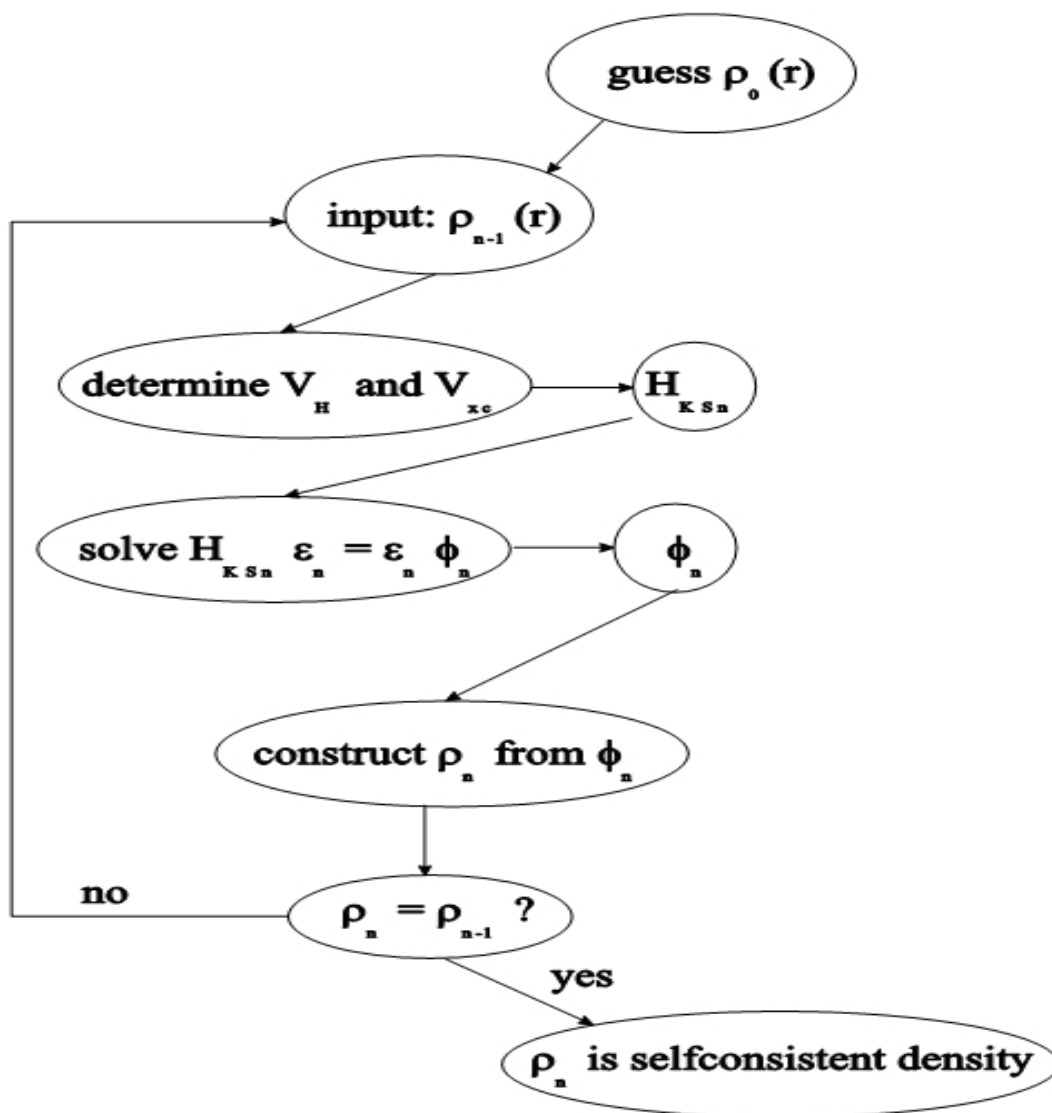


Figure (2.1): Flow chart for the n^{th} iteration in the self consistent procedure to solve Hartree-Fock or Kohn-Sham equations.

2.3.3 The exchange-correlation functional

The Kohn-Sham scheme described above was exact: apart from the preceding Born-Oppenheimer approximation, no other approximations were made. But we

neglected so far the fact that we do not know the exchange-correlation functional [44]. It is here that approximations enter our theory.

A widely used approximation-called the Local Density Approximation (LDA) – is to postulate that the exchange-correlation functional has the following form:

$$E_{xc}^{LDA} = \int \rho(\vec{r}) \epsilon_{xc}(\rho(\vec{r})) d\vec{r} \quad (2.18)$$

The function (not: functional) $\epsilon_{xc}(\rho)$ for the homogeneous electron gas, (The homogeneous electron gas, uniform electron gas is an imaginary solid where all nuclear charge is homogeneously smeared out over space. This material is completely isotropic, and identical on every length scale. Therefore the electron density is constant: $\rho = N/V$, with N the number of electrons in the material, and V its volume. The parameter ρ is the only thing we need to specify a particular homogeneous electron gas completely. If the electrons do not interact, we are in the case of the free electron gas, which can be solved analytically in a straightforward way. The problem is much more difficult for an interacting electron gas. Here numerical calculations for the total energy are possible by quantum Monte-Carlo. Subtracting the non-interacting kinetic energy and the Hartree energy gives a numerical result for the exchange-correlation energy. If this is done for several densities ρ the function $\epsilon_{xc}(\rho)$ is obtained. Note that $\epsilon_{xc}(\rho)$ is a function of ρ , not a functional) and is numerically known.

This postulate is somehow reasonable: it means that the exchange-correlation energy due to a particular density $\rho(\vec{r})$ could be found by dividing the material in infinitesimally small volumes with a constant density [45]. Each such volume contributes to the total exchange correlation energy by an amount equal to the exchange correlation energy of an identical volume filled with a homogeneous

electron gas, which has the same overall density as the original material has in this volume (see Fig. 2.2). No law of nature guarantees that the true E_{xc} is of this form, it is only a reasonable guess. By construction, LDA is expected to perform well for systems with a slowly varying density. But rather surprisingly, it appears to be very accurate in many other (realistic) cases too.

A next logical step to improve on LDA, is to make the exchange-correlation contribution of every infinitesimal volume not only dependent on the local density in that volume, but also on the density in the neighbouring volumes. In other words, the gradient of the density will play a role. This approximation is therefore called the Generalized Gradient Approximation (GGA) [46]. Although GGA performs in general slightly better than LDA, there are a few draw backs. There is only one LDA exchange-correlation functional, because there is a unique definition for ϵ_{xc} . But there is some freedom to incorporate the density gradient, and therefore several versions of GGA exist. Moreover, in practice one often fits a candidate GGA-functional with (hopefully only a few) free parameters to a large set of experimental data on atoms and molecules. The best values for these parameters are fixed then, and the functional is ready to be used routinely in solids. Therefore such a GGA-calculation is strictly spoken not an ab-initio calculation, as some experimental information is used. Nevertheless, there exist GGA's that are parameter free [42].

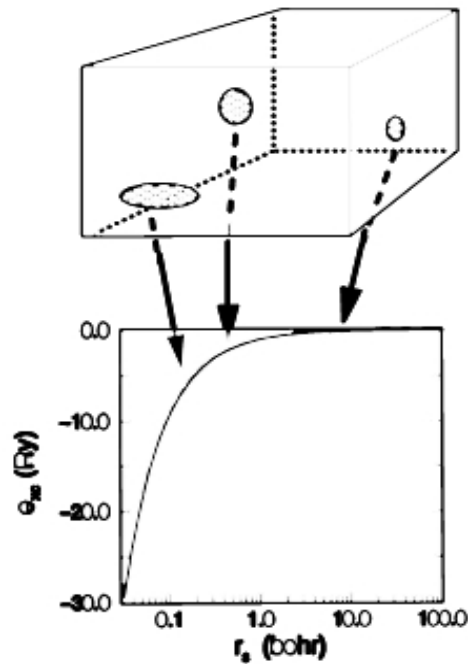
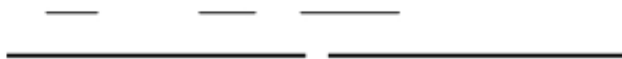


Figure (2.2): Illustration of the idea behind the LDA postulate. Every infinitesimally small volume of the material contributes to the exchange-correlation energy with an amount equal to the contribution of a homogeneous electron as that occupies that same infinitesimally small volume, and that has the same (overall) charge density as the charged density of the original material in that volume. The horizontal axis is proportional to the density of the homogeneous electron gas. The vertical axis displays the exchange-correlation energy of the homogeneous electron gas.



2.3.3 Level 3: Solving the equations

Irrespective whether one has used HF or DFT as level 2 approximation, one ends up with an infinite set of one-electron equations of the following type:

$$\underbrace{\left(-\frac{\hbar^2}{2m_e} \nabla_m^2 + \frac{e^2}{4\pi\epsilon_0} \int \frac{\rho(\vec{r}')}{|\vec{r}-\vec{r}'|} d\vec{r}' + V_\alpha + V_{ext} \right)}_{H_{sp}} \phi_m(\vec{r}) = \epsilon_m \phi_m(\vec{r}) \quad (2.19)$$

(m is an integer number that counts the members of the set). We call H_{sp} the single-particle Hamiltonian. For HF, V_α is the exchange operator[47]. The ϕ_m are true one-electron (or single-particle) orbital's for HF. Exchange is treated exactly, but correlation effects are not included at all. They can be added only in elaborations on the HF-method. For DFT, V_α is the exchange correlation operator, in the LDA, GGA or another approximation. Exchange and correlation are both treated, but both approximately.

The ϕ_m are mathematical single-particle orbitals. The similarity between the Hartree-Fock and Kohn-Sham equations means that the same mathematical techniques can be used to solve them. 'Solving' in most methods means that we want to find the coefficients c_p^m needed to express ϕ_m in a given basis set ϕ_p^b :

$$\phi_m = \sum_p^P c_p^m \phi_p^b \quad (2.20)$$

The wave functions ϕ_m belong to a function space which has an infinite dimension, P is therefore in principle infinite. In practice one works with a limited set of basis functions [48]. Such a limited basis will never be able to describe ϕ_m exactly, but one could try to find a basis that can generate a function that is 'close' to ϕ_m . Having chosen a basis (and hence a finite value for P) we realize that we can tackle the equations 2.19 as an eigen value problem. For a given m, substitute equation 2.20 in 2.19, and left-multiply with $\langle \phi_i^b |$ (I = 1 . . P), this leads to

$$\begin{bmatrix} \dots \\ \vdots \\ \dots \end{bmatrix} \begin{bmatrix} \langle \phi_i^b | \hat{H}_{sp} | \phi_j^b \rangle - \epsilon_m \langle \phi_i^b | \hat{H}_{sp} | \phi_j^b \rangle \\ \dots \end{bmatrix} \begin{bmatrix} \dots \\ c_1^m \\ \vdots \\ c_p^m \\ \dots \end{bmatrix} = \begin{bmatrix} 0 \\ \vdots \\ 0 \end{bmatrix} \quad (2.21)$$

We recognize here the matrix elements of the single-particle Hamiltonian in the basis states, and the overlap matrix elements S_{ij} . Diagonalization of the Hamiltonian matrix will lead to P eigen values and P sets of coefficients that express each of the P eigen functions in basis. The larger P , the better the approximation of the eigen function, but the more time-consuming the diagonalization of the matrix in equation 2.21[49].

2.4 The Local Spin Density Approximation (LSDA)

The local-density approximation (LDA) is an approximation of the exchange-correlation (XC) energy functional in density functional theory (DFT) by taking the XC energy of an electron in a homogeneous electron gas of a density equal to the density at the electron in the system being calculated (which in general is inhomogeneous). This approximation was applied to DFT by Kohn and Sham in an early paper.[50] The Hohenberg-Kohn theorem states that the energy of the ground state of a system of electrons is a functional of the electronic density, in particular the exchange and correlation energy is also a functional of the density (this energy can be seen as the quantum part of the electron-electron interaction). This XC functional is not known exactly and must be approximated [51]. LDA is the simplest approximation for this functional, it is local in the sense that the electron exchange and correlation energy at any point in space is a function of the electron density at that point only[53]. The LDA functional assumes that the per-electron exchange-correlation energy at every point in space is equal to the per-electron exchange-correlation energy of a homogeneous

electron gas[50]. The XC correlation functional is the sum of a correlation functional and an exchange functional [50]

$$E_{xc}=E_x +E_c \quad (2.22)$$

LDA uses the exchange for the uniform electron gas of a density equal to the density at the point where the exchange is to be evaluated,

$$E_{xc}^{LDA} = \int d^3r n(\vec{r}) \left(\frac{-3e^2}{4\pi} \right) (3\pi^2 n(\vec{r}))^{\frac{1}{3}} \quad (2.23)$$

in SI units where n is the electron density per unit volume at the point and e is the charge of an electron[54].

2.5 Generalized Gradient Approximation (GGA)

Many modern codes using DFT now use more advanced approximations to improve accuracy for certain physical properties. The DFT calculations in this study have been made using the Generalized Gradient Approximation (GGA) [49]. As stated above, the LDA uses the exchange-correlation energy for the uniform electron gas at every point in the system regardless of the homogeneity of the real charge density. For non uniform charge densities the exchange-correlation energy can deviate significantly from the uniform result. This deviation can be expressed in terms of the gradient and higher spatial derivatives of the total charge density. The GGA uses the gradient of the charge density to correct for this deviation. For systems where the charge density is slowly varying, the GGA has proved to be an improvement over LDA. Generalized gradient approximations (GGA's) seek to improve upon the accuracy of the local-spin-density (LSD) approximation in electronic-structure calculations. Perdew and *et al*,[46] have developed a GGA based on real-space cut-off of the spurious long-range components of the second-order gradient expansion for the exchange-correlation hole. We have found that this density functional performs well in numerical tests for a variety of systems: (1) Total energies

of 30 atoms are highly accurate. (2) Ionization energies and electron affinities are improved in a statistical sense, although significant inter configurationally and interterm errors remain. (3) Accurate atomization energies are found for seven hydrocarbon molecules, with a rms error per bond of 0.1 eV, compared with 0.7 eV for the LSD approximation and 2.4 eV for the Hartree-Fock approximation. (4) For atoms and molecules, there is a cancellation of error between density functionals for exchange and correlation, which is most striking whenever the Hartree-Fock result is furthest from experiment. (5) The surprising LSD underestimation of the lattice constants of Li and Na by 3–4 % is corrected, and the magnetic ground state of solid Fe is restored. (6) The work function, surface energy (neglecting the long-range contribution), and curvature energy of a metallic surface are all slightly reduced in comparison with LSD. Taking account of the positive long-range contribution, we find surface and curvature energies in good agreement with experimental or exact values. Finally, a way is found to visualize and understand the non locality of exchange and correlation, its origins, and its physical effects. Functionals that include the gradient of the charge density are collectively known as generalized gradient approximations (GGA). These functionals are the work horse of the current density functionals theory. In practice, E_{xc}^{GGA} is usually split into its exchange and correlation contributions.

$$E_{xc}^{GGA} = E_x^{GGA} + E_c^{GGA} \quad (2.24)$$

The exchange part can be written

$$E_x^{GGA} = E_x^{L(S)DA} - \sum_{\sigma} \left[F(S_{\sigma}) \rho_{\sigma}^{\frac{4}{3}}(r) dr \right] \quad (2.25)$$

And this can be reduced for spin σ as:

$$S_{\sigma}(r) = \left| \frac{\nabla \rho_{\sigma}(r)}{\rho_{\sigma}^{\text{inh}}(r)} \right| \quad (2.26)$$

Where S_{σ} is a local inhomogeneity parameter.

Chapter Three

Methodology

3.1 Introduction

The full-potential Linearized augmented plane wave (FLAPW) method has emerged as a widely used very robust and precise state of the art ab-initio electronic structure technique with reasonable computational efficiency to simulate the electronic properties of materials on the basis of density functional theory (DFT). Due to the high precision it is widely accepted that it provides the density functional answer to the problem. The shape of the charge density, the one-electron potential and the wave function is taken into account with high accuracy. The FLAPW method is an all-electron algorithm which is universally applicable to all atoms of the periodic table, in particular to transition metals and rare-earths and to multi-atomic systems with compact as well as open structures [55]. Due to the all-electron nature of the method, magnetism is included rigorously and nuclear quantities e.g. isomer shift, hyperfine field, electric field gradient (EFG), and core level shift are calculated routinely. Also open structures such as surfaces, clusters, organic and inorganic molecules as well as wires can be treated without problems. The capability of calculating atomic forces exerted on the atoms opens the path to structure optimization.

This chapter starts with an introduction of the APW-like and LAPW +Lo concepts to solve the Kohn-Sham equation for a periodic solid. Then, the concepts of FLAPW method and the Muffin Tin Approximation with full potential are described. Last the WIEN2K program and some of its applications are shown.

3.2 The Augmented Plane Wave (APW) method

In order to study the region near the nucleus (hyperfine fields for instance, or core level excitations) we have to search a basis set that help us without introducing pseudo-potential, such a basis set must be efficient. The first example of this will be the Augmented Plane Wave (APW) basis set. Right from the beginning it has to be said that the APW-method itself is of no practical use any more today. But for didactical reasons it is advantageous to discuss APW first, before going to its successors, LAPW and APW+Lo. The ideas that lead to the APW basis set are very similar to what made us to introduce the pseudo potential. In the region far away from the nuclei, the electrons are more or less ‘free’. Free electrons are described by plane waves[56]. Close to the nuclei, the electrons behave quite as they were in a free atom, and they could be described more efficiently by atomic like functions. Space is therefore divided now in two regions: around each atom[57] a sphere with radius R_α is drawn (call it S_α). Such a sphere is often called a *muffin tin* sphere, the part of space occupied by the spheres is the *muffin tin* region. The remaining space outside the spheres is called the interstitial region(call it I). One augmented plane wave(APW) used in the expansion of $\psi_{\vec{k}}^{\text{APW}}$ is defined as

$$\phi_{\vec{k}}^{\vec{K}}(\vec{r}, E) = \begin{cases} \frac{1}{\sqrt{V}} e^{i(\vec{k}+\vec{K})\cdot\vec{r}} & \vec{r} \in I \\ \sum_{l,m} A_{lm}^{\alpha,\vec{k}+\vec{K}} u_l^\alpha(r', E) Y_m^l(\hat{r}') & \vec{r} \in S_\alpha \end{cases} \quad (3.6)$$

The symbols $\vec{k} + \vec{K}$ and \vec{r} keep their usual meaning, V is the volume of the unit cell. Note that the APW basis set is k -dependent, as was the plane wave basis set. The position inside the spheres is given with respect to the centre of each sphere by $\vec{r}' = \vec{r} - \vec{r}_\alpha$ (see fig 3.1).

The length of \vec{r}' is r' , and the angles θ' and ϕ' specifying the direction of \vec{r}' in spherical coordinates, are indicated as \hat{r}' . The Y_m^l are spherical harmonics, the

$A_{lm}^{\alpha, \vec{k} + \vec{K}}$ are yet undetermined parameters as is E even it has dimension of

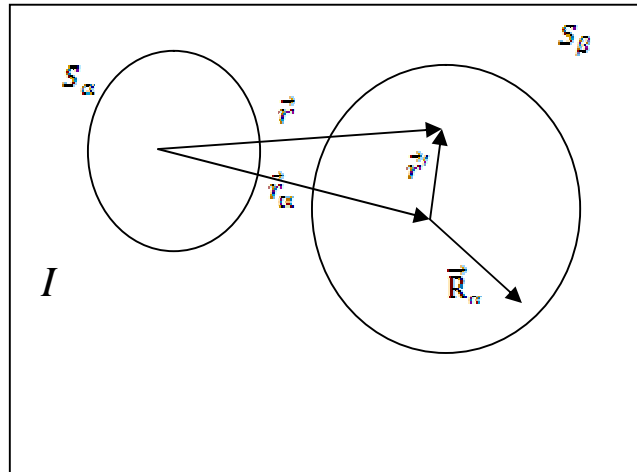


Figure (3.1): Division of a unit cell in muffin tin regions and the interstitial region, for a case with two atoms

energy. The u_l^α are solutions to the radial part of the Schrödinger equation for a free atom α , and this at the energy E . For a true free atom, the boundary condition that $u_l^\alpha(r, E)$ should vanish for $r \rightarrow \infty$, limits the number of energies E for which a solution u_l^α can be found. But as this boundary condition does not apply here, we can find a numerical solution for any E . Hence, the u_l^α themselves do not correspond to something physical, but that doesn't harm: they are only part of a basis function, not of the searched eigen function itself. And because they are close to how the actual eigen function will look like in that region of the crystal, they will do their job as basis function very efficiently. If an eigen function would be discontinuous, its kinetic energy would not be well-defined. Such a situation can therefore never happen, and we have to require that the plane wave outside the sphere matches the function inside the sphere over the complete surface of the sphere (in value, not in slope). That seems a weird thing to do: a plane wave is oscillating and has a unique direction built in, how can it match another function based on spherical harmonics over the entire surface of a sphere?

To see how this is possible, we expand the plane wave in spherical harmonics about the origin of the sphere of atom α :

$$\frac{1}{\sqrt{V}} e^{i(\vec{k}+\vec{K})\cdot\vec{r}'} = \frac{4\pi}{\sqrt{V}} e^{i(\vec{k}+\vec{K})\cdot\vec{r}'_\alpha} \sum_{l,m} i^l j_l(|\vec{k}+\vec{K}|r') Y_m^{l*}(\vec{k}+\vec{K}) Y_m^l(\vec{r}') \quad (3.7)$$

$j_l(x)$ is the Bessel function of order l , at the sphere boundaries (where $\vec{r}' = \vec{R}_\alpha$, which defines \vec{R}_α) to be equal to the lm -part of Eq.3.6 easily yields:

$$A_{lm}^{\alpha,\vec{k}+\vec{K}} = \frac{4\pi i^l e^{i(\vec{k}+\vec{K})\cdot\vec{r}'_\alpha}}{\sqrt{V} u_\alpha^l(\vec{R}_\alpha, E)} j_l(|\vec{k}+\vec{K}|R_\alpha) Y_m^{l*}(\vec{k}+\vec{K}) \quad (3.8)$$

At some choosing value ℓ_{\max} and treating the above equation at the boundaries of the sphere it will be clear that the muffin tin radii for different atoms should not be too different: if they were, a value for ℓ_{\max} that is suitable for each atom would not exist. So we can visualize the meaning of a single APW $\phi_{\vec{k}}^{\vec{R}_\alpha}(\vec{r}, E)$: it is an oscillating function that runs through the unit cell, whenever it encounters an atom on its path, the simple oscillating behavior is changed into something more complex inside the muffin tin sphere of that atom. At first sight it looks like we can now use the APW's as a basis set, and proceed in the same way as for the plane wave basis set in order to determine the coefficients $c_{\vec{k}}^{\vec{R}_\alpha}$ in the expansion of the searched eigen-function. However this does not work. We did not settle the parameter E yet. It turns out that in order to describe an eigen state $\psi_{\vec{k}}^{\vec{R}_\alpha}(\vec{r})$ accurately with APW's, one has to set E equal to the eigen value (or band energy) $\epsilon_{\vec{k}}^{\vec{R}_\alpha}$ of that state. But this is exactly what we are trying to determine! We are hence forced to start with a guessed value for $\epsilon_{\vec{k}}^{\vec{R}_\alpha}$ and take this as E . Now we can determine the APW's, and construct the Hamiltonian matrix elements and overlap matrix (the APW's are not orthogonal)[58]. The secular equation is determined, and our guessed $\epsilon_{\vec{k}}^{\vec{R}_\alpha}$ should be a root of it. Usually it is not, hence we have to try a second guess. Due to this new E , the APW's have to be determined again, and similarly for all matrix elements. With the help of root

determination algorithms, this guessing continues until a root say $\epsilon_{\vec{k}}^{n=1}$ is found. And then the whole procedure starts over for $\epsilon_{\vec{k}}^{n=2}$, etc.. In practice, $K_{max} \approx 3.5 au^{-1}$ is needed for sufficient accuracy. This is less than the typical value of 5.5 for plane waves and pseudo-potentials. As seen before, the basis set size can be estimated to be about $P = 131$ for APW, compared to roughly $P=270$ for plane waves. The calculation time (mainly determined by matrix diagonalization) scales with the third power of the basis set size, which would suggest APW to be 10 times faster than pseudo-potentials. However, with a plane wave basis set, P eigen values are found by a single diagonalization, while with APW one diagonalization is needed for every eigen value. This makes the APW method inherently slow, much slower than the pseudo-potential method.

3.3 The LAPW method

3.3.1 The regular LAPW method

The problem with the APW method was that the $u_{\vec{k}}^{\alpha}(r', E)$ have to be constructed at the -yet unknown- eigen energy $E = \epsilon_{\vec{k}}^n$ of the searched eigen state. It would be helpful if we were able to recover $u_{\vec{k}}^{\alpha}(r', \epsilon_{\vec{k}}^n)$ on the fly from known quantities. That is exactly what the Linearized Augmented Plane Wave method enables us to do. If we have calculated $u_{\vec{k}}^{\alpha}$ at some energy E_0 , we could make a Taylor expansion to find it at energies not far away from it:

$$u_{\vec{k}}^{\alpha}(r', \epsilon_{\vec{k}}^n) = u_{\vec{k}}^{\alpha}(r', E_0) + (E_0 - \epsilon_{\vec{k}}^n) \frac{\partial u_{\vec{k}}^{\alpha}(r', E)}{\partial E} \Big|_{E=E_0} + O(E_0 - \epsilon_{\vec{k}}^n)^2 \quad (3.9)$$

Substituting the first two terms of the expansion in the APW for a fixed E_0 gives the definition of an LAPW. This has a price: the energy difference $(E_0 - \epsilon_{\vec{k}}^n)$ is unknown and hence a yet undetermined $E_{\vec{k}m}^{\alpha, \vec{k}+\vec{K}}$ has to be

introduced

$$\phi_{\vec{k}}^{\vec{r}}(\vec{r}') = \begin{cases} \frac{1}{\sqrt{V}} e^{i(\vec{k}+\vec{K})\cdot\vec{r}'} & \vec{r}' \in I \\ \sum_{\ell,m} \left(A_{\ell m}^{\alpha,\vec{k}+\vec{K}} u_{\ell}^{\alpha}(r', E_0) + B_{\ell m}^{\alpha,\vec{k}+\vec{K}} \dot{u}_{\ell}^{\alpha}(r', E_0) \right) Y_m^{\ell}(\hat{r}') & \vec{r}' \in S_{\alpha} \end{cases} \quad (3.10)$$

In order to determine both $A_{\ell m}^{\alpha,\vec{k}+\vec{K}}$ and $B_{\ell m}^{\alpha,\vec{k}+\vec{K}}$, we will require that the function in the sphere matches the plane wave both in value and in slope at the sphere boundary. This can be done by using an expression similar to equation 3.2 and its radial derivative. This results in a 2×2 system from which both coefficients can be solved. Equation 3.10 is not the final definition of an LAPW yet. Imagine we want to describe an eigen state $\psi_{\vec{k}}^{\alpha}$ that has predominantly p-character ($\ell = 1$) for atom α . This means that in its expansion in LAPW's, the $A_{(\ell=1)m}^{\alpha,\vec{k}+\vec{K}}$ are large. It is therefore advantageous to choose E_0 near the centre of the p-band. In this way, the $O(E_0 - \epsilon_{\vec{k}}^{\alpha})^2$ term in equation 3.9 will remain small, and cutting after the linear term is certainly allowed. We can repeat this argument for every physically important (s-,p-, d- and f-states, i.e. up to $\ell = 3$) and for every atom. As a result, we should not choose one universal E_0 , but a set of well-chosen $E_{1,\ell}^{\alpha}$ to $\ell = 3$. For higher ℓ , a fixed value can be kept. The final definition of an LAPW is then

$$\phi_{\vec{k}}^{\vec{r}}(\vec{r}') = \begin{cases} \frac{1}{\sqrt{V}} e^{i(\vec{k}+\vec{K})\cdot\vec{r}'} & \vec{r}' \in I \\ \sum_{\ell,m} \left(A_{\ell m}^{\alpha,\vec{k}+\vec{K}} u_{\ell}^{\alpha}(r', E_{1,\ell}^{\alpha}) + B_{\ell m}^{\alpha,\vec{k}+\vec{K}} \dot{u}_{\ell}^{\alpha}(r', E_{1,\ell}^{\alpha}) \right) Y_m^{\ell}(\hat{r}') & \vec{r}' \in S_{\alpha} \end{cases} \quad (3.11)$$

With the $E_{1,\ell}^{\alpha}$ being fixed, the basis functions can be calculated once and for all. The same procedure as used for the plane wave basis set can now be applied. One diagonalization will yield P different band energies for this \vec{k} . The accuracy of a plane wave basis set was determined by $Kmax$. For the APW or LAPW basis set, it is not incorrect to use the same criterion.

However, a better quantity to judge the accuracy here is the product $R_{min}^\alpha K_{max}$ between the smallest muffin tin radius and K_{max} . This can be understood as follows. If the smallest muffin tin radius is increased, the closest point a plane wave can come to a nucleus moves farther away from the nucleus. The part of the wave function that need not to be described with plane waves any more, in general will have displayed the steepest behaviour, steeper than anywhere else in the interstitial region (it was closest to the nucleus). Less plane waves are needed to describe the remaining, smoother parts of the wave function. K_{max} can be reduced, and a good rule of thumb is that the product $R_{min}^\alpha K_{max}$ should remain constant in order to have comparable accuracy. Reducing K_{max} means reducing the size of the matrices, and because matrix diagonalization is very expensive, a larger R_{min}^α can significantly reduce the computation time. R_{min}^α can't be too large on the other hand, as the spherical harmonics are not suited to describe the wave functions in the region far away from the nuclei. Compared to a plane wave basis set, the LAPW basis set can be much smaller. The required K_{max} turns out to be $K_{max} = \frac{7.5 \leftrightarrow 9.0}{R_{min}^\alpha} \approx 4au^{-1}$, depending on the desired accuracy. This yields $P \approx 195$ as basis set size, compared to $P \approx 270$ for plane waves. The calculation time (mainly determined by matrix diagonalization) scales with the third power of the basis set size, which makes LAPW in this respect about 2 to 3 times faster than plane waves. There are other aspects however that slow down LAPW[59], such that in the end it is comparable in speed with plane waves.

3.3.2 LAPW with Local Orbital (LAPW+LO)

It was not explicitly stated so far which electron states are calculated with the LAPW method. Does it make sense to calculate the 1s orbital of Fe in

bcc-Fe? No, because this electron is extremely well bound to the nucleus (-514 Ry), and will behave almost exactly as if it were in a free Fe atom. Such a state is called a *core state*. The criterion for a core state is that it does not participate directly in chemical bonding with other atoms. Therefore, it must be contained entirely in the muffin tin sphere. States that leak out of the muffin tin sphere, are called *valence states*. Valence states participate in chemical bonds, and these states are treated by LAPW. Core states are treated as in free atoms, but subject to the potential due to the valence states. When applying this definition, it frequently happens that states with the same ℓ but a different principal quantum number n are both valence states. For instance, due to hybridization, Fe in bcc-Fe will have a non-negligible amount of 4p-character in its valence states that are about 0.2 Ry below the Fermi level. But the 3p-states that are 4.3 Ry below the Fermi level are not entirely confined in the core too. Such low-lying valence states are called *semi-core states*. It is not clear how $E_{1,\ell=1}^{Fe}$ should be chosen: close to 3p, close to 4p, at an intermediate value, : : :? None of the choices is optimal. This dilemma is solved by adding another type of basis function to the LAPW basis set, called a *local orbital* (LO). A local orbital is defined as:

$$\phi_{\alpha,LO}^{\ell m}(\vec{r}) = \begin{cases} 0 & \vec{r} \notin S_{\alpha} \\ \left(A_{lm}^{\alpha,LO} u_{\ell}^{\alpha}(r', E_{1,\ell}^{\alpha}) + B_{lm}^{\alpha,LO} \dot{u}_{\ell}^{\alpha}(r', E_{1,\ell}^{\alpha}) + C_{lm}^{\alpha,LO} \ddot{u}_{\ell}^{\alpha}(r', E_{1,\ell}^{\alpha}) \right) Y_{\ell}^m(\hat{r}') & \vec{r} \in S_{\alpha} \end{cases} \quad (3.12)$$

A local orbital is defined for a particular ℓ and m , and for a particular atom spheres of other atoms, hence its name *local orbital*. In the muffin tin sphere of atom α , the same $u_{\ell}^{\alpha}(r', E_{1,\ell}^{\alpha})$ and $\dot{u}_{\ell}^{\alpha}(r', E_{1,\ell}^{\alpha})$ as in the LAPW basis set are used, with as linearization energy $E_{1,\ell}^{\alpha}$ a value suitable for the highest of the two valence states (4p in our example)[60]. The lower valence state-that is much more free-atom-like-is sharply peaked at an energy $E_{1,\ell}^{\alpha}$. A single radial function $u_{\ell}^{\alpha}(r', E_{1,\ell}^{\alpha})$ at that same energy will be

sufficient to describe it. Local orbitals are not connected to plane waves in the interstitial region, they have hence no \vec{k} - or \vec{K} -dependence. The three coefficients $A_{lm}^{\alpha,LO}$, $B_{lm}^{\alpha,LO}$, $C_{lm}^{\alpha,LO}$ m are determined by requiring that the LO is normalized, and has zero value and zero slope at the muffin tin boundary (= it does not leak out of the muffin tin sphere). Adding local orbitals increases the LAPW basis set size. If for each atom local orbitals for p- and d-states are added, the basis set increases with 3+5=8 functions per atom [61] in the unit cell. This number is rather small compared to typical LAPW basis set sizes of a few hundred functions. The slightly increased computational time is a small price to be paid for the much better accuracy that local orbitals offer, and therefore they are always used.[62].

3.4 The FLAPW Method

One among the most accurate schemes for solving the Kohn–Sham equations is the full-potential Linearized-augmented-plane wave (FP-LAPW) method suggested by Andersen[63] on which WIEN code is based. Full-potential LAPW method (FLAPW)[24, 12] combines the choice of the LAPW basis set with the treatment of the full-potential and charge density without any shape approximations in the interstitial region and inside the muffin-tins. This generalization is achieved by relaxing the constant interstitial potential V_I^0 and the spherical muffin-tin approximation $V_{MT}^0(r)$ due to the inclusion of a warped interstitial $\sum V_I^{\vec{K}} e^{i\vec{K}r}$ (where \vec{K} are all reciprocal lattice vectors up to the largest value of K_{max}) and the non-spherical terms inside the muffin-tin spheres:

$$V(r) = \begin{cases} \sum_K V_I^{\vec{K}} e^{i\vec{K}r} & \text{interstitial region} \\ \sum_L V_{MT}^L(r) Y_L(\hat{r}) & \text{muffin - tin} \end{cases} \quad (3.12)$$

This method became possible with the development of a technique for obtaining the Coulomb potential for a general periodic charge density

without shape-approximations and with the inclusion of the Hamiltonian matrix elements due to the warped interstitial and non-spherical terms of the potential. The charge density n is represented analogously to Eq. (3.12), just exchanging by V .

3.5 WIEN2K code

The program package WIEN2k allows performing electronic structure calculations of solids using density functional theory (DFT). It is based on the full-potential (linearized) augmented plane-wave ((L)APW) + local orbitals (lo) method, one among the most accurate schemes for band structure calculations. In DFT the local (spin) density approximation (LDA) or the improved version of the generalized gradient approximation (GGA) can be used. WIEN2k is an all-electron scheme including relativistic effects and has many features.

3.6 Computational considerations

In the newest version WIEN2k [64] the alternative basis set (APW+lo) is used inside the atomic spheres for the chemically important orbitals, whereas LAPW is used for the others [65, 60]. In addition new algorithms for the computer intensive general eigen solver were implemented. The combination of algorithmic developments and increased computer power has led to a significant improvement in the possibilities of simulating relatively large systems on moderate computer hardware. Now, PCs or a cluster of PCs can be used efficiently instead of the powerful workstations or supercomputers that were needed about a decade ago. Several considerations are essential for a modern computer code and were made in the development of the new WIEN2k package [65]: Accuracy: extremely important in the present case. It is achieved by the well-balanced basis set,

which contains numerical radial functions that are recalculated in each iteration cycle. Thus these functions adapt to effects due to charge transfer or hybridization, are accurate near the nucleus and satisfy the cusp condition. The PW convergence can be essentially controlled by one parameter, namely the cut-off energy corresponding to the highest PW component. There is no dependence on selecting atomic orbitals or pseudo-potentials. It is a full-potential and all electron method. Relativistic effects (including spin orbit coupling) can be treated with a quality comparable to solving Dirac's equation. All atoms in the periodic table can be handled. Efficiency and good performance should be as high as possible. The new mixed basis APW+Lo/LAPW optimally satisfies this criterion. The smaller matrix size helps to save computer time and thus larger systems can be studied. The scaling is less than N^3 : Parallelization: the program can run in parallel, either in a coarse grain version where each k-point is computed on a single processor, or—if the memory requirement is larger than that available on a single CPU—in a fine grain scheme that requires special attention for the eigen solver, the most time consuming part. Both options, full and iterative diagonalization, are implemented to (automatically) select the most efficient routines. Architecture: the hardware in terms of processor speed, memory access and communication is crucial. Depending on the given architecture, optimized algorithms and libraries are used during installation of the program package. Portability requires the use of standards as far as possible, such as FORTRAN90, MPI, BLAS (level 3), SCALAPACK, etc. User friendliness is achieved by a web based graphical user interface (GUI), called w2web. The program package provides an automatic choice of default options and is complemented by an extensive User's Guide.

3.7 Applications of WIEN2k

3.7.1. Systems

The problems considered so far in QM calculations using the LAPW method (employed in various versions of the WIEN2K code) have covered a wide spectrum, including in particular insulators, semiconductors, (transition) metals up to f -electron systems or inter metallic compounds. The band structure can directly be compared to experiment in weakly correlated cases. However, the electronic structure of highly correlated systems such as the high T_c superconductors or the often-discussed late transition metal oxides would require treatments beyond LDA or GGA. In some solids magnetism plays an important role and as long as the magnetic moments are ordered in a collinear arrangement (e.g., Ferro-, ferri- or antiferromagnets) a proper description is relatively easy. Recently an extension to non-collinear magnetic systems (e.g., canted spins or spin spirals) has been provided.

3.7.2 Band structure and density of states (DOS)

In solid state physics, the electronic band structure (or simply band structure) of a solid describes ranges of energy that an electron is "forbidden" or "allowed" to have. It is due to the diffraction of the quantum mechanical electron waves in the periodic crystal lattice. The band structure of a material determines several characteristics, in particular its electronic and optical properties. The density of states (DOS) of a system describes the number of states at each energy level that are available to be occupied. A high DOS at a specific energy level means that there are many states available for occupation. A DOS of zero means that no states can be occupied at that energy level. The energy band structure and the corresponding density of states are the dominant quantities that determine

the electronic structure of a system. Their inspection provides information about the electric property (metal, insulator or semiconductor) and gives insight into the chemical bonding. By looking at site decomposed partial densities of states one can find a hint for the strength of interactions between the orbitals of the constituting atoms. The band structure is useful e.g., in connection with photoelectron spectra [66]. A three-dimensional band mapping is possible by angle-dependent very-low-energy diffraction and photoemission.

3.7.3. Electron densities

Electron density is the measure of the probability of an electron being present at a specific location. In molecules, regions of electron density are usually found around the atom, and its bonds. The electron density is the key quantity in DFT. By taking its Fourier transform the static structure factors can easily be obtained, which can be compared with the X-ray diffraction measurements. The comparison, however, is delicate, since the experiments are taken at finite temperature and must be corrected for thermal smearing, absorption and extinction. Determining the static structure factors from the experimental data requires a model in order to allow a comparison with theory [67].

3.7.4. Total energy and phase transitions

With the total energy the relative stability of different phases can be computed. In such a case it is advisable to keep as many parameters constant as possible in order to have a cancellation of systematic errors. These parameters can be, for example, the size of the atomic spheres, the plane-wave cut-off, the k-mesh, the DFT functional [68], the treatment of relativity, etc. Energy differences are often rather small and thus a consistent treatment of the systems to be compared will help to minimize

these computational effects. A few examples can be found in applications to metals [69], an insulator CaCl₂ [70] or a defect structure [71]. In each of these cases a new interpretation for the interplay between the structure of a solid and the electronic structure is given.

3.7.5. Forces and structure optimization

Closely related to the total energy is the structure optimization that is often needed in this context. In cases where the atoms occupy general positions that are not fixed by the crystal symmetry, the knowledge of the forces acting on the atoms helps to optimize the structure parameters. Forces can be computed in WIEN2k and are crucial for such optimizations [45].

3.7.6 Equilibrium volume and bulk modulus

A series of total energy calculations as a function of volume can be fitted to an equation of states according to Murnaghan's equation:

$$E(V) = \frac{B_0 V}{B'_0} \left[\frac{(V_0/V)^{B'_0}}{B'_0} + 1 \right] + C$$

The equilibrium volume and the bulk modulus can be calculated from the above equation by plotting total energy versus volume .

Chapter Four

Crystal Structure

4.1 Introduction

This is the story of how materials are made up from atoms. There are about 100 kinds of atoms in all the Universe, and whether these atoms form trees or tyres, ashes or animals, water or the air we breathe, depends on how they are put together. The same atoms are used again and again. Structure determines not only the appearance of materials, but also their properties. When an electrical insulator can become a superconductor, we begin to understand how important it is to understand the structure of materials [72]. Every year we are making rapid progress in developing new tools to understand structure; X-rays and accelerators, electron microscopes and nuclear reactors are among many physical and chemical techniques. One of the most important tools is of course the computer, both for calculating structures and visualizing them. Combining computers with communication means that the secrets of structure, and the beauty of structure, can be revealed to everyone.

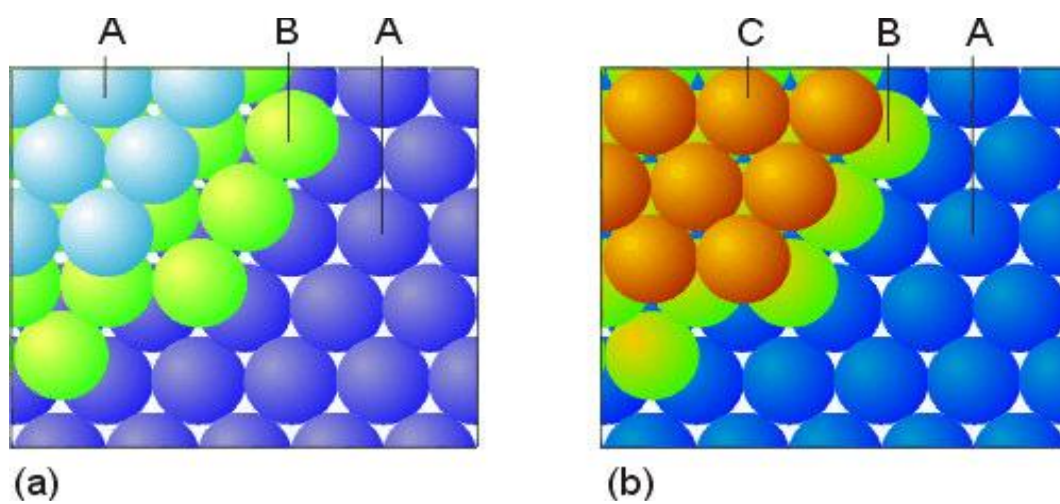
4.2 crystal structure

In mineralogy and crystallography, a crystal structure is a unique arrangement of atoms in a crystal. A crystal structure is composed of a motif, a set of atoms arranged in a particular way, and a lattice. Motifs are located upon the points of a lattice, which is an array of points repeating periodically in three dimensions. The points can be thought of as forming identical tiny boxes, called unit cells, that fill the space of the lattice. The lengths of the edges of a unit cell and the angles between them are called the lattice parameters. The symmetry properties of the crystal are embodied in

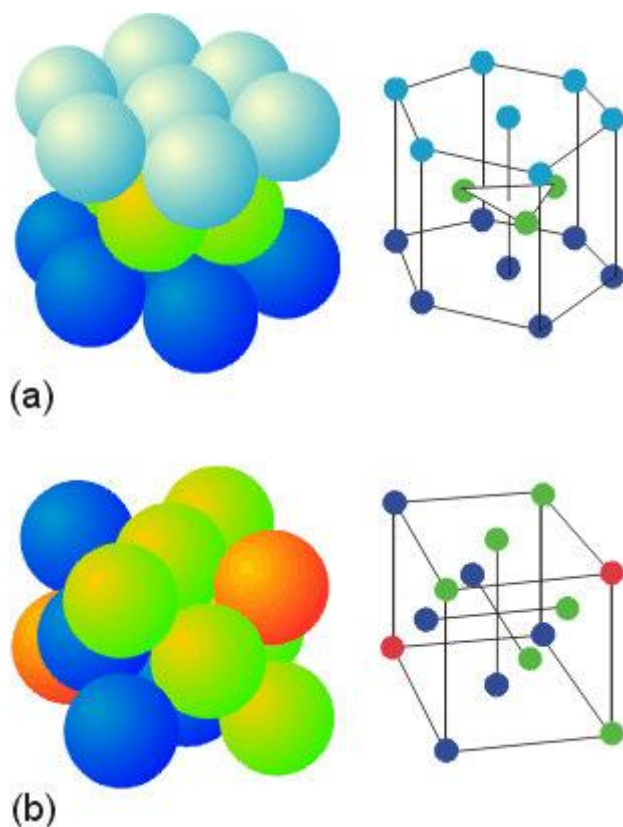
its space group [73]. A crystal's structure and symmetry play a role in determining many of its properties, such as cleavage[73], electronic band structure, and optical properties.

4.2.1 How do Atoms Pack Together?

The crystal structures of many metals can be described by close-packing of spheres (atoms). Similarly, many simple oxides to be discussed later can conveniently be considered to consist of close-packing of oxygen ions while the metal ions occupy voids in the close-packed structures. Let us therefore briefly discuss close-packing of spheres (atoms or ions). Consider an atom as a small hard sphere and make a layer of identical atoms so that the empty space between the atoms is minimum (layer A). Let us now add a second layer (B) such that the atoms in this second layer sit in one set of the hollows of the first layer. When we add a third layer of spheres, the spheres can be placed in two different positions: the spheres in the third layer can be placed directly over the spheres in layer A, and if we continue this stacking, the stacking sequence becomes ABABAB... as illustrated in figure (4-1-a)[74]. This type of close-packed stacking is called hexagonal close packing (hcp) of the spheres because it gives crystal structures with hexagonal symmetry. The third layer (layer C) could alternatively be placed such that the spheres in this layer will not be directly over either the atoms in the A or B layers, see figure (4-1-b). The stacking sequence is now ABCABC... and this close packing is known as cubic close packing (ccp) as this gives rise to a cubic (face-centered) crystal structure. The following figure shows how the two close-packed structures appear when their hexagonal and face-centered cubic unit cells are emphasized.



Figure(4.1) ABABAB...(hcp) close-packing (a) and ABCABC...(fcc) close-packing (b) of spheres. From Shriver and Atkins; *Inorganic Chemistry*.



Figure(4.2) Schematic views of the hcp (a) and fcc (b) structure types. From Shriver and Atkins; *Inorganic Chemistry*.

Less close-packed arrangements

Some metals and ionic compounds choose for various reasons to arrange themselves in less close-packed structures, as exemplified in the following two figures.

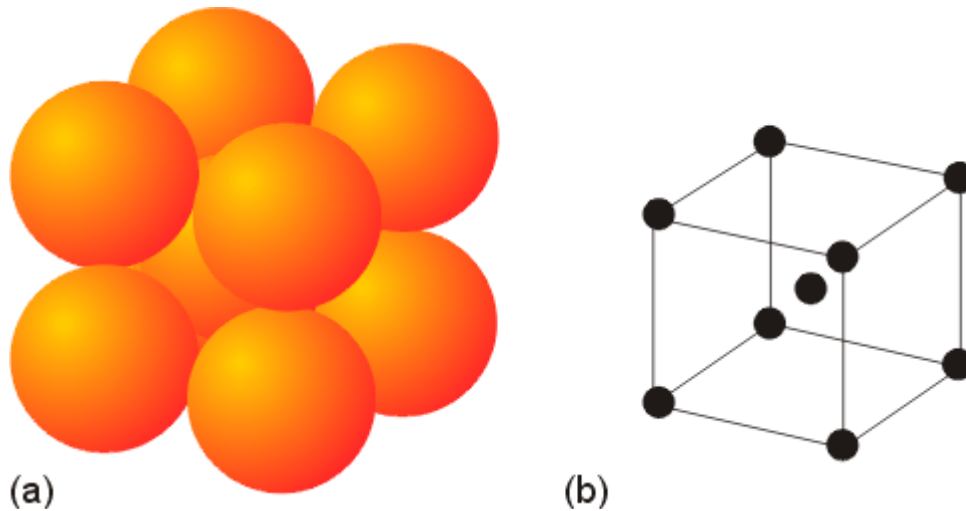


Figure (4.3) Body-centered cubic (bcc) packing of spheres

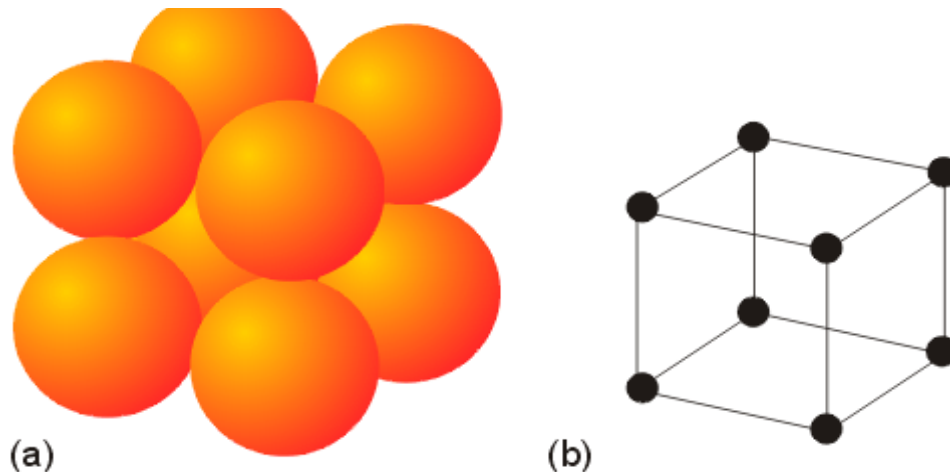


Figure (4.4) Simple cubic (sc) packing of spheres.

4.2.2 Unit Cell

The crystal structure of a material or the arrangement of atoms in a crystal can be described in terms of its unit cell. The unit cell is a tiny box containing one or more motifs, a spatial arrangement of atoms. The units cells stacked in three-dimensional space describe the bulk arrangement of

atoms of the crystal [75]. The unit cell is given by its lattice parameters, the length of the cell edges and the angles between them, while the positions of the atoms inside the unit cell are described by the set of atomic positions (x_i, y_i, z_i) measured from a lattice point. Although there are an infinite number of ways to specify a unit cell, for each crystal structure there is a conventional unit cell, which is chosen to display the full symmetry of the crystal. However, the conventional unit cell is not always the smallest possible choice. A **primitive unit cell** of a particular crystal structure is the smallest possible volume one can construct with the arrangement of atoms in the crystal such that, when stacked, completely fills the space. This primitive unit cell does not always display all the symmetries inherent in the crystal. A Wigner-Seitz cell is a particular kind of primitive cell which has the same symmetry as the lattice. In a unit cell each atom has an identical environment when stacked in three-dimensional space. In a primitive cell, each atom may not have the same environment. There are only seven possible crystal systems that atoms can pack together to produce an infinite 3D space lattice in such a way that each lattice point has an identical environment to that around every other lattice point.

4.2.3 Classification of crystals by symmetry

The defining property of a crystal is its inherent symmetry, by which we mean that under certain operations the crystal remains unchanged. For example, rotating the crystal 180 degrees about a certain axis may result in an atomic configuration which is identical to the original configuration. The crystal is then said to have a twofold rotational symmetry about this axis. In addition to rotational symmetries like this, a crystal may have symmetries in the form of mirror planes and translational symmetries, and also the so-called compound symmetries which are a combination of translation and

rotation/mirror symmetries [76]. A full classification of a crystal is achieved when all of these inherent symmetries of the crystal are identified.

4.2.4 Crystal system

The crystal systems are a grouping of crystal structures according to the axial system used to describe their lattice. Each crystal system consists of a set of three axes in a particular geometrical arrangement [77]. There are seven unique crystal systems. The simplest and most symmetric, the cubic (or isometric) system, has the symmetry of a cube, that is, it exhibits threefold rotational axes oriented at 109.5 degrees (the tetrahedral angle) with respect to each other. These threefold axes lie along the body diagonals of the cube. This definition of a cubic is correct, although many textbooks incorrectly state that a cube is defined by three mutually perpendicular axes of equal length – if this were true there would be far more than 14 Bravais lattices. The other six systems, in order of decreasing symmetry, are hexagonal, tetragonal, rhombohedral (also known as trigonal), orthorhombic, monoclinic and triclinic. Some crystallographers consider the hexagonal crystal system not to be its own crystal system, but instead a part of the trigonal crystal system. The crystal system and Bravais lattice of a crystal describe the (purely) translational symmetry of the crystal.

4.2.5 The Bravais lattices

When the crystal systems are combined with the various possible lattice centerings, we arrive at the Bravais lattices. They describe the geometric arrangement of the lattice points, and thereby the translational symmetry of the crystal. In three dimensions, there are 14 unique Bravais lattices which are distinct from one another in the translational symmetry they contain. All crystalline materials recognized until now fit in one of these arrangements [78]. The Bravais lattices are sometimes referred to as *space lattices*. The

crystal structure consists of the same group of atoms, the *basis*, positioned around each and every lattice point. This group of atoms therefore repeats indefinitely in three dimensions according to the arrangement of one of the 14 Bravais lattices. The characteristic rotation and mirror symmetries of the group of atoms, or unit cell, is described by its crystallographic point group.

4.2.6 Point and space groups

The crystallographic point group or crystal class is the mathematical group comprising the symmetry operations that leave at least one point unmoved and that leave the appearance of the crystal structure unchanged [79]. These symmetry operations can include reflection, which reflects the structure across a reflection plane, rotation, which rotates the structure a specified portion of a circle about a rotation axis, inversion which changes the sign of the coordinate of each point with respect to a centre of symmetry or inversion point and improper rotation, which consists of a rotation about an axis followed by an inversion. Rotation axes (proper and improper), reflection planes, and centres of symmetry are collectively called symmetry elements. There are 32 possible crystal classes. Each one can be classified into one of the seven crystal systems. The space group of the crystal structure is composed of the translational symmetry operations in addition to the operations of the point group. These include pure translations which move a point along a vector, screw axis, which rotate a point around an axis while translating parallel to the axis, and glide planes, which reflect a point through a plane while translating it parallel to the plane. There are 230 distinct space groups.

4.3 Some simple structures for oxides and other ionic compounds

The structures of ionic compounds can often be seen as close-packing

of the large anions, while the normally smaller cations occupy the interstitial voids [78]. (Note that once the structure is established, the interstices occupied by cations are not any longer considered interstitial; they are part of the ideal (reference) structure.). In judging the packing of ions it is useful to recall some important principles of ionic radii; the size of the elements increase down a group of the periodic table (resulting from the larger orbital of the outermost shell). Further, the size of the elements as a rule of thumb decreases from left to right through a period of the periodic table (resulting from increased nuclear charge). Finally, and most importantly in this context: Negatively charged ions (anions) are much larger than their neutral atoms and positively charged ions (cations) are much smaller than their neutral atoms. One may also recall that the effective size increases with the coordination number. In the following we look at some example structures possessed by oxides.

4.3.1 The Rock Salt (NaCl) structure

The ionic radius of the sodium ion is 1.16 angstroms and that of the chloride ion is 1.67 angstroms. The ratio of radii for the cation and anion is thus $r_{+}/r_{-} = 1.16/1.67 = 0.695$. With a radius ratio of 0.695, the cubic holes are too large ($r_{\text{hole}}/r = 0.732$) to be suitable. The sodium ions will prefer to occupy octahedral holes in a closest-packed structure [79]. As it happens, the chloride ions in NaCl pack in a cubic closest-packed structure.

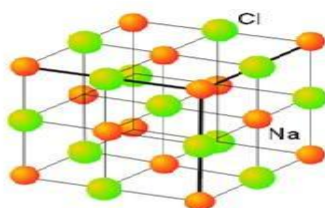


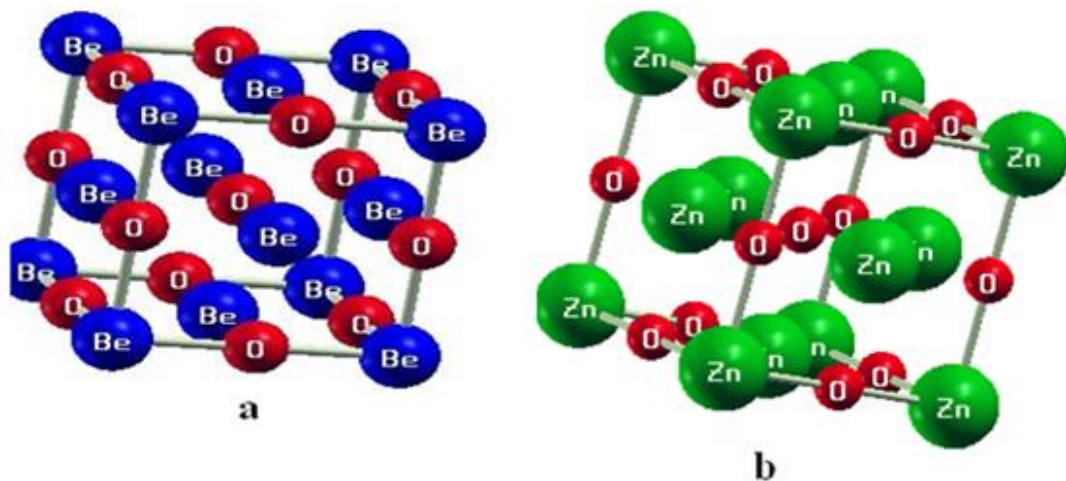
Figure (4.5) The rock salt (RS) structure.

It is clear that the lattice of NaCl is a face-centered cubic (fcc), the basis consists of one Na atom and one Cl atom separated by one-half the body

diagonal of a unit cell[80]. There are four units of NaCl in each unit cube, the basis, Na at (0,0,0) and Cl at (0.5, 0.5, 0.5), the space group is $Fm\bar{3}m$ with number 225 and the primitive s vectors for (RS) are :

$$\mathbf{r}_{a_1} = \frac{a}{2} \hat{y} + \frac{a}{2} \hat{z} \quad \mathbf{r}_{a_2} = \frac{a}{2} \hat{x} + \frac{a}{2} \hat{z} \quad \mathbf{r}_{a_3} = \frac{a}{2} \hat{x} + \frac{a}{2} \hat{y} \quad (4.1)$$

In our study Be, Zn will be placed at the position of Na and O will be placed at the position of Cl.

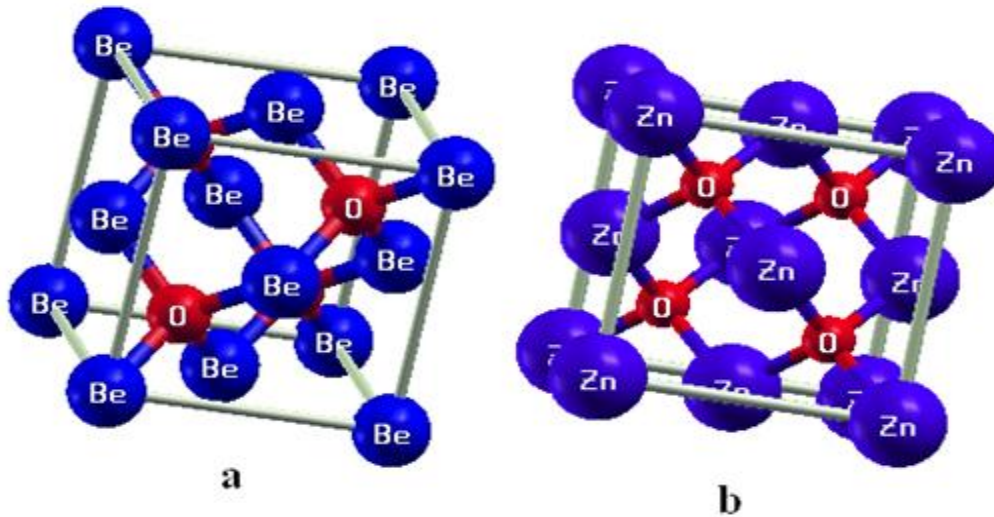


Figure(4.6) BeO(a) and ZnO(b)compounds in the rock salt structure(RS)

4.3.2 The zinc blende (ZB) structures

This structure is named after different mineral forms of zinc sulphide (ZnS). The zinc blende structure can be considered as a cubic close-packing of sulphide ions with the zinc ions occupying every other tetrahedral void. Each zinc ion is thus tetrahedrally coordinated by four sulphide ions and vice versa, also we can say that each Zn atom is placed on one fcc lattice and each S atom on other fcc lattice as illustrated in figure (4-7a,b) for BeO and for ZnO. In this structure the basis: Zn at: (0,0,0) and S at: (0.25,0.25,0.25) [80], the space group is $F\bar{4}3m$ with number 216 and the Primitive vector of (ZB) are:

$$\mathbf{r}_{a_1} = \frac{a}{2} \hat{y} + \frac{a}{2} \hat{z} \quad \mathbf{r}_{a_2} = \frac{a}{2} \hat{x} + \frac{a}{2} \hat{z} \quad \mathbf{r}_{a_3} = \frac{a}{2} \hat{x} + \frac{a}{2} \hat{y} \quad (4.1)$$



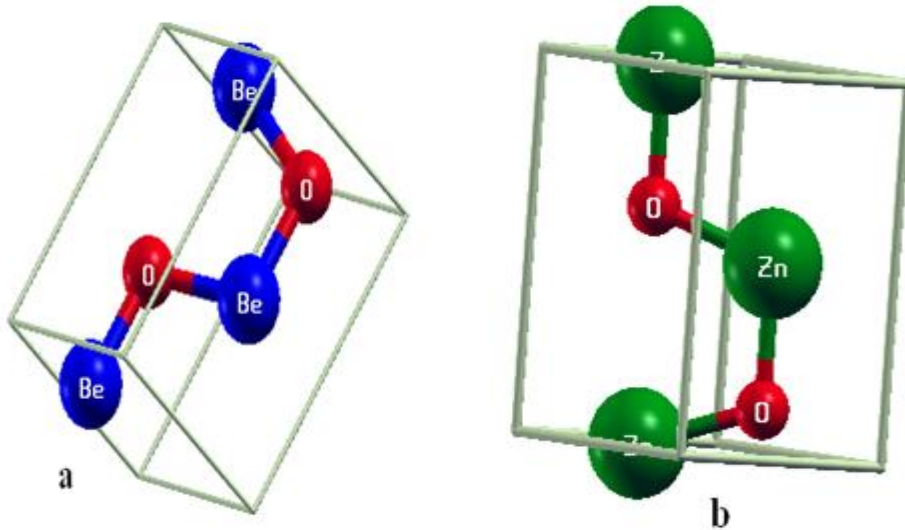
Figure(4.7) BeO(a) and ZnO(b) compound in the zinc-blende structure(ZB)

4.3.3 The wurtzite (W) structure

Zinc sulfide crystallizes in two different forms: Wurtzite and Zinc Blende. The ionic radius of the Zn^{+2} ion is 0.74 angstroms and that of S^{-2} ion is 1.70 angstroms. The ratio of radii for the cation and anion is thus $r_+/r_- = 0.74/1.70 = 0.44$ [81]. With a radius ratio of 0.44, one might expect the zinc(II) ions to occupy octahedral holes; however, the value of 0.44 is only slightly larger than $r_{\text{hole}}/r = 0.414$ for an octahedral hole. In this case, the zinc(II) ions occupy tetrahedral holes. If the sulfide ions originally adopt a hexagonal closest-packed structure, the ZnS crystal is Wurtzite. If the sulfide ions originally adopt a cubic closest-packed structure, the ZnS crystal is Zinc Blende. In the wurtzite structure the basis: Zn at $(1/3, 2/3, 0)$ and S at: $(1/3, 2/3, u)$ where $u = 3/8$ with $c/a = \sqrt{8/3}$, the space group is $P6_3\text{-}mc$ with number 186 and the primitive vectors are

$$\mathbf{r}_{a_1} = \frac{a}{2} \hat{x} + \frac{\sqrt{3}}{2} a \hat{y} \quad \mathbf{r}_{a_2} = \frac{a}{2} \hat{x} + \frac{\sqrt{3}}{2} a \hat{y} \quad \mathbf{r}_{a_3} = c \hat{z} \quad (4.3)$$

BeO and ZnO adopt the wurtzite structure as shown in figure (4.8a,b).



Figure(4.8): BeO (a) and ZnO(b) compounds in the wurtzite structure(W).

4.3.4 Cesium Chloride structure (CsCl)

The ionic radius of the cesium ion is 1.88 angstroms and that of the chloride ion is 1.67 angstroms. In this case the cation is the larger ion, and the ratio of radii for the anion and cation is $r_-/r_+ = 1.67/1.88 = 0.888$ [9]. With a radius ratio of 0.888, the smaller ion is expected to prefer a cubic hole. In this structure there is only one molecule per primitive cell (figure (4.9)), with basis Cs at (0, 0, 0) at the corners and Cl at (0.5, 0.5, 0.5) body-centered positions[10]. In this structure each atom may be viewed as at the center of a cube of atoms of the opposite kind, so the number of nearest neighbors or coordination number is eight, the space group for this structure is pm_3m with number of 221[79], the primitive vectors are:

$$\vec{a}_1 = a\hat{x} \quad \vec{a}_2 = a\hat{y} \quad \vec{a}_3 = a\hat{z} \quad (4.4)$$

ZnO adopt this structure but BeO compound don't.

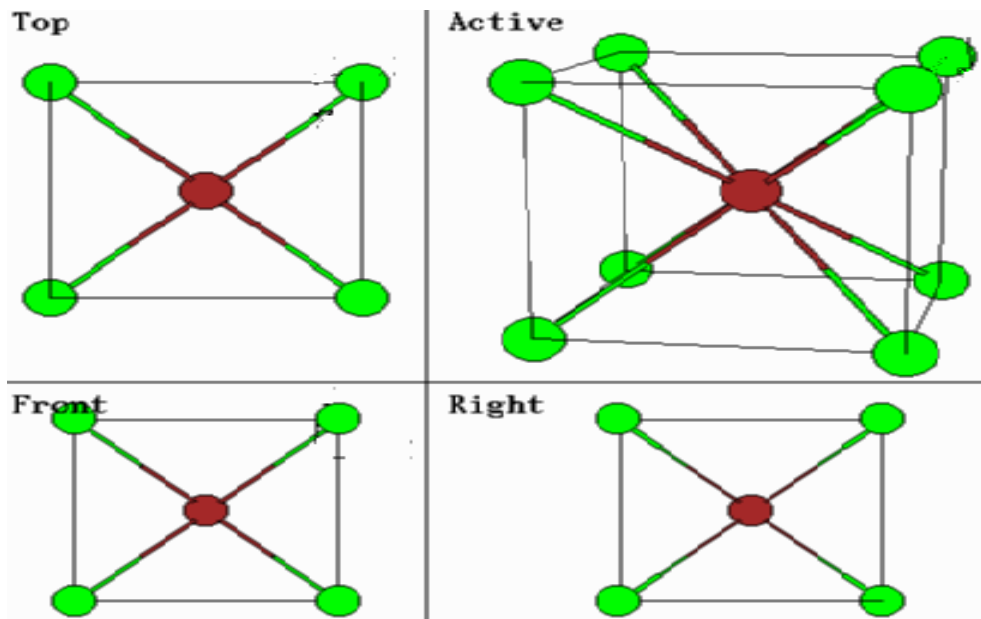


Figure.(4.9) the cesium chloride structure (CsCl)

4.4 Computational details

The structural phase transition of BeO and ZnO have been investigated under high pressure with full-potential linear augmented wave (FL-APW), WIEN2K computer code[82] within the local density approximation(LDA), generalized gradient approximation (GGA) and Cohen-Wu (which is a GGA improved). The FP-LAPW results for the crystal change density were obtained with LDA which proposed by Perdew and Wang[80], GGA which proposed by Perdew and his co-workers[83] and Cohen-Wu which proposed by Walter Kohn. The FP-LAPW method was used to calculate the electronic structure and the total energy of BeO and ZnO in the wurtzite, zinc-blende and rocksalt phases. This method has been successfully applied to study structural phases transitions of certain semiconductors [84,85]. The Zn 3d (Be doesn't has 3d) orbital is treated as part of the valence state, which increases the number of plane waves in the basis set, in order to decrease the structural properties of ZnO accurately. The FP-LAPW program, WIEN2K, was used to solve the Kohn-Sham equations. In FP-LAPW method, the wave function is expanded in atomic orbitals in spherical regions around the

atomic positions while in the regions between the spheres, it is expanded in plane wave. The wave functions and their derivatives are made continuous at the boundary of the sphere. The FP-LAPW places no restrictions on the form of crystalline potential and is known to yield reliable structural parameter for semiconductors, metals, and insulators. Relativistic effect is included in the calculations. Spin-orbit effects are not included in the calculations. Plane cut-off was chosen (by test, see tables 1-5 in next chapter) from the condition $R_{\text{mt}}K_{\text{max}}= 8$ for LDA, $R_{\text{mt}}K_{\text{max}}=9$ for GGA and $R_{\text{mt}}K_{\text{max}}=9$ for Cohen-Wu calculations, where K_{max} is the plane wave cut-off and R_{mt} is the atomic sphere radius (muffin-tin radius). A sufficiently dense k-point grid was used to achieve a good and very close convergence of total energy. For BeO we used $K_{\text{point}} = 3000$ with reduced $K=165$ and matrix $=12 \times 12 \times 9$ for wurtzite and $k_{\text{point}} = 9361$ with reduced $k=506$ and matrix $=21 \times 21 \times 21$ for both zinc-blende and rock salt structures, while for ZnO $K_{\text{point}} = 6000$ with reduced $k=624$ and matrix of $(22 \times 22 \times 12)$ for wurtzite and $K_{\text{point}}=9500$ with reduced $k=286$ and matrix $=21 \times 21 \times 21$.

A highly efficient and accurate tetrahedron integration scheme is used for the k-space integration. The calculated bulk properties are obtained by fitting the calculated total energy to the Murnaghan's equation of state [87]. In order to keep the same degree of convergence for all the lattice constants studied, we kept the values of the sphere radii constant over all the range of lattice spacing considered. For BeO compound we have considered R_{mt} (Be)=1.41 and R_{mt} (O)=1.41 Angstrom, also for ZnO we considered R_{mt} (Zn)=1.82A, R_{mt} (O)=1.62A for wurtzite, ZB and RS structures. The Zn 3d electrons are treated as part of the valence band since they are relatively high in energy even though they continue a well localized and narrow band. FP-LAPW schemes make no shape approximation to the potential and the

charge density. In addition to obtain a good agreement with the experiment. This makes the calculations much easier to converge; even we need a large value for $R_{\text{mt}}K_{\text{max}}$ in order to have reasonable number of plane waves to describe 3d state correctly. The lattice harmonics (angular momenta) up to $l=10$ are used for the expansion inside the muffin-tin spheres for the development of the wave function of the charge density and potential. The ground state properties are obtained by minimization of the total energy with respect to the volume of the unit cell. In the zinc blende and rock salt structures, the volume is directly related to the lattice constant(a), while for the wurtzite structure this minimization are performed using three independent parameters, lattice constants(a & c), and the internal cell parameter(u). Equilibrium values were found by calculating total energies for asset of values of the c/a ratio and the volume per unit cell to determine the optimum value of u . The equilibrium value and bulk modulus were determined by calculating total energies for asset of volumes and fitting these to the Murnaghan's equation of state [88]. We calculate the total energy for 7 different values of c/a and find the energy minimum by fitting the resulting values to a parabola. Freezing a_0 and c/a_0 at the best values just found, we vary the parameter u and find the new minimum of the total energy. Finally, with c/a and u fixed at their optimized values, we vary a_0 and calculate the total energy for 7 different volumes, which we fit again by Murnaghan's equation of state [82].

The k -integration over the Brillouin zone is performed with the Monk horst-pack[83]scheme. The number of sampling k -point in the irreducible Brillouin zone is 624, 506 and 506 for wurtzite, zinc-blende, and rock salt structures respectively, which correspond to $21 \times 21 \times 21$ k -point meshes for zinc-blende and rock salt phases and $22 \times 22 \times 12$ k -point meshes for the wurtzite phase.

Chapter Five Results, Discussions and Conclusion

5.1 Introduction

BeO compound is very important to be studied under high pressure because it possesses both ionic and covalent bonds and because of its role in fabrication as a catalyst, moderator and other applications. ZnO compound also is very important to be studied under high pressure because of the role that the d-electrons play in hybridization, covalent bonds, polarity and narrow energy band gap where few valence electrons will gain enough energy to make transition (easy transition from the valence band to the conduction band)[89].

5.2 BeO compound

The main aim of studying this compound is to investigate the stability of its wurtzite structure, we also studied the zinc-blende and the rocksalt structures and the transition pressure from W to RS, and from ZB to RS structures, we also calculated the structural parameter and the energy band gap for each phase by using the FLAPW method depending on the density functional theory. In the beginning of this study we made many tests to find the suitable Rk_{\max} , the suitable number of K_{points} , u and the c/a for wurtzite.

5.2.1 General considerations

5.2.1.1 Finding Rk_{\max}

R is the average value of the R_{mt} for all atomic spheres taken in account and K_{\max} is the maximum value for the K vector in the reciprocal lattice. Tables(5.1) and (5.2) show the tests done for choosing Rk_{\max} , where we took the same number of K_{points} , the same R_{mt} for all structures and the lattice parameters were fixed through the test for each phase[90]. We run

self-consistency cycle (SCF) and take the total energy for each run, we look for the minimum energy. From table(1) and table(2) we found that the best Rkmax is 8 for LDA, 9 for GGA and 9 for Wu-Cohen.

Table(5.1): Test to find Rk_{\max} for RS,ZB structures by LDA and GGA approximations

No.	RKmax	Etot (total energy(no.	Rkmax	Etot (total energy
1	6	-179.04204	1	6	-180.215100
2	6.5	-179.045149	2	6.5	-180.256032
3	7	-179.068125	3	7	-180.297453
4	7.5	-179.088066	4	7.5	-180.301256
5	8	-179.132574	5	8	-180.307832
6	8.5	-179.132563	6	8.5	-180.309897
7	9	-179.132573	7	9	-180.315603
8	9.5	-179.131443	8	9.5	-180.312175
9	10	-179.120276	9	10	-180.301901

Table (5.2) :Test to find Rk_{\max} for W structure by LDA, GGA and Cohen-Wu methods

LDA			GGA			Wu-Cohen		
No.	RK _{max}	E _{tot}	No.	RK _{max}	E _{tot}	No.	RK _{max}	E _{tot}
1	6	-358.221489	1	6	-360.621548	1	6	-359.402984
2	6.5	-358.222134	2	6.5	-360.630115	2	6.5	-359.487634
3	7	-358.223011	3	7	-360.630879	3	7	-359.511237
4	7.5	-358.223328	4	7.5	-360.631011	4	7.5	-359.599845
5	8	-358.223527	5	8	-360.631332	5	8	-359.689756
6	8.5	-358.223512	6	8.5	-360.631511	6	8.5	-359.887435
7	9	-358.223436	7	9	-360.631612	7	9	-359.97995
8	9.5	-358.223357	8	9.5	-360.631600	8	9.5	-359.97243
9	10	-358.222518	9	10	-360.631421	9	10	-359.965314

5.2.1.2 How to select R_{MT} radii:

R_{mt} is the atomic sphere radius (muffin-tin-radius) for atoms under study, the WIEN2k code can set this R_{mt} automatically (by default 2a.u.) but it is recommended to set R_{mt} and *NOT* use the default, taking the following consideration into account:

- 1- Choose the radii as large as possible, this will save computer time.
- 2- Choosing them smaller will make the calculations more expensive (you will need more plane waves), but a little bit more accurate (PW's are better basis functions, reduced linearization error).
- 3- If core charge leaks out of the spheres (check **:NEC01** in case.scf Whether too much charge is missing) you can increase the sphere of the atom where the core charge leaks out.
- 4- Do not make your R_{mt} 's too different!!! (even when geometry would allow), but atoms with d or (f) states may be 10-15% larger.
- 5- Identical atoms (elements) should have identical R_{MT} 's. For BeO compound we choose $R_{mt} = 1.41a.u$ for both atoms by doing reduction of 10% of the default value.

5.2.1.3 Choice of the k-point mesh

For a periodic system, integrals in real space over the (infinitely extended) system are replaced by integrals over the (finite) first Brillouin zone in reciprocal space, by virtue of Bloch's theorem. In WIEN2K code, such integrals are performed by summing the function values of the integrand (for instance: the charge density) at a finite number of points in the Brillouin zone, called the **k**-point mesh. Choosing a sufficiently dense mesh of integration points is crucial for the convergence of the results, and is therefore one of the major objectives when performing convergence tests. Here it should be noted that there is no variational principle governing the convergence with respect to the **k**-point mesh. This means

that the total energy does not necessarily show a monotonous behaviour when the density of the \mathbf{k} -point mesh is increased[91].

Monkhorst-Pack mesh

In order to facilitate the choice of \mathbf{k} -points, the WIEN2K package offers the possibility to choose \mathbf{k} -points according to the scheme proposed by Monkhorst and Pack [91]. This essentially means that the sampling \mathbf{k} -points are distributed homogeneously in the Brillouin zone, with rows or columns of \mathbf{k} -points running parallel to the reciprocal lattice vectors that span the Brillouin zone.

The concept of equivalent \mathbf{k} -points

In comparing different structures, if the two structures have the same unit cell, the comparison should always be done using the same \mathbf{k} -point set, so that possible errors from a non-converged \mathbf{k} -point sampling tend to cancel out. A similar strategy can also be applied when comparing structures with different unit cells. We refer to this concept here as 'equivalent \mathbf{k} -point sampling': The structure with a large unit cell has a smaller Brillouin zone associated with it. The \mathbf{k} -points sampling along this smaller Brillouin zone should be chosen as a subset of the \mathbf{k} -mesh in the larger Brillouin zone.

Reduced \mathbf{k} -points and symmetry

Apart from the translational symmetry of the Bravais lattice, the crystal structure under investigation may often have additional point group symmetries. These can be used to reduce the number of \mathbf{k} -points which are needed in the actual calculation substantially. To perform the integrals in the Brillouin zone, it is sufficient to sample the contribution from a subset of non-symmetry-equivalent \mathbf{k} -points only. Therefore the integrand (e.g. the charge density) is calculated only at these points. The integrand with

the full symmetry can be recovered from its representation by non-symmetry-equivalent \mathbf{k} -points whenever this is required [91].

Add inversion to K mesh

We have to add inversion to K-mesh in all cases except when you do *spin Polarized (magnetic) calculations WITH spin-orbit coupling* (this breaks time-inversion symmetry and thus one must not add inversion symmetry (eigen-values at $+\mathbf{k}$ and $-\mathbf{k}$ may be different)[91].

Shift the k-mesh:

Shifting of k mesh means that it will add (x,x,x) to all generated k-points, thus shifting them from high symmetry points (lines) to more "general" points with a higher weight. By this procedure (known also as "*special k-point methods*") one generates an equally "dense" mesh, but with less basis points. Usually a shift is *recommended*: When we are interested in "gaps" of semiconductors, they are often located at Gamma or X (or at some other BZ-border point). With shifted meshes we will NOT have those high-symmetry points in our mesh, thus the gap may seem to be smaller/larger than expected.

Tests for ZB with GGA, RS with LDA and Wurtzite with Wu-Cohen methods were done to choose the best K-points as seen in tables (3),(4)and(5), running (scf) and looking for the minimum energy . It is clear that best k-points for ZB and RS is 9261 with 286 reduced K-points and matrix $(21 \times 21 \times 21)$, while for wurtzite is 6300 with 364 reduced K-point and matrix $(22 \times 22 \times 12)$.

Table (5.3): Choosing best k-point for ZB structure by GGA method

no.	K _{point}	K _{reduced}	Matrix	E _{total} (RY)
1	729	35	9×9×9	-180.315603
2	1000	47	10×10×10	-180.315601
3	1331	56	11×11×11	-180.315602
4	1728	72	12×12×12	-180.315603
5	2744	104	14×14×14	-180.315602
6	3375	120	15×15×15	-180.315601
7	4096	145	16×16×16	-180.315601
8	4913	165	17×17×17	-180.315602
9	5832	195	18×18×18	-180.315602
10	6859	220	19×19×19	-180.315602
11	8000	256	20×20×20	-180.315602
12	9261	286	21×21×21	-180.315606
13	10648	328	22×22×22	-180.315603
14	12167	364	23×23×23	-180.315602

Table (5.4): Choosing K-point for RS structure by LDA method

no.	K _{point}	K _{reduced}	Matrix	E _{total} (RY)
1	729	35	9×9×9	-179.048047
2	1000	47	10×10×10	-179.048044
3	1331	56	11×11×11	-179.048048
4	1728	72	12×12×12	-179.048046
5	2744	104	14×14×14	-179.048046
6	3775	120	15×15×15	-179.048048
7	4096	145	16×16×16	-179.048045
8	4913	165	17×17×17	-179.048048
9	5832	195	18×18×18	-179.048045
10	6859	220	19×19×19	-179.048047
11	8000	256	20×20×20	-179.048047
12	9261	286	21×21×21	-179.048068
13	10648	328	22×22×22	-179.048046
14	12167	364	23×23×23	-179.048047

Table (5.5):Choosing K-point for wurtzite structure by Wu-Cohen

no.	K _{point}	K _{reduced}	Matrix	E _{total} (RY)
1	430	60	9*9*5	-359.818812
2	900	96	11*11*6	-359.951678
3	1200	147	13*13*7	-359.967980
4	1800	192	14*14*8	-359.974941
5	2300	240	16*16*8	-359.978093
6	2800	297	17*17*9	-359.979431
7	3200	333	18*18*9	-359.979991
8	3800	400	19*19*10	-359.980250
9	4500	440	20*20*10	-359.980376
10	5500	528	21*21*11	-359.980437
11	6000	624	22*22*12	-359.980479
12	6700	672	23*23*12	-359.818812
13	7500	732	24*24*12	-359.951678
14	8000	793	24*24*13	-359.967980
15	8500	845	25*25*13	-359.974941

5.2.1.4 Optimization

Most of the more complicated structures have free internal structural parameters, which can either be taken from experiment or optimized using the calculated forces on the nuclei.

Some suggestions about how to optimize a structure in WIEN2K:

- Start calculation by generating struct.file with arbitrary parameters.
- Initialize your file by introducing Rkmax , G_{max} and number of k-points.
- Run lapw and SCF cycle.
- Choose optimize(v, c/a) job, then x-optimize and choose vary volume with constant a, b, c for optimizing volume to find lattice parameters or vary c/a with constant volume for determining the ratio of c/a of wurtzite structure, in both cases we have to enter values like(-15,-10,-5,0,5,10,15)%
- After running optimize-job we plot energy curve versus volume or c/a.

5.2.1.4.1 Wurtzite structure

In this study c/a ratio was found by taking 7 values (-8,-4,-2,0,2,4,8%), for each value writing down a , c , c/a and run SCF to find minimum energy as shown in Tables (5.6, 5.7, 5.8), fitting these data to a Fortran program called polyfit and then getting the best value for c/a , this was done for LDA ($c/a=1.626$), GGA($c/a=1.6311$), and Wu-Cohen($c/a=1.6319$) methods.

For LDA $R_{mt}=1.41$ a.u.for Be and O, $Rk_{max}=8$, $G_{max}=14$, $K_{point}=6300$

Table(5.6): Finding c/a by LDA method

no.	Percent	a=b (a.u)	C (a.u)	c/a	E_{total} (RY)
1	-8.0	5.30435	7.93945	1.4967809	-358.205777
2	-4.0	5.22963	8.16794	1.5618581	-358.214231
3	-2.0	5.19381	8.28099	1.5943960	-358.216161
4	0.0	5.15895	8.39328	1.6269357	-358.216710
5	2.0	5.12501	8.50482	1.6594738	-358.215975
6	4.0	5.09195	8.61564	1.6920119	-358.214038
7	8.0	5.02829	8.83516	1.7570904	-358.206902

For GGA $R_{mt}=1.41$ a.u.for Be and O, $Rk_{max}=9$, $G_{max}=16$, $K_{point}=6300$

Table(5.7) Finding c/a by GGA method

Tries	Percent	a=b (a.u)	C (a.u)	c/a	E_{total} (RY)
1	-8	5.30435	7.90561	1.4904013	-360.618841
2	-4	5.22963	8.13313	1.5552018	-360.628237
3	-2	5.19381	8.24570	1.5876014	-360.630527
4	0	5.15895	8.35751	1.6200021	-360.631368
5	2	5.12501	8.46857	1.6524007	-360.630865
6	4	5.09195	8.57891	1.6847986	-360.629107
7	8	5.02829	8.79750	1.7496008	-360.622160

For Wu-Cohen $R_{mt}=1.41$ a.u.for Be and O, $Rk_{max}=9$, $G_{max}=16$, $K_{point}=6300$

Table(5.8) Finding c/a by Wu-Cohen method

no.	ratio	a	c	c/a	Etot
1	-8	5.29443	7.75739	1.46520	-359.967289
2	-4	5.25578	7.87189	1.49776	-359.976761
3	-2	5.18174	8.09844	1.56288	-359.979707
4	0	5.11171	8.32187	1.62800	-359.977024
5	4	5.04532	8.54233	1.69312	-359.969511
6	8	4.98224	8.75998	1.75824	-359.964114

Secondly the u value which controls the position of the atom in the unit cell is founded, taking different values of u , running SCF calculation and writing down the total energy for each value as shown in Table(5.9). This is also done for LDA (u=0.378), GGA & Wu-Cohen (u=0.377).

Table(5.9):Finding u by LDA method

no.	U	E _{total} (RY)	no.	U	E _{total} (RY)	no.	U	E _{total} (RY)
1	0.357	-358.20393	10	0.366	-358.20857	17	0.375	-358.21041
2	0.358	-358.20462	11	0.367	-358.20891	18	0.376	-358.21046
3	0.359	-358.20524	12	0.368	-358.2092	19	0.377	-358.21049
4	0.36	-358.20581	13	0.369	-358.20947	20	0.378	-358.2105
5	0.361	-358.20638	14	0.370	-358.2097	21	0.379	-358.21048
6	0.362	-358.2069	15	0.371	-358.2099	22	0.38	-358.21043
7	0.363	358.20737	16	0.372	-358.21007	23	0.381	-358.21036
8	0.364	-358.20781	15	0.373	-358.21021	24	0.382	-358.21027
9	0.365	-358.20821	16	0.374	-358.21033	25	0.383	-358.21015

Table(5.10): Finding u by GGA method

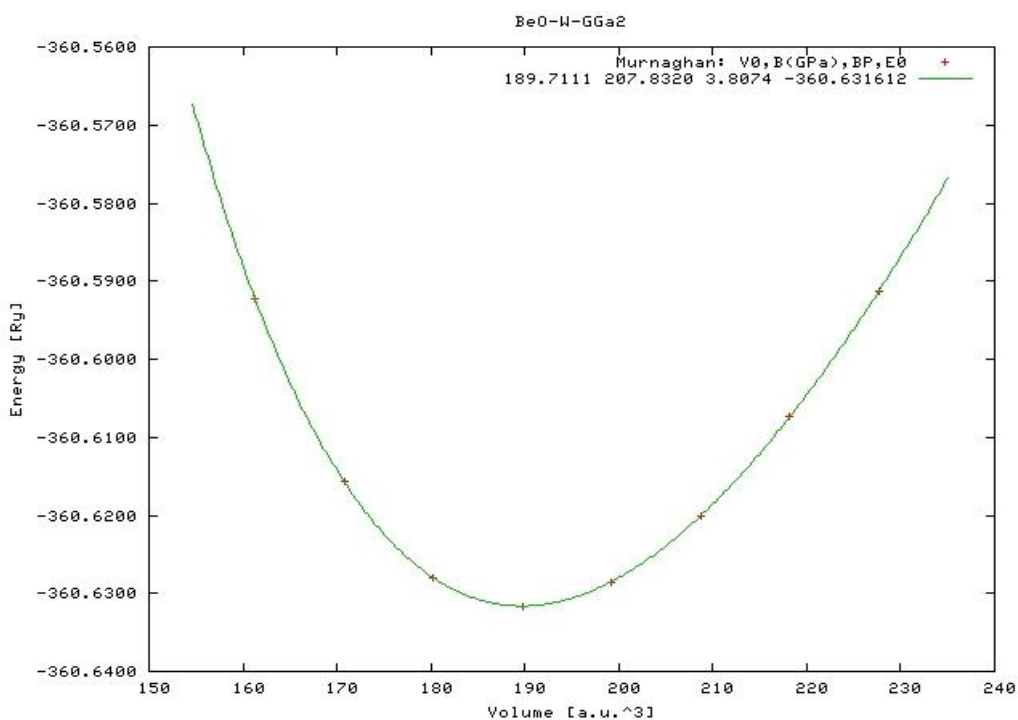
no.	U	E _{total} (RY)	no.	u	E _{total} (RY)
1	0.367	-360.626868	8	0.3900	-360.632090
2	0.369	-360.627383	9	0.3800	-360.632037
3	0.372	-360.632034	10	0.3820	-360.631856
4	0.374	-360.631933	11	0.3840	-360.631576
5	0.376	-360.631723	12	0.3860	-360.631577
6	0.377	-360.632113	13	0.3880	-360.631118
7	0.378	-360.632115	14	0.3900	-360.630578

After finding c/a and u, a and c will be found by optimizing job, choosing optimization vary volume with constant a= b, c and use 7 values for optimization (-15,-10,-5,0,5,10,15%) and looking for the minimum energy, fitting the results with the Murnaghan's equation and plotting the energy versus volume, the values of minimum volume, bulk modulus, its first derivative with respect to volume and minimum energy can be obtain from the graph. (the same way for LDA, GGA, Wu-Cohen)

$$\text{The volume of the unit cell for wurtzite(hcp)} \quad V = \frac{\sqrt{3}}{2} a^2 c \quad (1)$$

$$\text{by rewriting this equation} \quad V = \frac{\sqrt{3}}{2} a^3 (c/a) \quad (2)$$

$$a = \left[\frac{2V}{\sqrt{3}(c/a)} \right]^{1/3} \quad (3)$$



Figure(5.1) Energy vs. volume for ZB of BeO by GGA method we can find a., substituting the volume (V) from the graph and c/a in equation (3)

1-For LDA, $V= 180.3017(a.u)^3$, $c/a=1.626$, $a.=5.04022a.u. =2.6675A$

2- For GGA, $V=189.7111(a.u)^3$, $c/a=1.6311$, $a.=5121a.u. =2.709A$

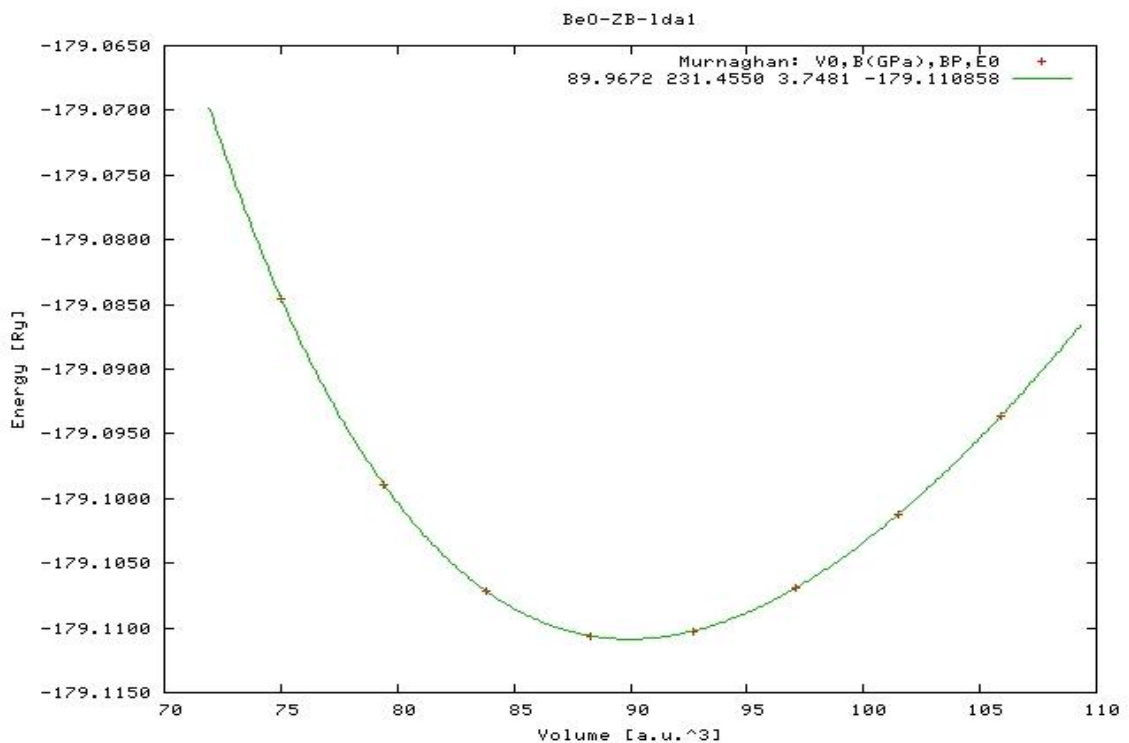
3-For Wu-Cohen, $V=185.7742(a.u)^3$, $c/a=1.6319$, $a.=5.085a.u.=2.6905A$

Table(5.11):Structural parameters for wurtzite structure

method	a.(A)		c/a		u		volume $V_0(A)^3$	B(GPa) ^a		B'	$E_{min}(RY/mol)$
	present	other	Present	other	present	other		present	other		
LDA	2.6675	2.65	1.626	1.624	0.378	0.378	26.72	232.6	224	3.7	-358.22
GGA	2.709	2.703	1.6311	1.635	0.377	0.377	28.11	207.8	203	3.8	-360.62
Cohen	2.6905	2.698	1.6319	1.633	0.376		27.53	216.8	239	3.8	-359.98

5.2.1.4.2 Zinc-blende structure(ZB)

The same way of calculation is used in (ZB) structure to find the lattice parameters, for this structure the $R_{mt}=1.41a.u.$,the number of K-point is 9261 with reduced $K_{point}= 286$ and matrix of $21 \times 21 \times 21$, the Be atom set at (0,0,0), while O atom sets at (1/4,1/4,1/4) positions, for LDA $Rk_{max}=8$, $G_{max}=14$, while for GGA and Wu-Cohen $Rk_{max}=9$, $G_{max}=16$.



Figure(5.2) Energy vs. volume for ZB of BeO by LDA method

The volume of the unit cell for ZB(fcc) is $V = \frac{a^3}{4}$ (4)

And can be rewritten for a., $a = [4.V]^{1/3}$ (5)

Using equation(5) and substitute V from the graphs we get a. ,

1- for LDA, $V=89.967(a.u.)^3$, $a. = 7.11a.u. =3.7639 \text{ \AA}$

2- for GGA, $V =94.8352(a.u.)^3$, $a.= 7.239a.u. =3.8306 \text{ \AA}$

3-for Cohen $V=92.7613(a.u.)^3$, $a. = 7.186a.u. = 3.8025 \text{ \AA}$

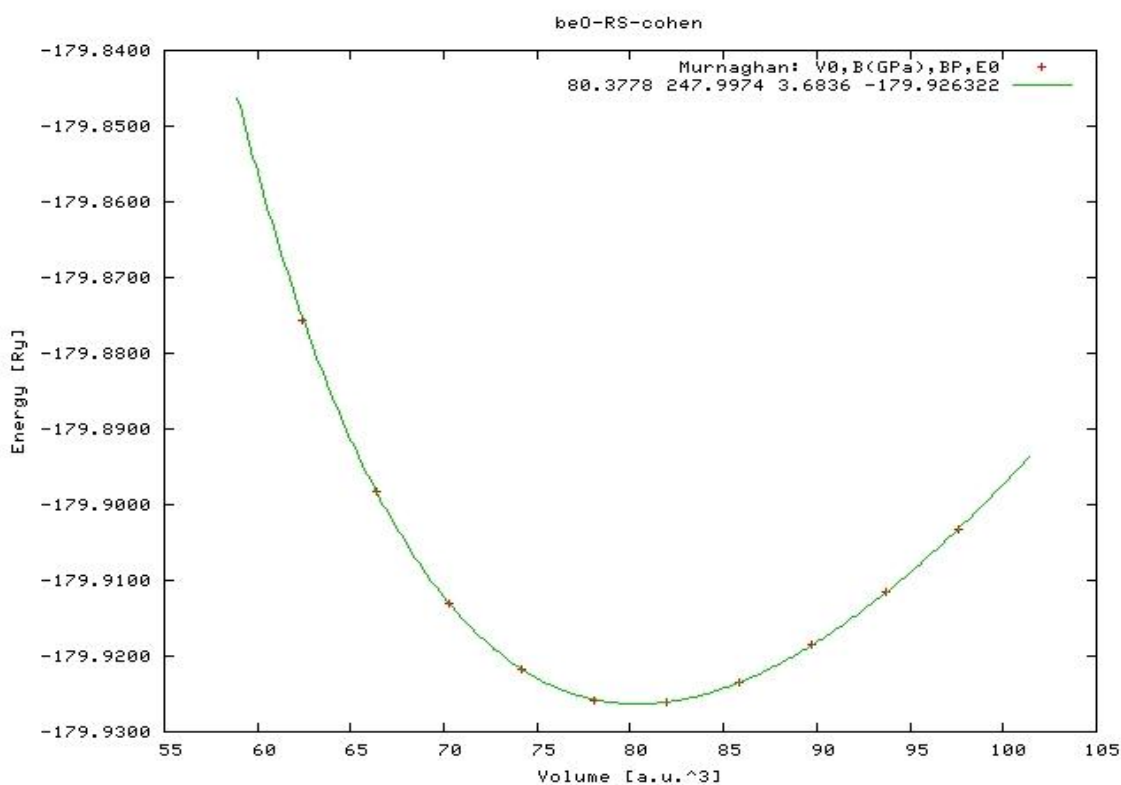
Table(5.12) Structural parameters for ZB structure

method	a. (A)		V ₀ (A) ³		B(GPa) ^a		B'	E(RY/mol.)
	present	other	present	other	present			
LDA	3.7639	3.737	89.967	231.5	224	3.748	-179.1109	
GGA	3.8306	3.810	94.835	207.5	201	3.666	-180.3156	
Cohen	3.8025	3.8	92.761	215.2	228	3.828	-179.9893	

(a) reference[92]

5.2.1.4.3 Rocksalt structure (RS)

The way of calculations and initial values are the same as in ZB structure the different only in the positions of the atoms where Be at (0,0,0) and O at (1/2,1/2,1/2).

**Figure(5.3)** Energy vs. volume for RS of BeO by Wu-Cohen method

Since RS is fcc the volume of the unit cell as in equation(4) and a. can be found from equation(5), for fcc the lattice constants are equal $a=b=c$

1- for LDA, $V=77.9951(a.u.)^3$, $a.=6.7823a.u. =3.5890A$

2-for GGA, $V=82.2512(a.u.)^3$, $a.=6.9035a.u. =3.6531A$

3-for Wu-Cohen, $V=80.3778(a.u.)^3$, $a.=6.8506a.u. =3.6252A$

Table(5.13) Structural parameters for RS structure

method	a.(A)		V ₀ (A) ³	B(GPa) ^a		B'	E(RY/mol.)
	present	other		present	other		
LDA	3.5890	3.577	77.995	263.1	264	3.522	-179.0479
GGA	3.6531	3.648	82.251	231.8	231	3.587	-180.2453
Cohen	3.6252		80.378	248	262	3.684	-179.9263

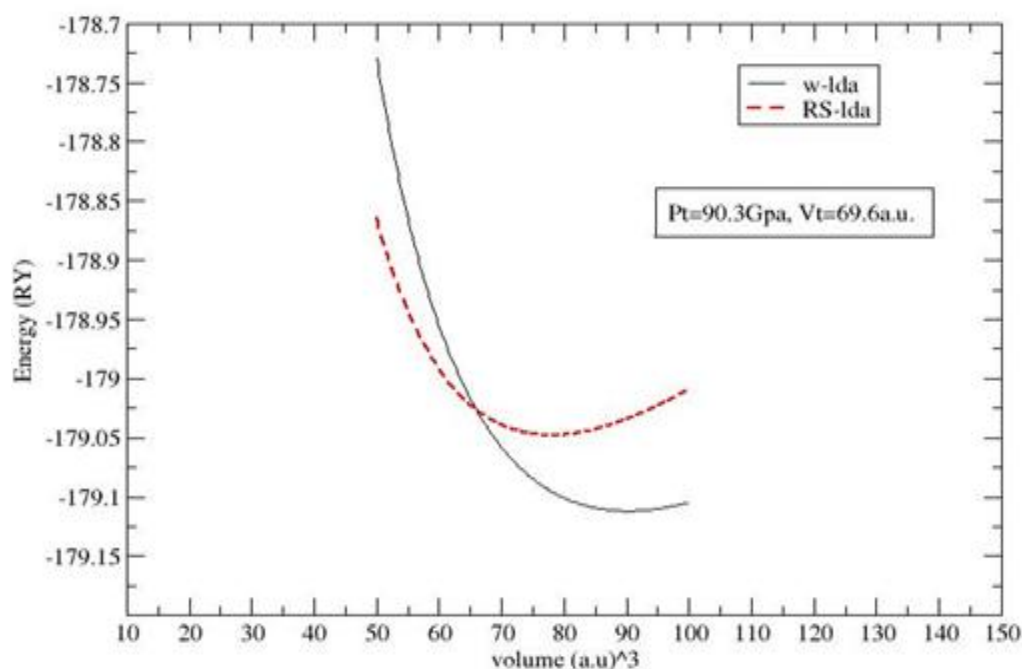
a) reference[92]

5.2.1.5 Transition phases

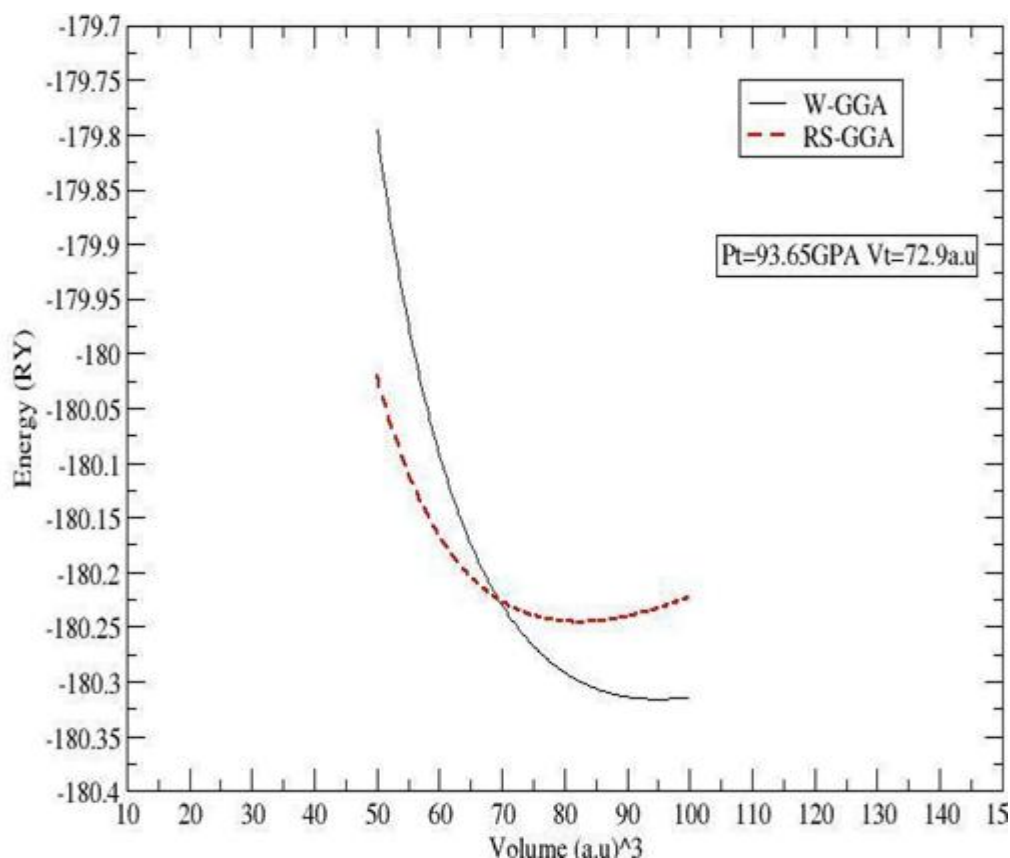
The forces that act on the nuclei causes optimization of the unit cells which means that the lattice parameters change into new values and this causes the structure to come into new structure, this happen at embedded pressure with certain values called the transition pressure, here we are seeking the transition pressure by the equation:

$$P_t = -\frac{\Delta E}{\Delta V} \quad (6)$$

Fig(4) shows the EOS for both WZ &RS structures using LDA method. The transition pressure was found to be 90.3 GPa and the transition volume was found to be 69.6a.u. (10.3A)

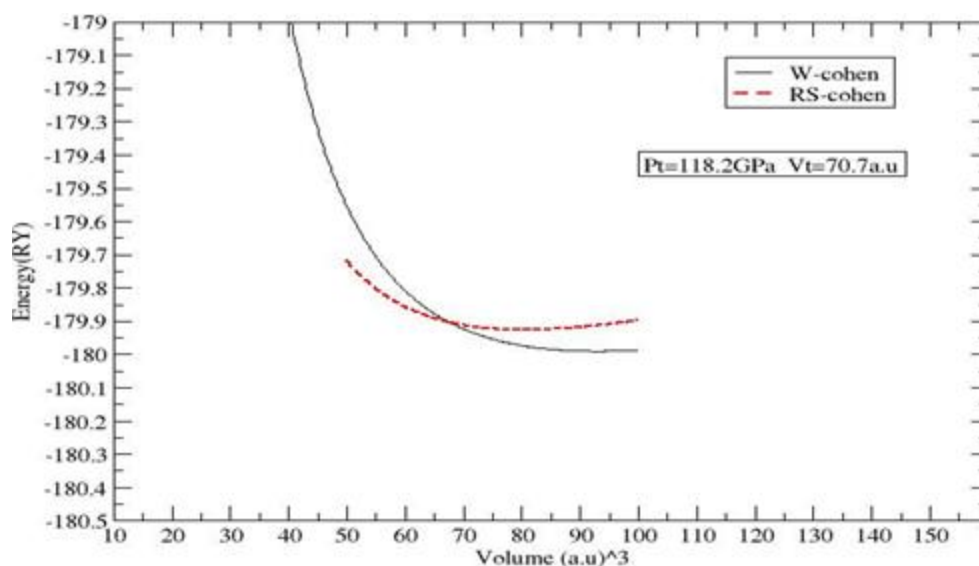
**Figure(5.4)** Total energy vs. volume for W , RS of BeO by LDA method

Figure(5.5) shows the EOS for WZ & RS structures using GGA method. The transition pressure was found to be 93.65 GPa and the transition volume was $72.9\text{a.u.}^3 = (10.8\text{\AA})^3$.



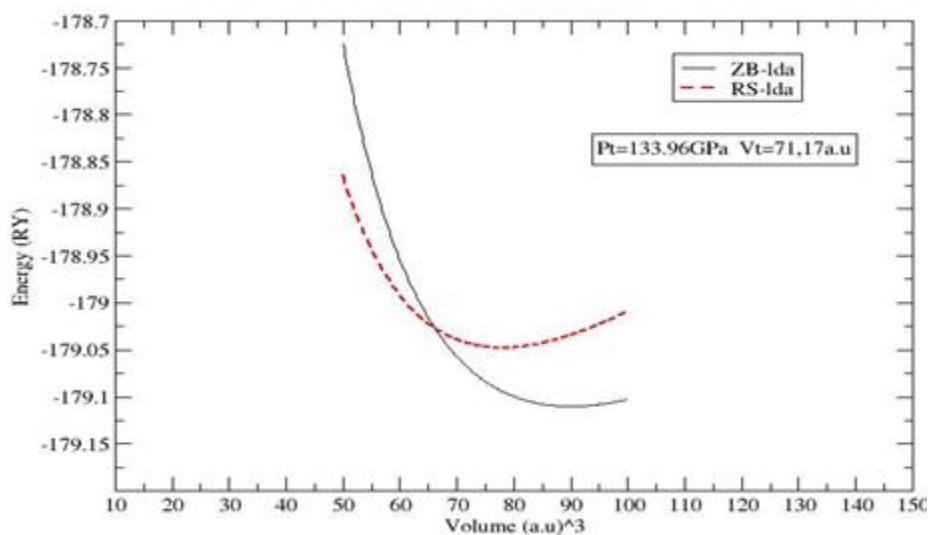
Figure(5.5) Total energy vs. volume for W, RS of BeO by GGA method

Fig(5.6) also shows the EOS for both WZ & RS structures but by using the Wu=Cohen method. The transition pressure was found to be 118.2 GPa while the transition volume was found to be $70.7\text{a.u.}^3 = (10.48\text{\AA})^3$.



Figure(5.6) Total energy vs. volume for W, RS of BeO by Wu-Cohen method

Fig(5.7) shows the EOS for ZB & RS structures by using LDA method. The transition pressure was found to be 133.96GPa and the transition volume was $71.17\text{a.u.}^3=(10.55\text{\AA}^3)$.



Figure(5.7) Total energy vs. volume for ZB,RS of BeO by LDA method

Fig(5.8) shows the EOS for ZB & RS structures by using GGA method. The transition pressure was found to be 146.47 GPa and the transition volume was $70.6\text{a.u.}^3=(10.47\text{\AA}^3)$.

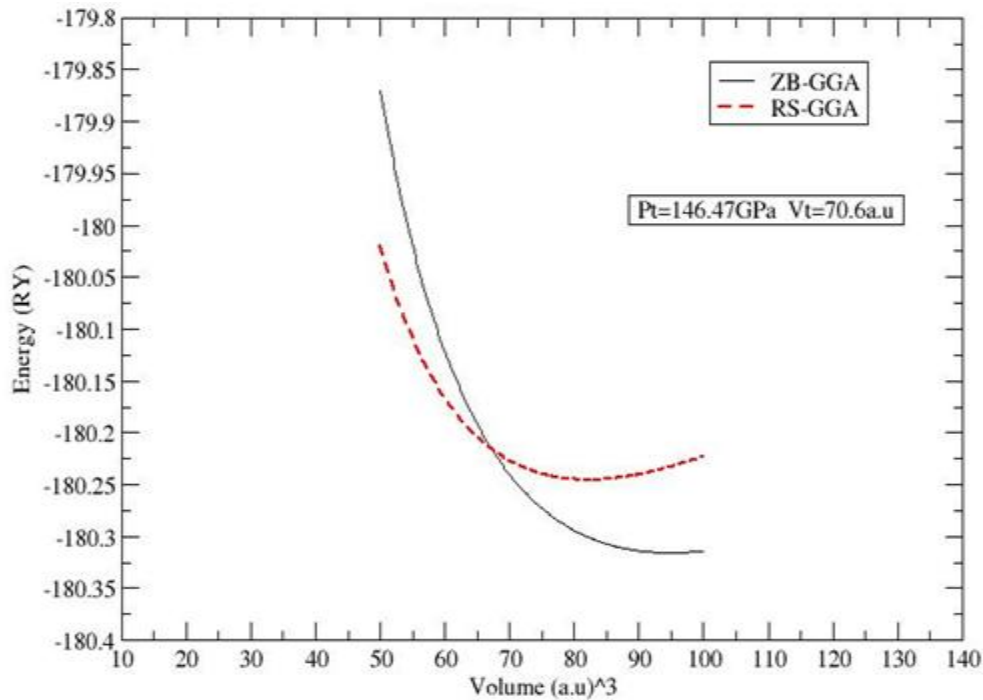


Figure (5.8) Total energy vs. volume for ZB, RS of BeO by GGA method

Figure (5.9) shows the EOS for ZB & RS structures by using Wu-Cohen method. The transition pressure was found to be 140.45GPa and the transition volume was found to be $71.96\text{a.u.}^3=(10.66\text{\AA}^3)$.

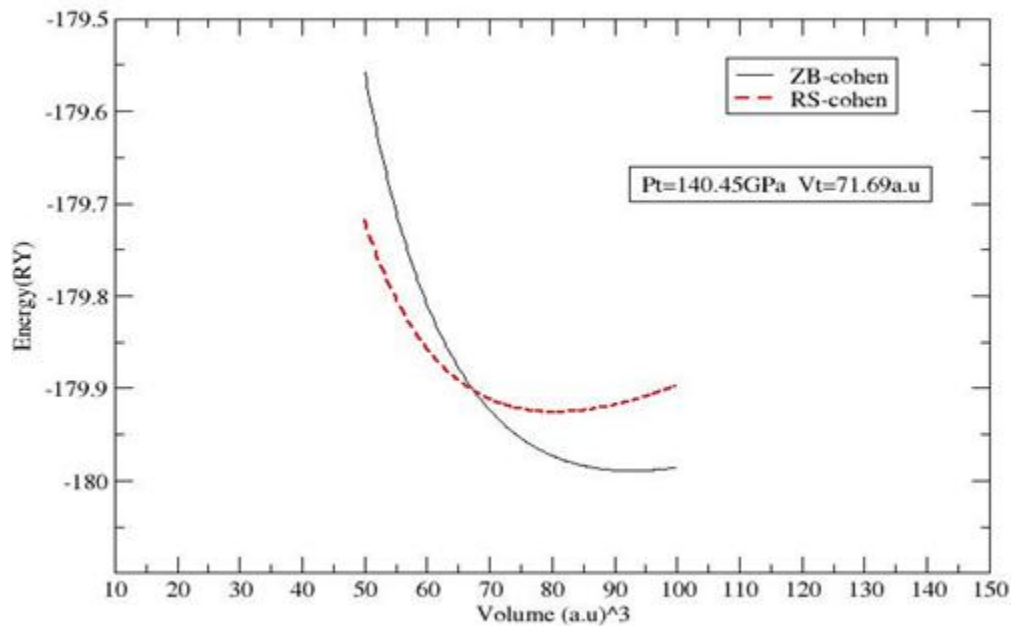


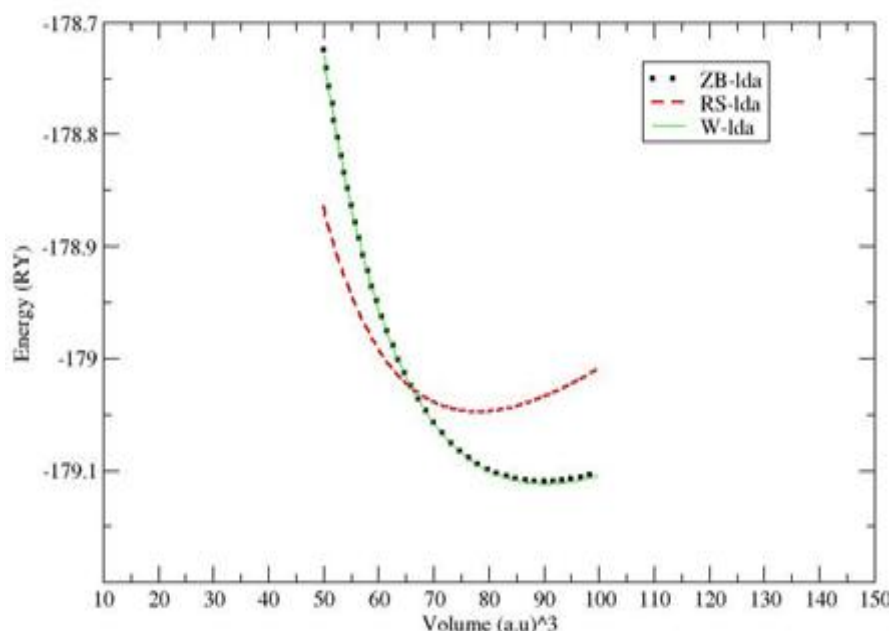
Figure (5.9) Total energy vs. volume for ZB,RS of BeO by Wu-Cohen method

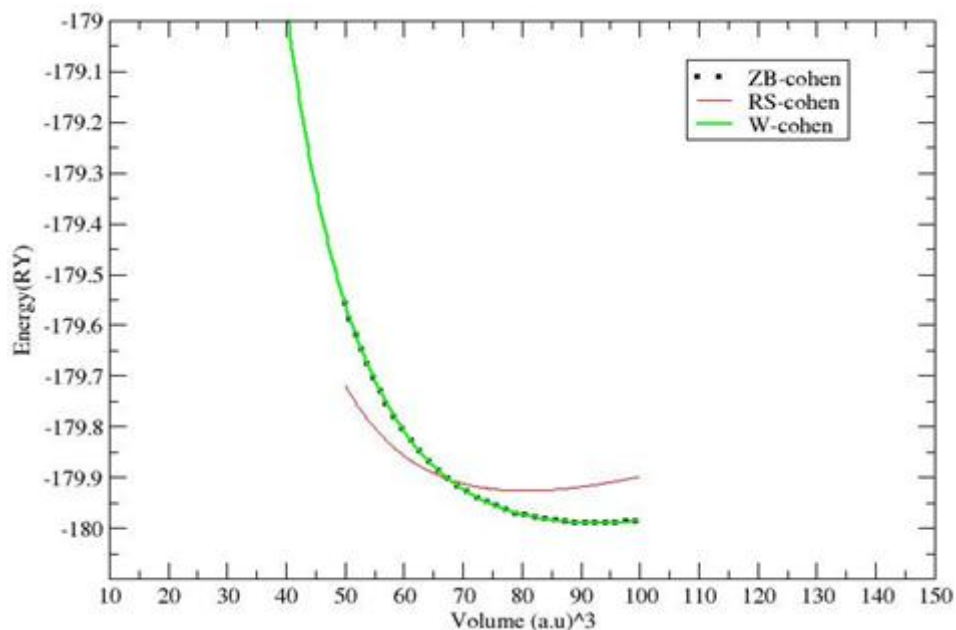
Table(5.14):Shows all the transition pressure and volume for BeO structures

structure	method	Pt(GPa)		$V_t(\text{a.u.})^3$	
		present cal.	other cal. ^b	present cal.	other cal. ^b
W-RS	LDA	90.3	93.8	69.6	69.98
	GGA	93.65	95.4	72.9	70.2
	Wu-Cohen	118.2		70.7	
ZB-RS	LDA	133.96	126.5	71.17	70.04
	GGA	146.47	147.1	70.6	69.74
	Wu-Cohen	140.45		71.69	

(a) reference[93]

Using a Fortran program called polyfit and the graphic program called grace we get all the figures in this study. Figures (5.10) and (5.11) shows that the green curve (wurtzite structure) is the basic one and the other curves (for ZB & RS structures) lay over it, and this mean that the wurtzite structure is the ground state for BeO and it crystallizes in wurtzite at room temperature, also the table(5.11) shows that it has minimum binding energy.

**Figure(5.10)** Total energy vs. volume for W,ZB & RS of BeO by LDA method



Figure(5.11) Total energy vs. volume for W,ZB and RS of BeO by Wu-Cohen method

Transition from W to ZB couldn't be calculated as shown in figure (5.12) and (5.13) since the curves laid over each other.

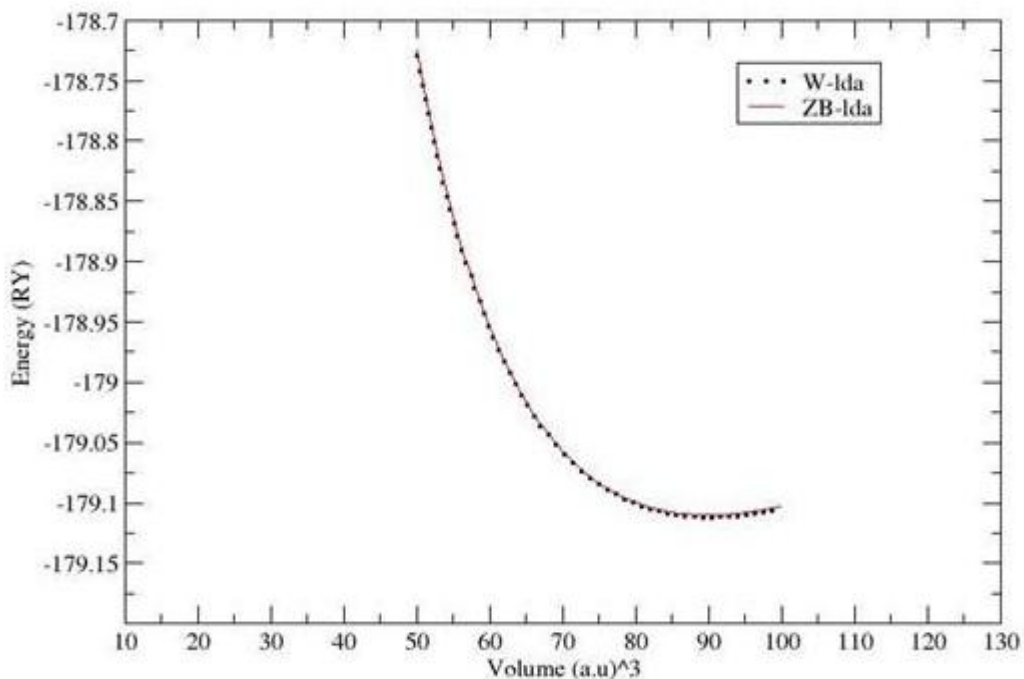
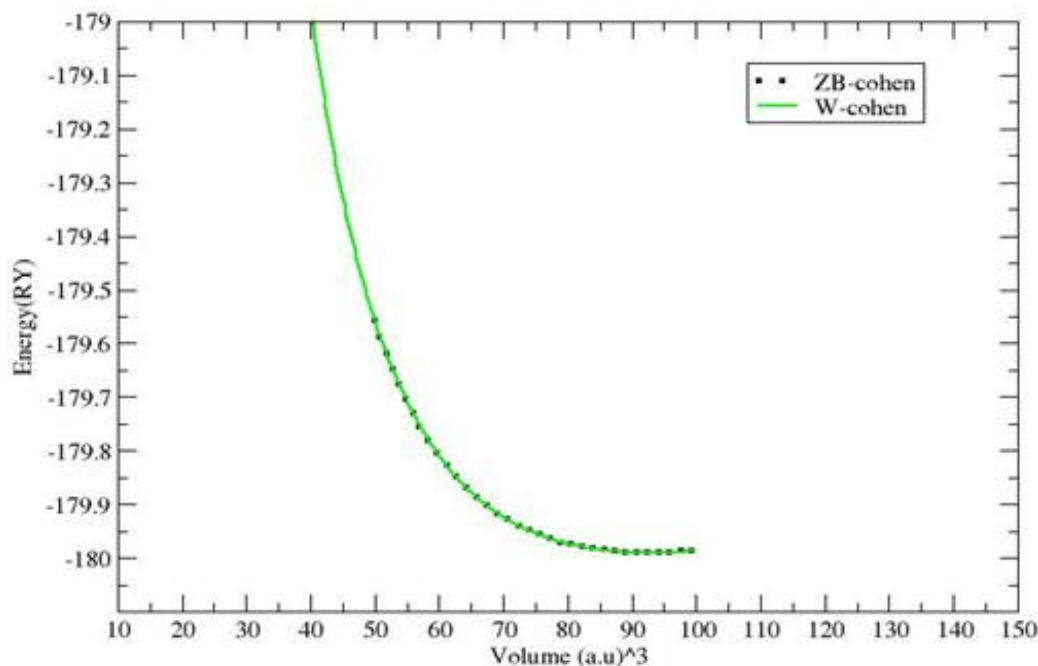


Figure (5.12) Total energy vs. volume for W and ZB of BeO by LDA method



Figure(5.13) Total energy vs. volume for W and ZB of BeO by Wu-Cohen method

5.2.1.6 Band structure

Using WIEN2K code which depends on FLAPW it was very easy to study the band structure and calculate the band gap for each structure of BeO compound, band gap is very important because by calculating it we can determine whether the compound is metal, semiconductor or insulator.

After the optimization job and calculating the structural parameters, we use the exact structural parameters to calculate the band structure, going to generate structure file and initialize calculation, then run SCF calculation and after that choose band structure form the task f the WIEN2K, edit the Fermi energy, run the spaghetti lapw and then plot the band structure to get a graph showing the nature of the band gap and the width of the bands for any structure as shown in figures(5.14),(5.15),(5.16) and(5.17).

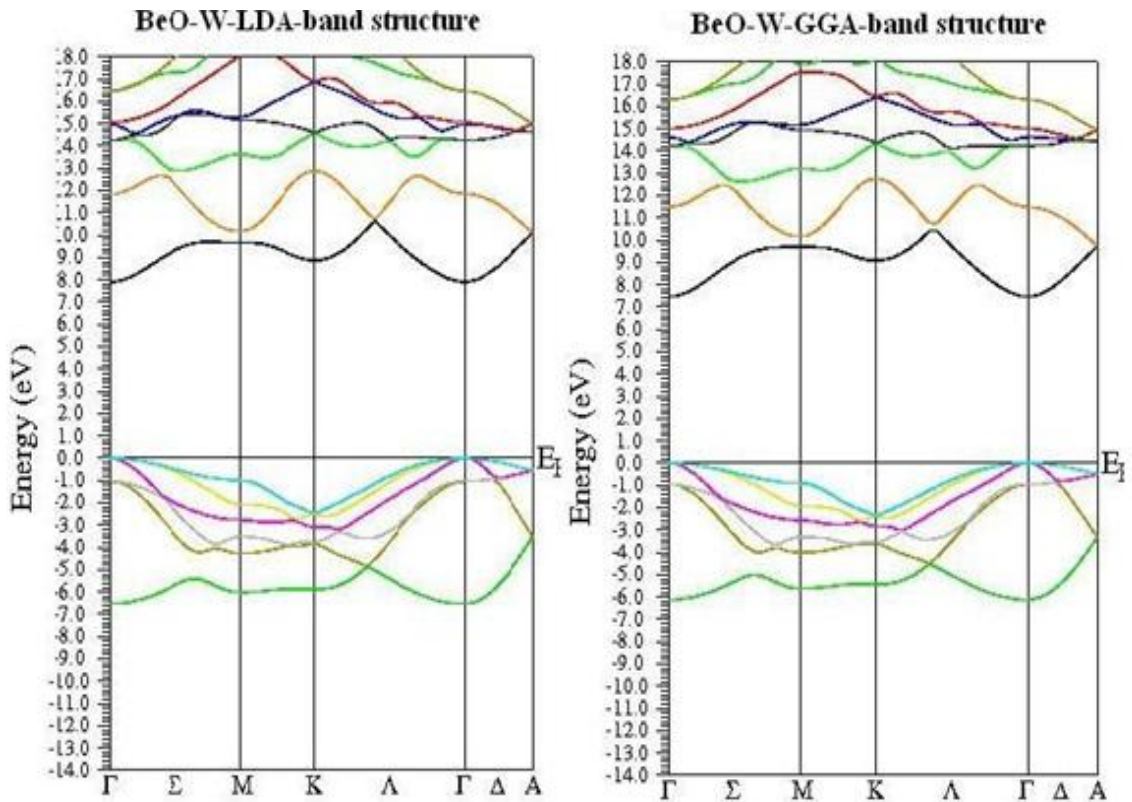
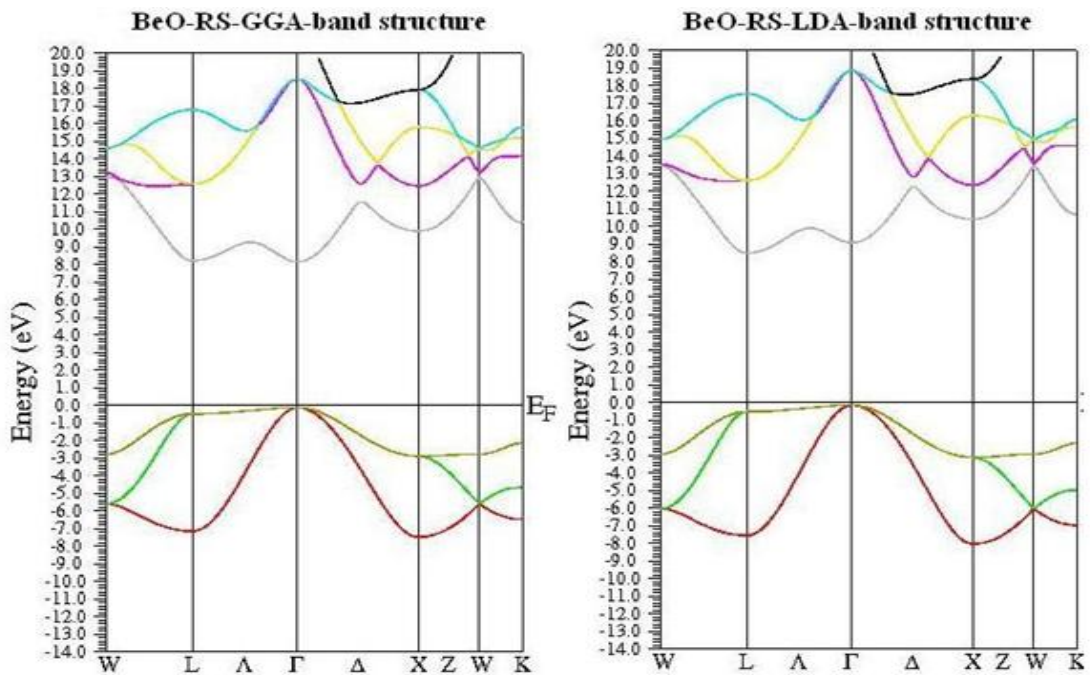


Figure (5.14) The band structure for wurtzite by LDA and GGA methods



Figure(5.15) The band structure for rocksalt by LDA and GGA methods

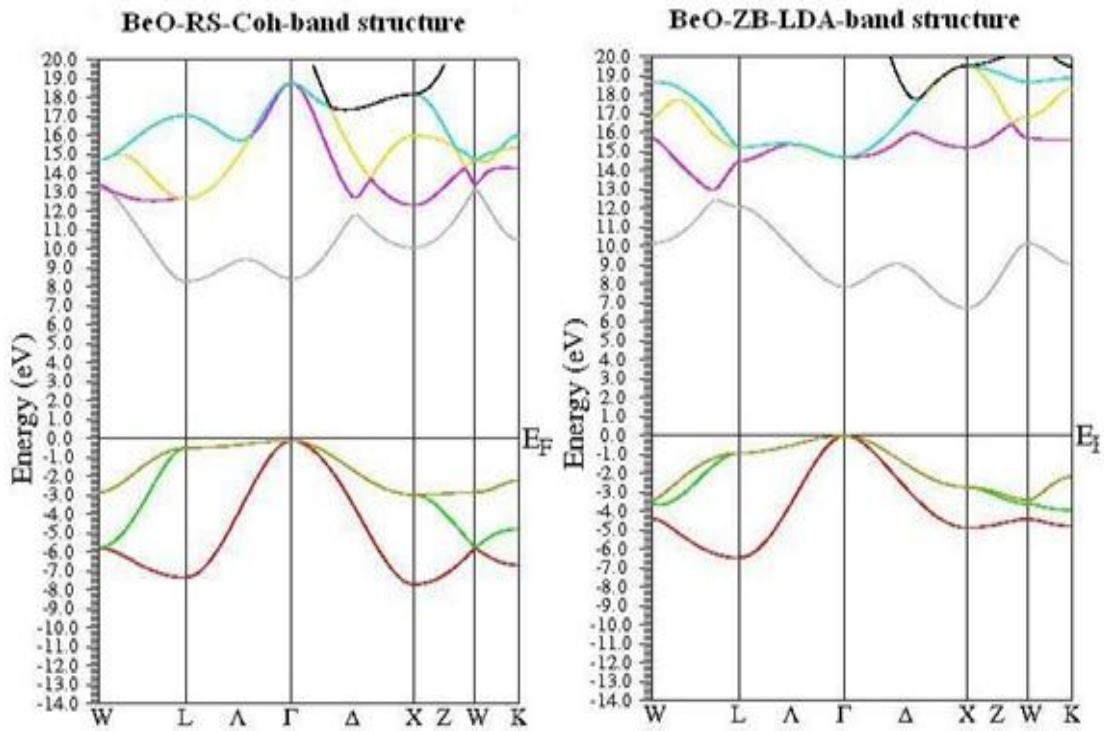


Figure (5.16) The band structure for RS by Wu-Cohen and ZB by LDA methods

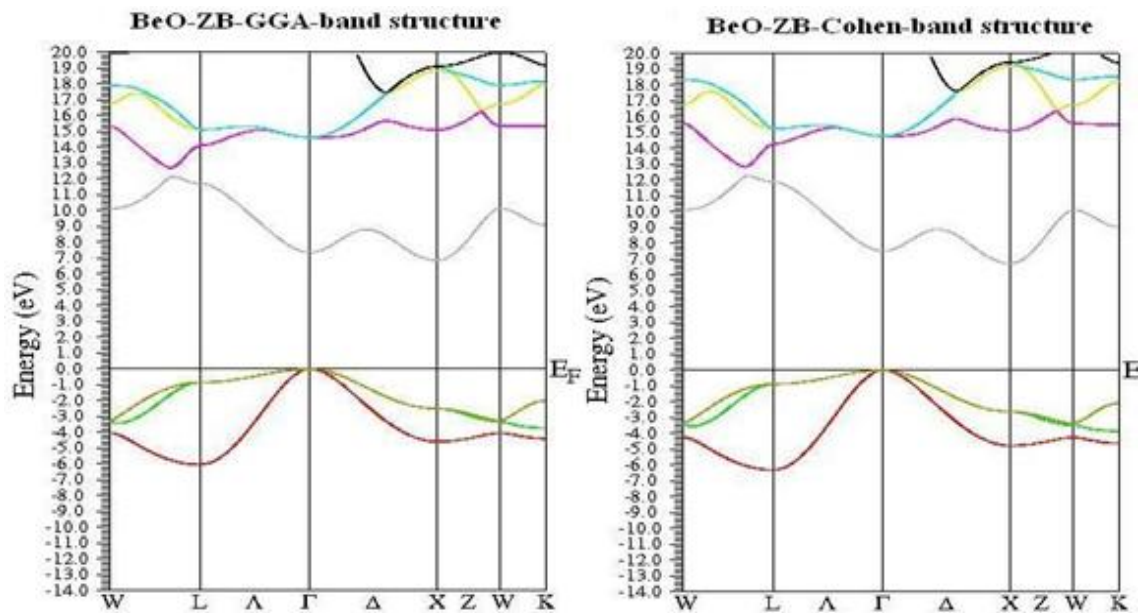


Figure (5.17) The band structure for ZB by GGA and Cohen methods

Browsing the spaghetti it will be very easy to calculate the band gap for each structure, the energy band gap for wurtzite was found to be 7.74 eV

for the LDA calculations, 7.211eV for GGA and 7.45eV for Cohen calculations corresponds to indirect transition at the Γ point. For zinc-blende, the energy band gap was found to be 6.736eV for LDA , 6.854ev for GGA and 6.747eV for Cohen calculations corresponding for indirect transition at the Γ point. Finally for the rocksalt, the energy band gap was found to be 8.36eV for LDA, 8.047eV for GGA and 8.177eV for Cohen calculations corresponding also to indirect transition at the Γ point.

Table(5.15): The band gap for BeO compound (*b*) reference[93]

Structure	method	present cal.	other cal. ^b	experimental result
Wurtzite (W)	LDA	8.356	8.05	7-10eV
	GGA	8.047		
	Cohen	8.177		
rocksalt (RS)	LDA	6.736	6.88	
	GGA	6.854		
	Cohen	6.747		
Zincblende (ZB)	LDA	7.75	7.54	
	GGA	7.211		
	Cohen	7.45		

5.3 ZnO compound

For this compound the same procedures have been done as for the compound (BeO), the lattice constant for each structure of this compound which (RS, ZB, CsCl, and W), the transition pressure from phase to phase and the energy band gap for each structure have been calculated to determine whether this compound is a metal, semi-metal, semiconductor or insulator by the LDA, GGA, and Wu-Cohen approximations. As done before I found the suitable number of K-points by, suitable Rkmax by test, for LDA Rkmax found to be 8, for GGA and Wu-Cohen it was found to be 9, and the suitable k-point = 9261 with reduced $k_{\text{point}} = 286$ and matrix = $21 \times 21 \times 21$ for RS, ZB, and CsCl while for W $K_{\text{point}} = 6000$ with reduced $k = 624$ and matrix = $22 \times 22 \times 12$.

5.3.1 Optimization

The same procedures are used for BeO will be used here for ZnO, we are going to find best u , c/a and lattice parameter a and c for wurtzite, zinc-blende, rock-salt and cesium-chloride structures. In this study, $R_{\text{mt}} = 1.77 \text{ a.u.}$ for Zn and 1.59 a.u. for O, $R_{\text{kmax}} = 8$ for LDA and 9 for GGA and Wu-Cohen, $G_{\text{max}} = 14$ for LDA, 16 for GGA and Wu-Cohen in all structures.

5.3.1.1 Wurtzite Structure

For this structure u was found to be 0.38 by LDA, 0.382 by GGA and 0.379 by Wu-Cohen method, table(16) shows the structural parameters, optimized volume, bulk modulus and minimum energy for this structure.

Table(5.16): The structural parameters for W structure. (c) reference[94]

method	a=b (A)		c/a	$V_0 \text{ (A.)}^3$	B (GPa)		B'		Emin (RY)
	found	other			Found	Others ^c	found	Others ^c	
LDA	3.18	3.29	1.63	307.1138	164.4	162	4.9971	5.01	-7473.166345
GGA	3.28		1.618	333.7014	128.66		4.4818		-7485.627888
Cohen	3.22		1.631	318.9665	146.294		4.6725		-7483.379513

5.3.1.2 Zinc-blende Structure

Table(17) shows the lattice parameters, optimized volume, bulk and minimum energy also other calculations for this structure.

Table(5.17):Structural parameters for ZB structure. (c) reference[94]

method	a=b=c (A)		V_0 (A.) ³	B (GPa)		B'	Emin (RY)
	present	other ^c		present	other ^c	present	
LDA	4.496	4.614	153.334	164.581	170.4	4.9376	-3736.5824
GGA	4.624		166.848	128.751		4.8165	-3742.8143
Cohen	4.554		159.37	147.193		4.8773	-3741.6894

5.3.1.3 Rock-salt Structure

Table(18) shows the lattice parameters, optimized volume, bulk and minimum energy also other calculations for this structure.

Table(5.18):Structural parameters for RS structure. (c) reference[94], (d) reference[95]

method	a=b=c (A)		V_0 (A.) ³	B (GPa)		B'	Emin (RY)
	Present	other ^c		Present	other ^d	present	
LDA	4.2136	4.28	126.218	202.561	260	4.5846	-3736.5681
GGA	4.3372		137.648	159.946		4.2612	-3742.7939
Cohen	4.269		131.267	182.229		4.5458	-3741.6743

5.3.1.4 Cesium-chloride Structure

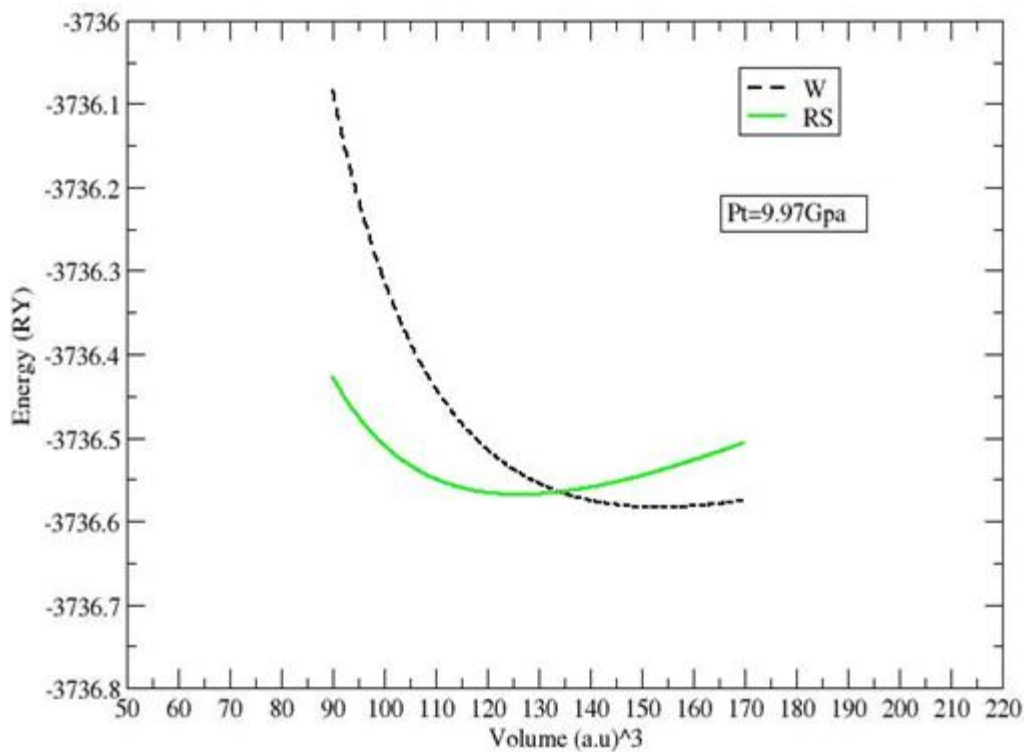
Table(5.19) shows the lattice parameters, optimized volume, bulk and minimum energy also other calculations for this structure

Table(5.19): Structural parameters for CsCl structure. (d)reference[95]

method	a=b=c (A)		V_0 (A.) ³	B (GPa)		B'	Emin (RY)
	Present	other ^c		Present	other ^d	present	
LDA	4.147	4.21	120.333	195.9	185.6	4.4771	-3736.4811
GGA	4.2653		129.198	127.5		3.5696	-3742.7073
Cohen	4.1997		124.978	176.5		4.8572	-3741.589

5.3.2 Transition phases

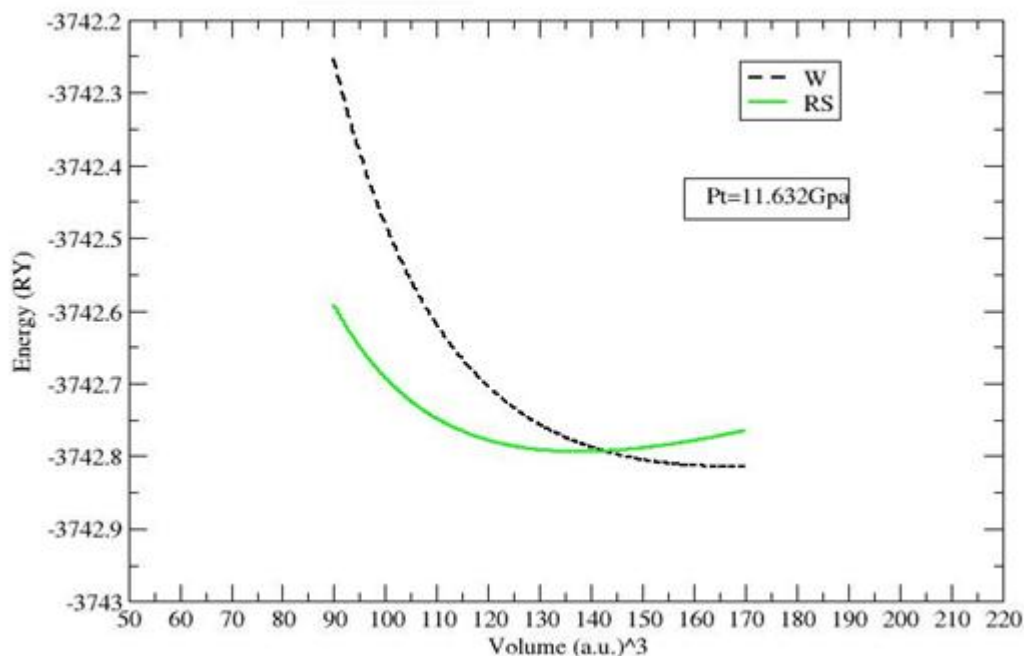
Figure(5.18) shows the EOS for both WZ & RS structures using LDA method. The transition pressure was found to be 9.97GPa and the transition volume was found to be 148.85a.u.(22.06Å)



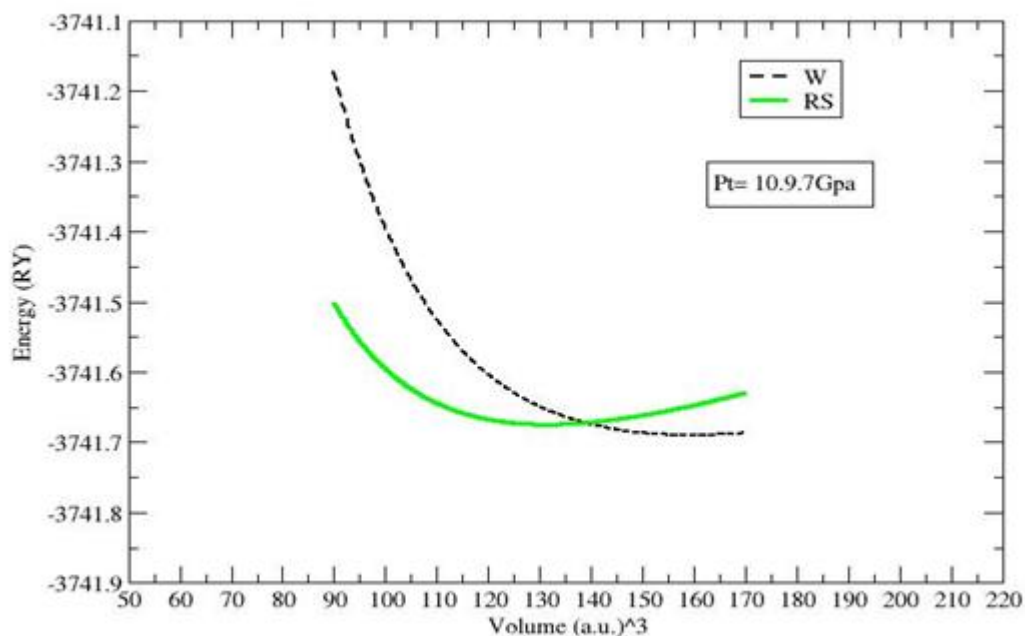
Figure(5.18) Total energy vs. volume for W,RS of ZnO by LDA method

Fig(5.19) shows EOS for both WZ & RS structures using GGA method. The transition pressure was found to be 11.632 GPa and the transition volume was found to be $152.1(\text{a.u.})^3=(22.54\text{\AA}^3)$.

Fig(5.20) shows EOS for both WZ & RS structures using Wu-Cohen method. The transition pressure was found to be 10.97 GPa and the transition volume was found to be $152.054(\text{a.u.})^3=(22.53\text{\AA}^3)$.



Figure(5.19) Total energy vs. volume for W,RS of ZnO by GGA method



Figure(5.20) Total energy vs. volume for W,RS of ZnO by Wu-Cohen method

Fig(5.21) shows EO'S for both W & CsCl structures using LDA method. The transition pressure was found to be 54.87Gpa and the transition volume was found to be $131.89(\text{a.u.})^3 = (19.54\text{\AA})^3$

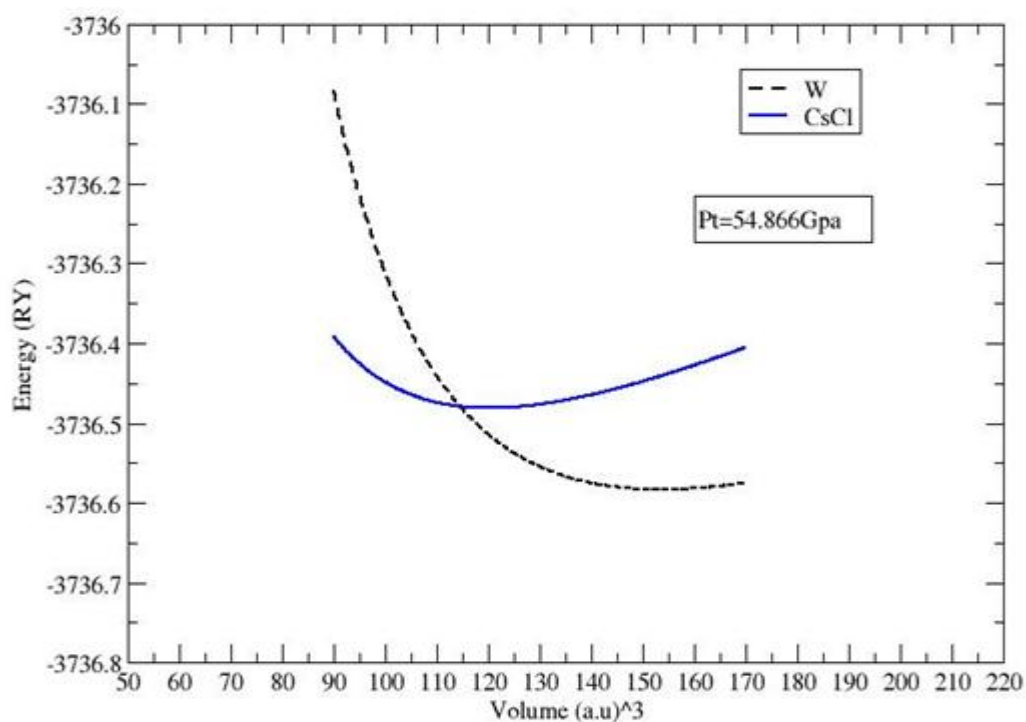


Figure (5.21) Total energy vs. volume for W, CsCl of ZnO by LDA method.

Figure (5.22) shows EO'S for both WZ & CsCl structures using GGA method. The transition pressure was found to be 52.63 GPa and the transition volume was found to be $134.641(\text{a.u.})^3 = (19.95\text{\AA})^3$.

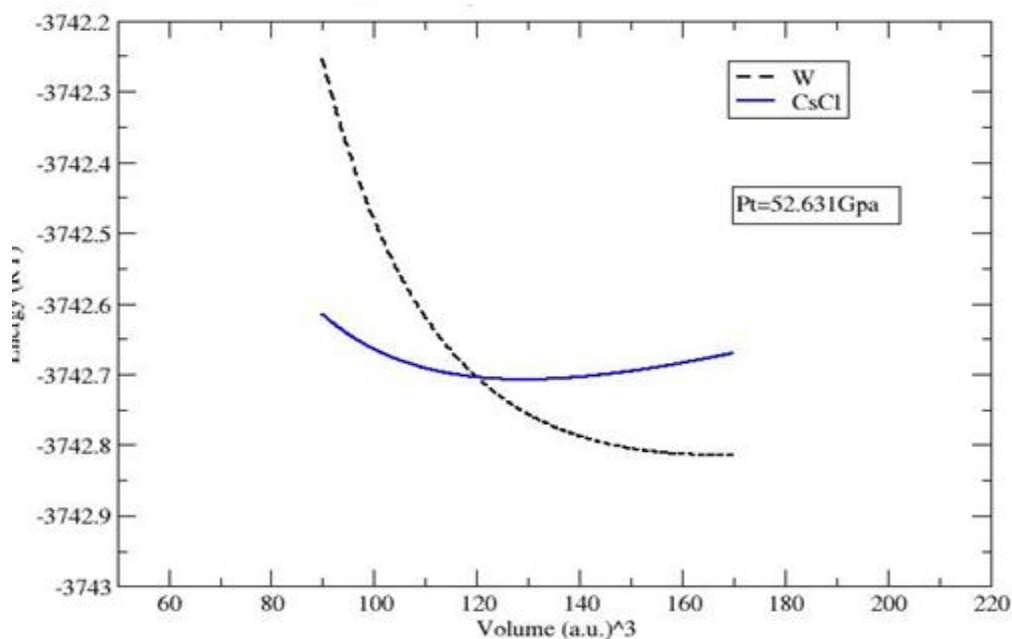


Figure (5.22) Total energy vs. volume for W, CsCl of ZnO by GGA method

Figure (5.23) shows EOS for both WZ & CsCl structures using Wu-Cohen method. The transition pressure was found to be 53.26 GPa and the transition volume was found to be $128.55(\text{a.u.})^3=(19.04\text{Å}^3)$

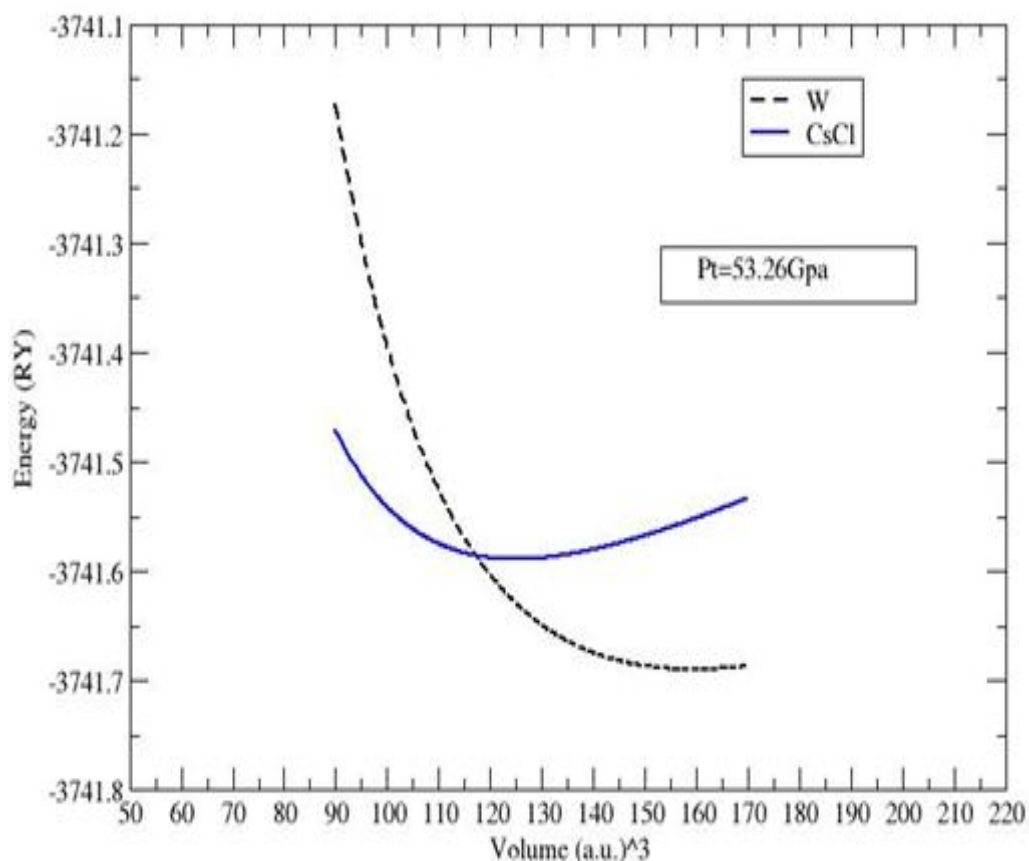


Figure (5.23) Total energy vs. volume for W, CsCl of ZnO by Wu-Cohen method

Figures (5.24),(5.25)and (5.26) shows EOS for both ZB & RS structures using LDA, GGA and Wu-Cohen methods. The transition pressure was found to be 13.07 GPa, 10.898 GPa and 5.72 GPa and the transition volume was found to be $150.59(\text{a.u.})^3=(22.31\text{Å}^3)$, $158.37(\text{a.u.})^3=(23.47\text{Å}^3)$ and $151.18(\text{a.u.})^3=(22.4\text{Å}^3)$ respectively.

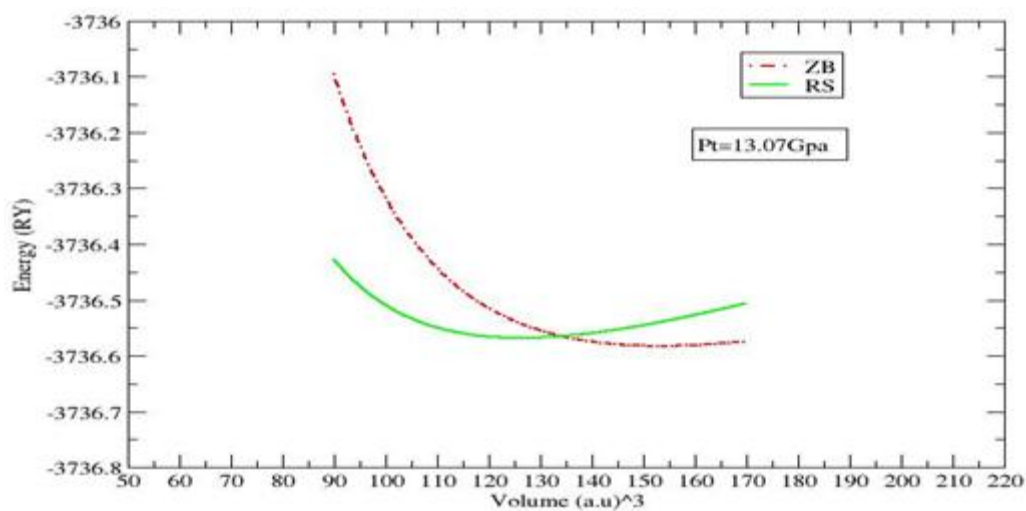


Figure (5.24) Total energy vs. volume for ZB, RS of ZnO by LDA method

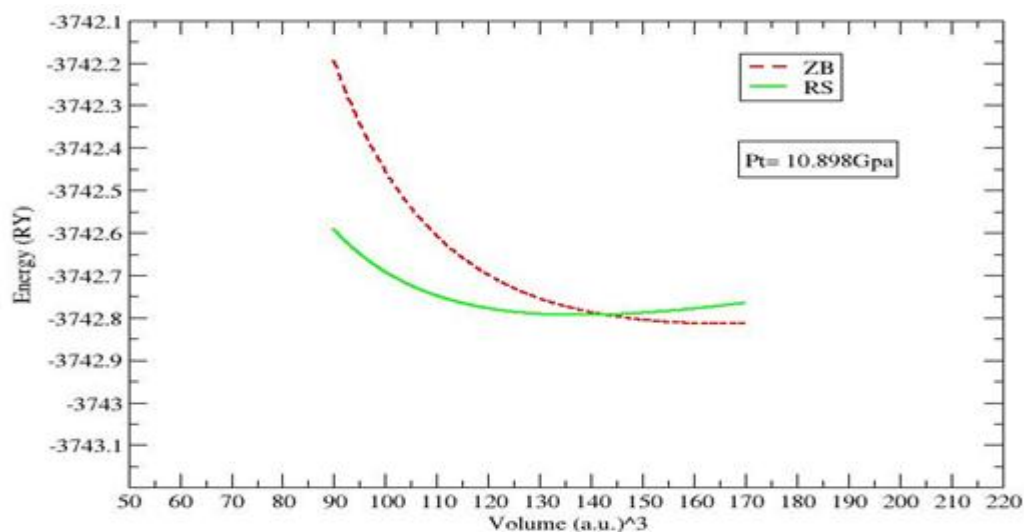


Figure (5.25) Total energy vs. volume for ZB, RS of ZnO by GGA method

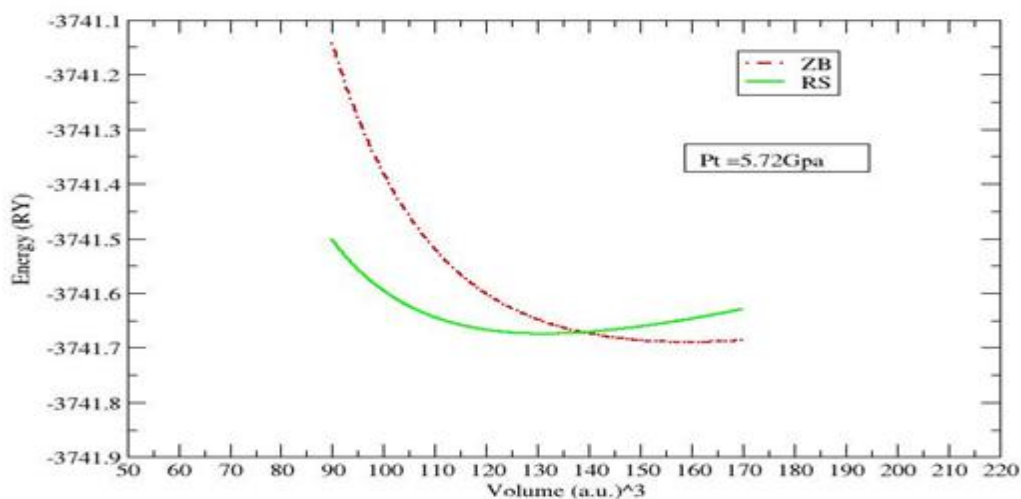


Figure (5.26) Total energy vs. volume for ZB, RS of ZnO by Wu-Cohen method

Figures (5.27), (5.28) and (5.29) shows the EO'S for both ZB & CsCl structures using LDA, GGA and Wu-Cohen methods. The transition pressure was found to be 51.96 GPa, 44.04GPa and 48.85 GPa respectively, where the transition volume was found to be $132.76(\text{a.u.})^3=(19.67\text{\AA}^3)$, $137.47(\text{a.u.})^3=(20.37\text{\AA}^3)$ and $33.34(\text{a.u.})^3=(19.76\text{\AA}^3)$.

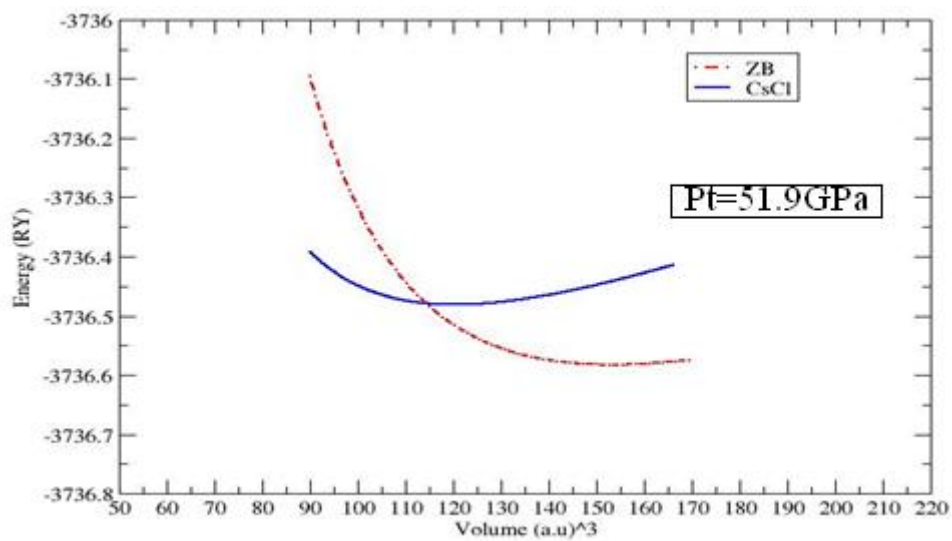


Figure (5.27) Total energy vs. volume for ZB, CsCl of ZnO by LDA method.

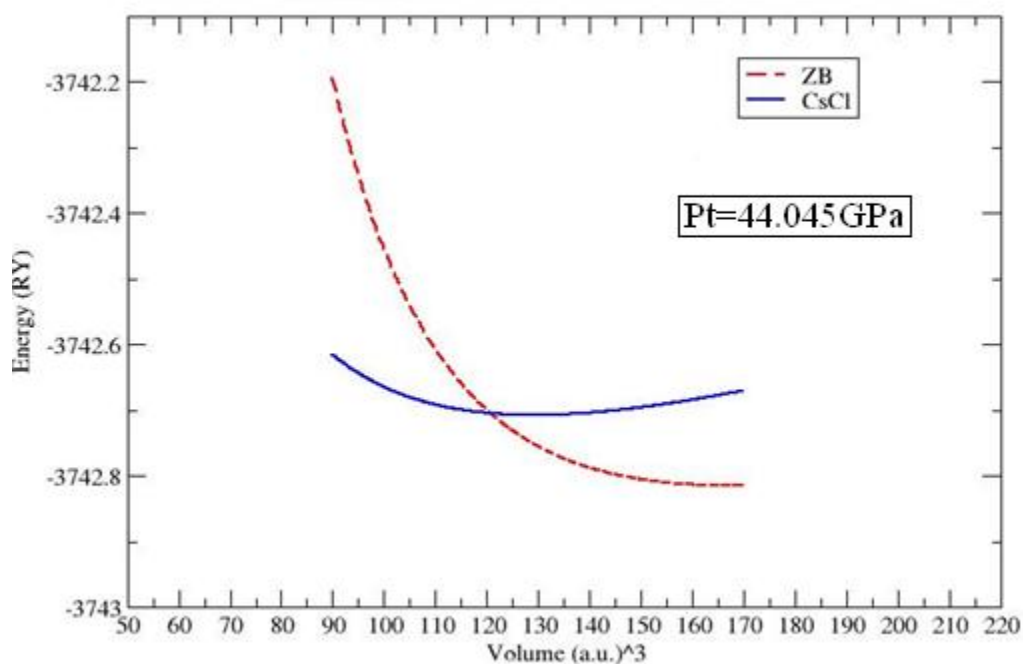


Figure (5.28) Total energy vs. volume for ZB, CsCl of ZnO by GGA method.

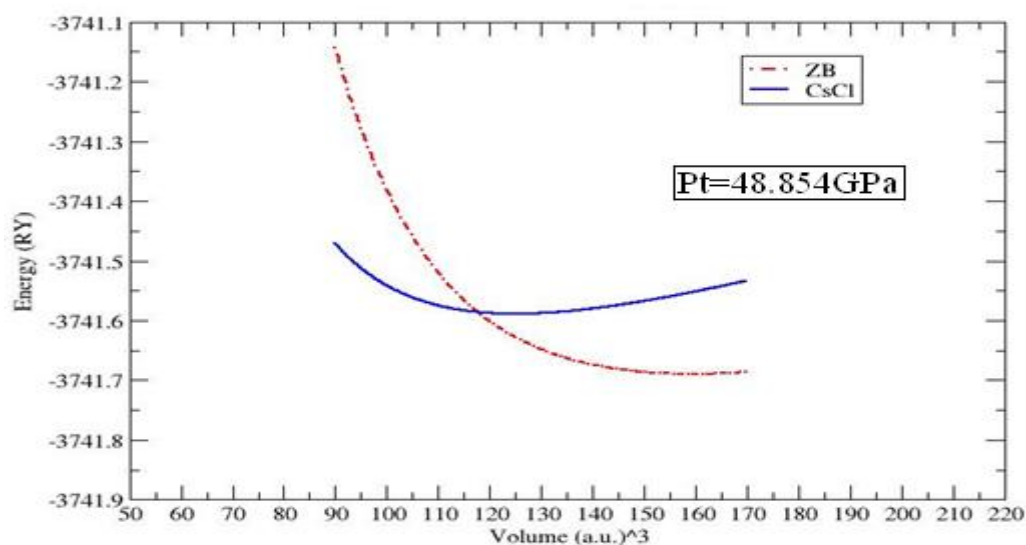


Figure (5.29) Total energy vs. volume for ZB, CsCl of ZnO by Wu-Cohen method.

The last phase transition from RS to CsCl structures as shown in figures(5.30), (5.31) and (5.32) using LDA, GGA and Wu-Cohen methods. The transition pressure was found to be 137.86Gpa, 117.37Gpa and 191.15Gpa respectively, where the transition volume was found to be $86.89(\text{a.u.})^3=(12.87\text{\AA}^3)$, $95.896(\text{a.u.})^3=(14.2\text{\AA}^3)$ and $91.13(\text{a.u.})^3=(13.5\text{\AA}^3)$ respectively.

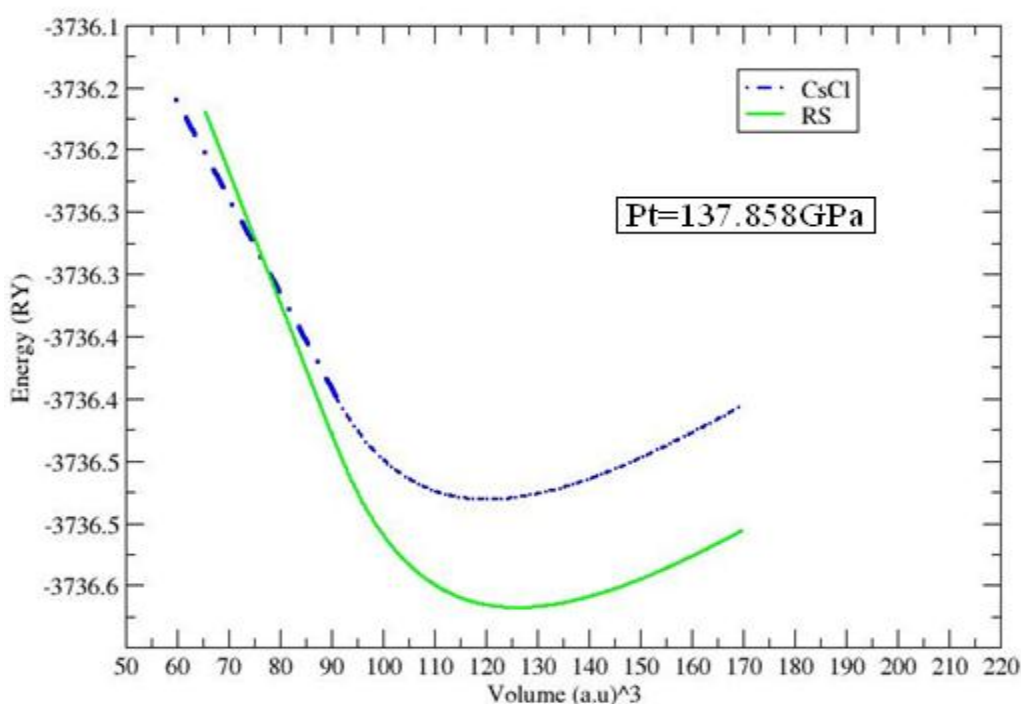


Figure (5.30) Total energy vs. volume for RS, CsCl of ZnO by LDA method.

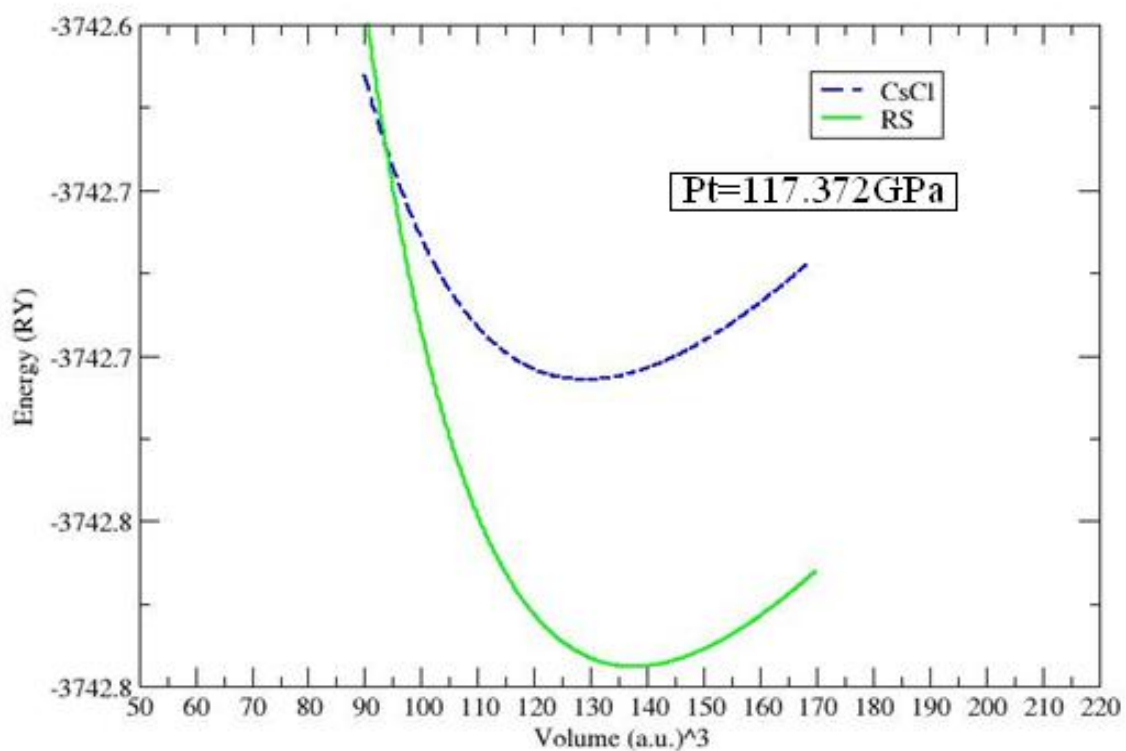


Figure (5.31) Total energy vs. volume for RS, CsCl of ZnO by GGA method.

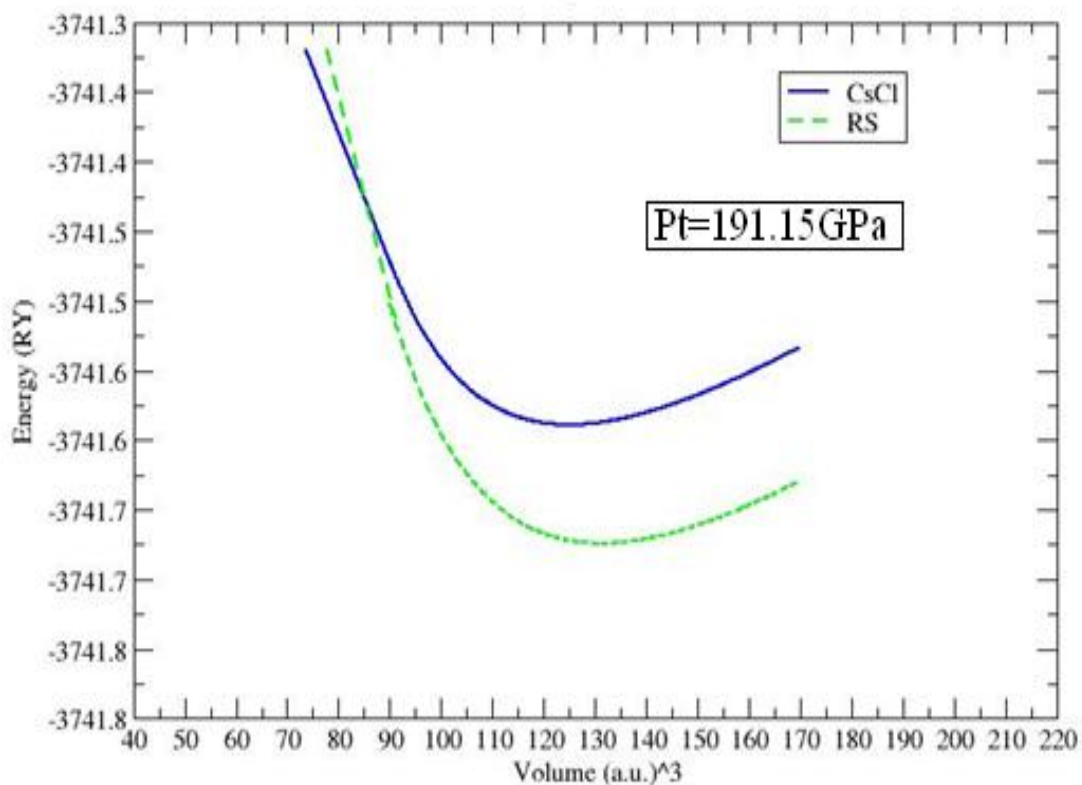


Figure (5.32) Total energy vs. volume for RS, CsCl of ZnO by Wu-Cohen method.

Table(5.20): shows the transition pressure & volume for all phases

Structure	Method	Pt (GPa)		Vt(A ³)	
		present	Other ^d	present	Other ^c
W-RS	LDA	9.97	9.5	22.06	22.8
	GGA	11.632		22.54	
	Cohen	10.97		22.53	
W-CsCl	LDA	54.87	51.4	19.54	20.5
	GGA	52.63		19.95	
	Cohen	53.26		19.04	
ZB-RS	LDA	13.07	14.05	22.31	22.03
	GGA	10.898		23.47	
	Cohen	5.72		22.4	
ZB-CsCl	LDA	51.96	50.3	19.67	21.092
	GGA	44.04		20.37	
	Cohen	48.85		19.76	
RS-CsCl	LDA	137.86	154.7	12.87	18.2
	GGA	117.37		14.2	
	Cohen	191.15		13.5	

(a) reference[94], (d) reference[95]

Figure (5.33), figure (5. 34) and fig(5.35) show the four structure together on laid on one graph using LDA, GGA and Wu-Cohen methods . These graphs also show that the ZnO compound can be found in WZ structure at ground state and no transition from WZ to ZB could be calculated, also the graphs show that the wurtzite structure is the ground state.

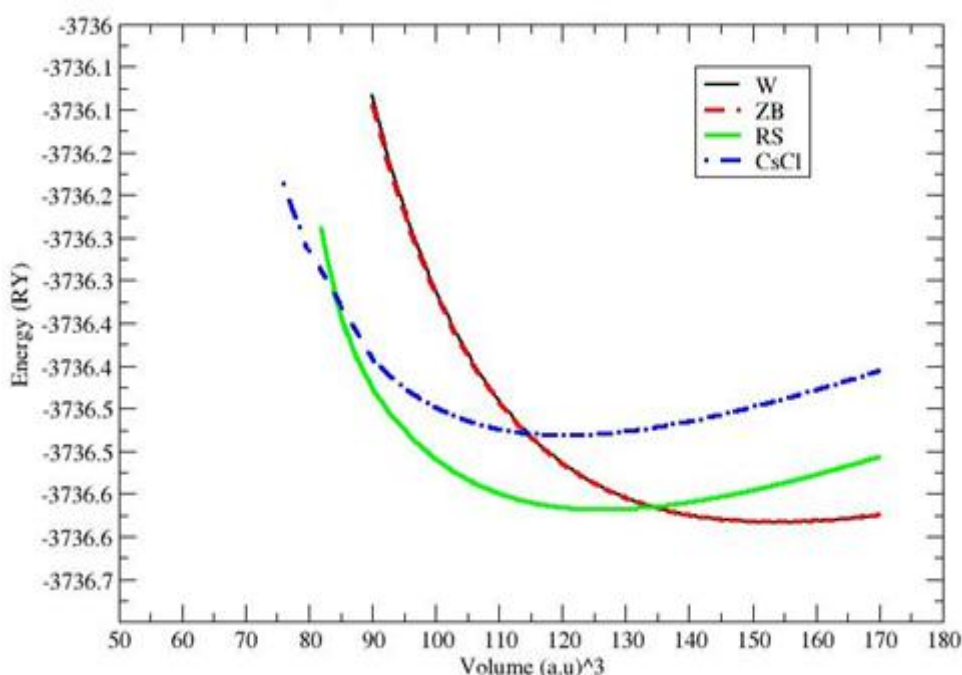
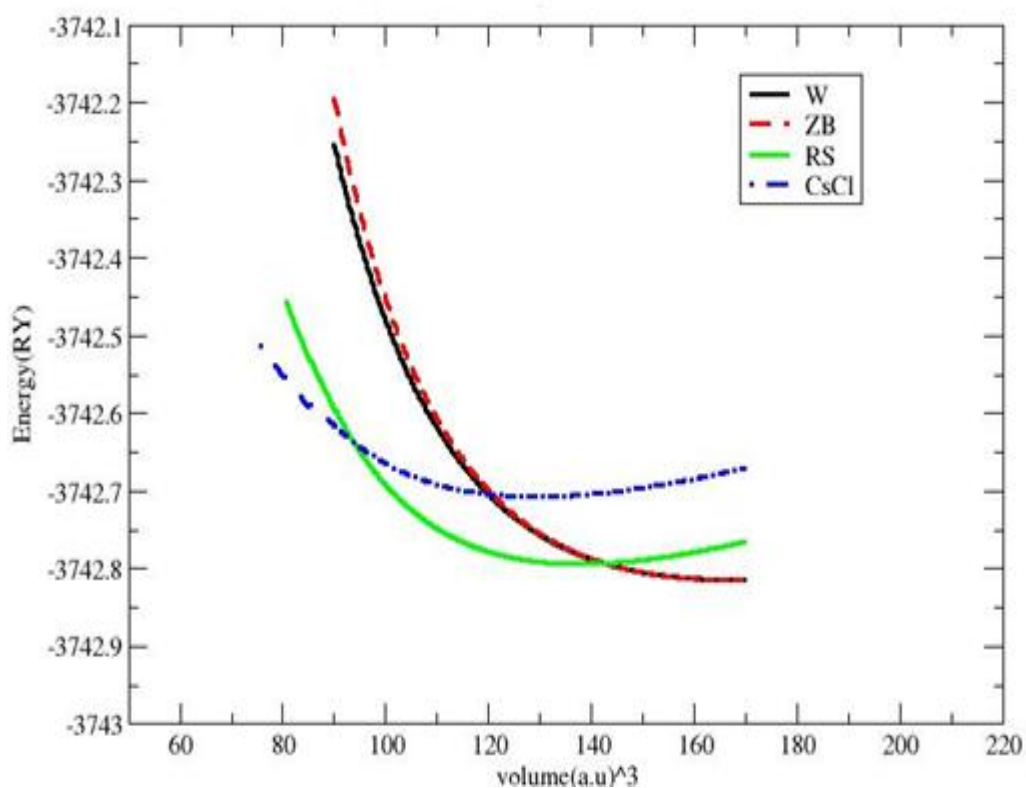
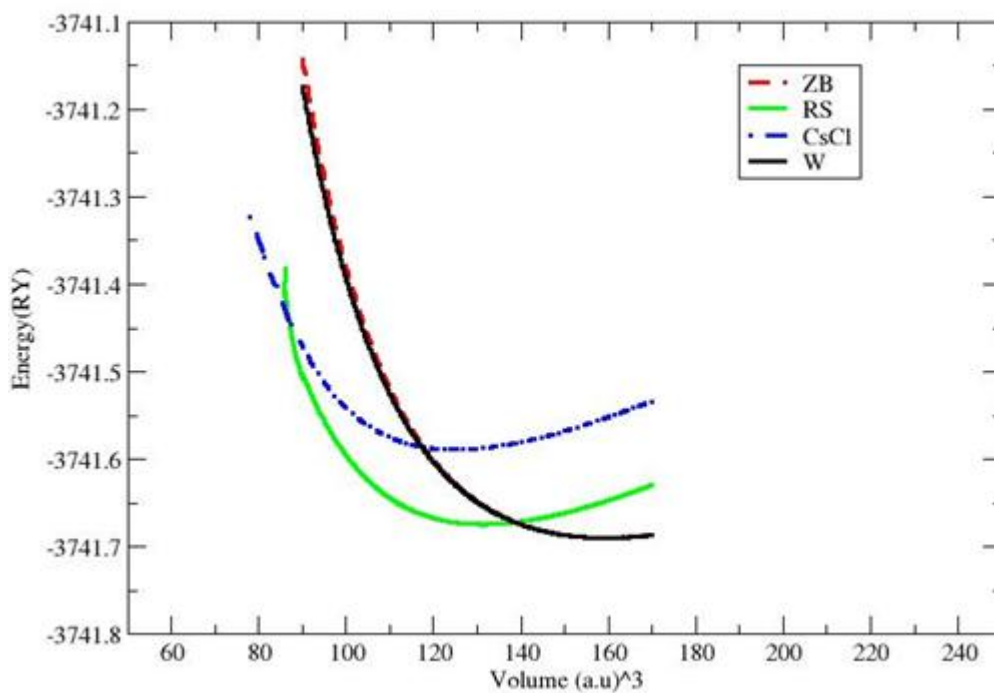


Figure (5.33) Total energy vs. volume for W,ZB, RS and CsCl of ZnO by LDA method.



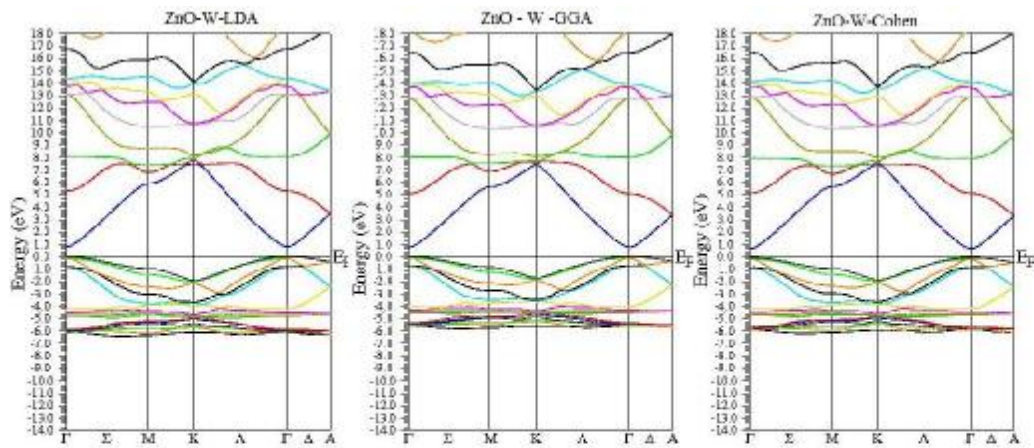
(5.34) Total energy vs. volume for W,ZB, RS and CsCl of ZnO by GGA method.



(5.35) Total energy vs. volume for W,ZB, RS and CsCl of ZnO by Wu-Cohen method.

5.3.3 Band structure

The same way was done for BeO compound will be done for ZnO where the energy gap was calculated for all structures using all methods (LDA, GGA and Wu-Cohen). Fig(36), fig(37), fig(38) and fig(39) show the energy band gap for WZ, ZB, RS and CsCl structure



Figure(5.36) ZnO band structure of W by LDA, GGA and Wu-Cohen method

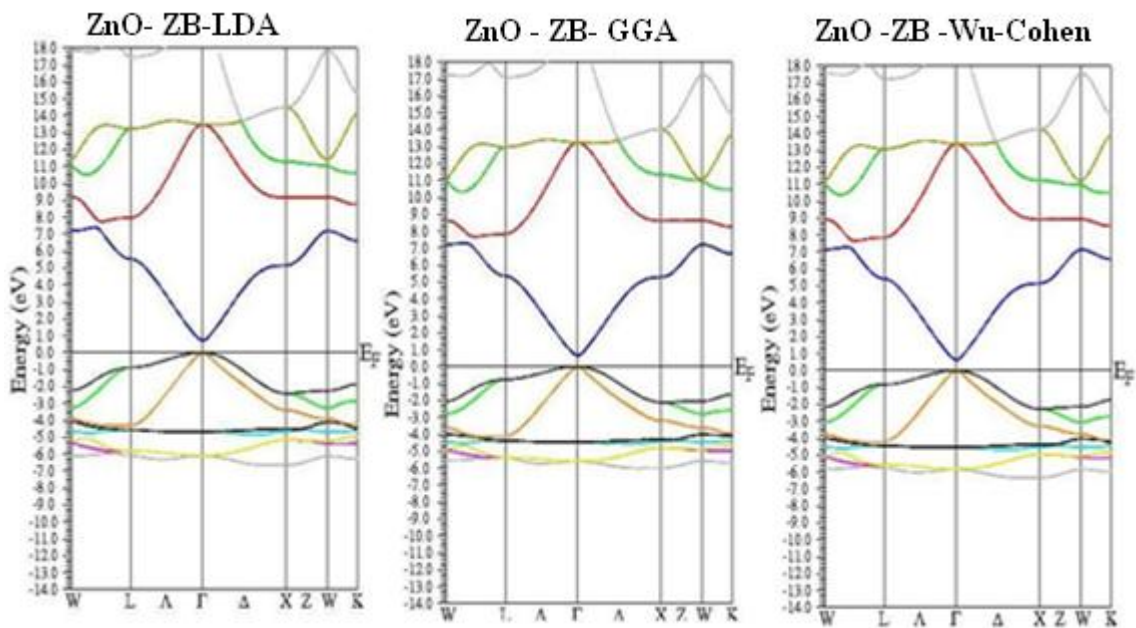


Figure (5.37) ZnO band structure of ZB by LDA, GGA and Wu-Cohen method

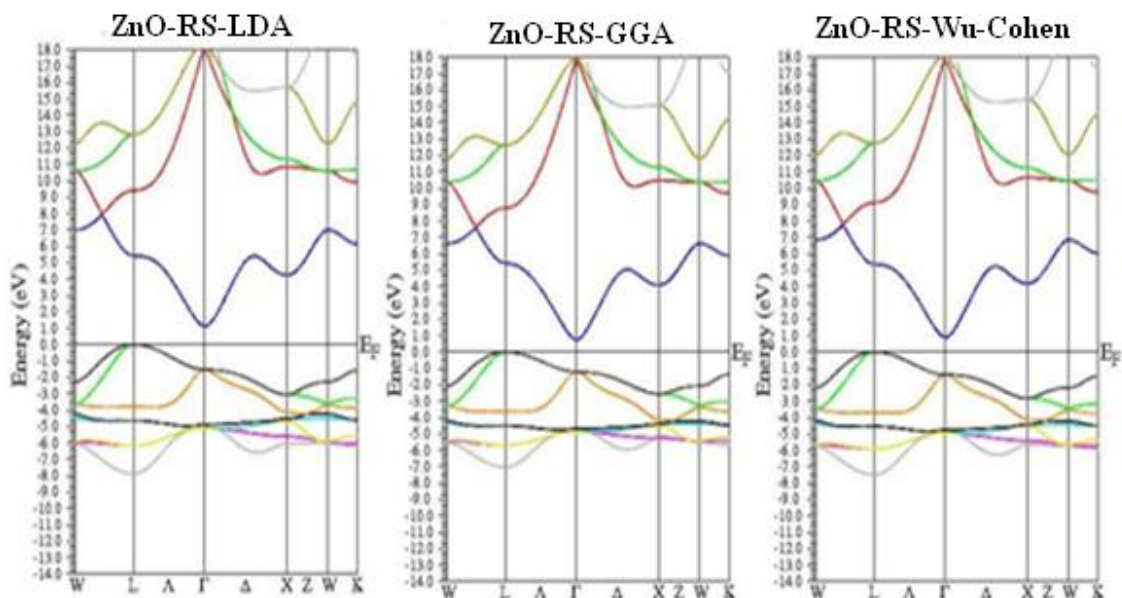


Figure (5.38) ZnO band structure of RS by LDA, GGA and Wu-Cohen method.

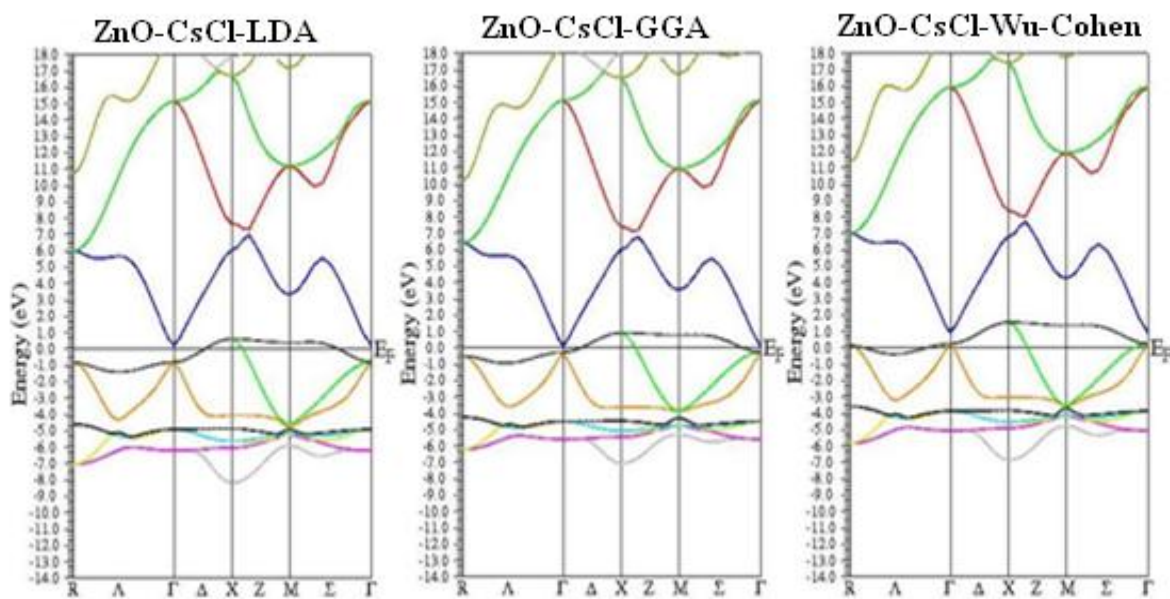


Figure (5.39) ZnO band structure of CsCl by LDA, GGA and Wu-Cohen method.

Figure (5.36) shows the energy band gap for W structure and it found to be 0.79659 eV by LDA, 0.75716eV by GGA and 0.69006 eV by Cohen calculations which correspond direct transition at Γ point. Figure (5.37) shows the energy band gap for ZB which found to be 0.71671eV by LDA, 0.65801eV by GGA and 0.61331eV by Wu-Cohen calculation which correspond to direct transition at Γ point too. Figure (5.38) shows the energy gap for RS and found to be 1.13737eV by LDA, 0.75755eV by GGA and 0.89867eV by Cohen calculations which correspond to indirect transition at Γ point. Fig(39) shows energy band gap for CsCl structure which is found to be 1.14287eV for LDA, 0.31864eV for GGA and 0.37643eV for Cohen calculations which correspond to direct transition at Γ point as shown in Table (5.21).

Table(5.21) The energy band gap for all ZnO structures.

Structure	Method	energy band gap(eV)	
		Present	Other ^e
WZ	LDA	0.79659	0.15 – 3.5
	GGA	0.75716	
	Cohen	0.69006	
ZB	LDA	0.71671	
	GGA	0.65801	
	Cohen	0.61331	
RS	LDA	1.13737	
	GGA	0.75755	
	Cohen	0.89867	
CsCl	LDA	1.14287	
	GGA	0.31864	
	Cohen	0.37643	

(e)reference[96]

5.4 Conclusion

The study of BeO and ZnO compounds shows the importance of these compounds, it gives a good understanding about the stability, electronic structure and phase transition of these two compounds.

In this study the Full-Potential Augmented plane Wave (FP-LAPW) method with LDA, GGA and Wu-Cohen approximations is used to investigate the structural properties and stability of the WZ, ZB, and RS phases of BeO compound and the WZ, ZB, RS, and CsCl phases for ZnO compound. FP-LAPW method is also used to calculate the equation of state (EOS's) of WZ, ZB, RS structures for both BeO and ZnO compounds where CsCl structure for ZnO compound. From these (EOS's) the lattice parameter a , the bulk modulus B , the pressure derivative B' , the equilibrium volume of the crystal v_0 and the transition pressure have been investigated. Also the energy band gap was calculated using the same method for all structures mentioned above. The main results and conclusion of this study can be summarized as follows:

- 1- The calculated structural parameters (a , B , B') using FP-LAPW method are found to be in good agreement with the available experimental data and other theoretical results.
- 2- The phase transition for BeO compound occur from WZ to RS and from ZB to RS. The transition pressure from WZ to RS was found to be 90.3, 93.65 , 118.2Gpa and the transition pressure from ZB to RS was found to be 133.96, 146.47, 140.45 GPa for LDA, GGA and Wu-Cohen approximations respectively.
- 3- For ZnO the phase transition occur from WZ to RS, from WZ to CsCl, from ZB to RS, from ZB to CsCl and from RS to CsCl, the transition pressure was found to be 9.97, 11.632, 10.97 GPa from WZ to RS, 54.87, 52.63, 53.26 GPa from WZ to CsCl, 13.07,

10.898, 5.72 GPa from ZB to RS, 51.96, 44.04, 48.85GPa from ZB to CsCl and 137.86, 117.37, 191.15GPa from RS to CsCl using LDA, GGA and Wu-Cohen approximations respectively.

- 4- The energy band gap for BeO compound was calculated for WZ, ZB and RS structures and found to be 7.75eV, 7.211eV, 7.45eV for WZ, 6.736eV, 6.854eV, 6.747eV for ZB and 8.356eV, 8.047eV, 8.177eV for RS using LDA, GGA and Wu-Cohen approximations respectively.
- 5- For ZnO compound the energy band gap was calculated for WZ, ZB, RS and CsCl structures and was found to be 0.797eV, 0.757eV, 0.69eV for WZ, 0.717eV, 0.66eV, 0.613eV for ZB, 1.14eV, 0.76eV, 0.9eV for RS and 1.43eV, 0.319eV, 0.376eV for CsCl structures using LDA, GGA, Wu-Cohen approximations respectively.
- 6- This study shows that BeO compound is insulator since it has a large band gap in all its phases (WZ, ZB, RS).
- 7- BeO compound can be found in WZ or ZB structures as a ground state and originally in WZ structure since this structure has a minimum binding energy and RS is unstable since it exists at high pressure.
- 8- ZnO behaves as semiconductor in the wurtzite and zinc-blende since it has a large energy gap in all their structures. For rock-salt it has energy band gap about 1.14eV, 0.76eV, 0.9 eV by LDA, GGA and Wu-Cohen approximations which lead to non-metallic behaviour. For CsCl structure the energy gap by LDA is 1.14eV which lead to non-metallic behaviour, while by GGA and Wu-Cohen approximations its about 0.3 eV which lead to metallic behaviour.

REFERENCES

- [1] Ves S. shawarz U. Christensen N. E., Syassen K., and Cardona M **Phys. Rev. B42**, 9113(1990) .
- [2] Nelmes R. J., McMahon m. I., Wright N. G. and Allan D.R. **Phys. Rev. Lett. 73, 1805**(1994).
- [3] San-Miguel A., Polian A., Gauthier M. and Itie J. P. **Phys. Rev. b48, 8683**(1993).
- [4] schröer P., kruger P. and Pollmann J. **Phys. Rev. B48, 18264** (1993).
- [5] Hasse M. A., Qui L., Depuydt J. M., Luo H., Samarath N. and Furdyana J. K. **Appl. Phys. Lett.59, 1273**, (1991).
- [6] Gaines J., drenten R., Haberen K. W., Marshall., Mensz P. M. and Petruzzello J. **Appl. Phys. lett. 62, 2462**.(1993).
- [7] Fuchs M., Bockstede M., Pehlke E. and Scheffler M. **Phys. Rev. B57, 2134** (1998).
- [8] V.E. Henrich and P. A. Cox, **The surface Science of Material Oxides** (Cambridge University Press, Cambridge, 1994).
- [9] V.E. Herick, **Rep. Prog. Phys. 48, 1481** (1985).
- [10] Björn baumeier, Peter Krüger, and johannes Pollmann **Phys. Rev. B 75, 045323** (2007)
- [11] Yingxiang Cai, Songtao Wu, Rui Xu, and Jie Yu. **Phys, Rev. B 73, 184104** (2006).
- [12] <http://www.azom.com/details.asp?ArticleID=263>
- [13] A.P. Jephcoat, R. J. Hemley, H. K. Mao, R. E. Cohen, and M. J. Mehl, **Phys. Rev. B 37, 4727**, (1988) .
- [14] J. C. Phillips, **Rev. Mod. Phys. 42, 317**, (1970) .
- [15] K.J. Chang, S. Froyen, and M. L. Cohen, **J. Phys. C 16, 3475** (1983)
- [16] P.E. Van Camp and V. E. Van Doren, **J. Phys.: Condens. Matter,**

- 3865**, (1996) .
- [17] J. C. Boettger and J. M. Wills, **Phys. Rev. B** **54**, **8965**, (1996).
- [18] C.-J. Park, S.-G. Lee, Y.-J. Ko, and K. J. Chang, **Phys. Rev. B** **59**,**13501**, (1999).
- [19] Y.Mori et. al., **AIRAPT Conf.**, **17**, **518** (1999).
- [20] C.L. Freeman, F. Claeysens, N. L. Allan, and J. H. Harding, **Phys. Rev. Lett.** **96**, **066102** (2006) .
- [21] P.B.Sorokin,A. S.Fedorov, and L. A. Chernozatonskii, **Phys. Solid State** **48**, **398** (2006) .
- [22] B. Soul de Bas, H. E. Dorsett, and M. J. Ford, **J. Phys. Chem.Solids** **64**, **495** (2003) .
- [23] http://www.wikipedia.org/wiki/Zinc_oxide#American_process
- [24]<http://www.zincoxide.unicore.com/Applications/>
- [25] H. Karzel, W. Portzel, M. Köfferlein, W. Schiessl, M. Steiner, U. Hiller, and G. M. Kalvius **Phys. Rev. B** **vol 53**, **N17**, (1996).
- [26] Manabu Usuda and Noriaki Hamada, **arXiv:cod-mat/0202308**, **V1**, (2002).
- [27] J.A. Sans, A.Segura ,F.J.Manjón , b.Mari ,A.Muñoz, M.J. Herrera-Cabrera, **Microelectronics jour.** **36** ,**928-932**, (2005).
- [28] L.Hedin, **Phys. Rev.** **139**, **A796**;L.Hedin and S.lundqvist,in **Solid State Physics**,edited by F.Seitz,and D.Turnbull, and H.Ehreneich, Vol. 23, p.1,(1969).
- [29] F. Aryasetiawan in **Strong Coulomb Correlations in Electronic structure Calculation**, edited by V.I.Anisimov,(2000).
- [30] T. Takeda and J.kübler, **J. Phys. F** **9**,**661** (1976).
- [31] K. Schwarz, P. Balaha, G. K. H. Madsen, **Computer Phys. Communications** **147**, **71-76** (2002) .
- [32] Ph. Kurz and F. Forster, **Phys. Rev. B** **69**, **024415** (2004).

- [33] R. O. Jones and O. Gunnarsson, **Rev. Mod. Phys.** **61**, **689** (1989).
- [34] D. R. Hartree, Proc. Cambridge **Philos. Soc.** **24**, **89** (1928).
- [35] J. C. Slater, **Phys. Rev.** **35**, **210** (1930).
- [36] V. Fock, **Z. Phys.** **61**, **126** (1930).
- [36] C. Coulson, **Rev. Mod. Phys.** **32**, **170** (1960).
- [37] L. H. Thomas, Proc. **Cambridge Philos. Soc.** **23**, **542** (1927).
- [38] E. Fermi, **Z. Phys.** **48**, **73** (1928).
- [39] E. H. Lieb, **Rev. Mod. Phys.** **48**, **553** (1976).
- [40] P. A. M. Dirac, Proc. **Cambridge Philos. Soc.** **26**, **376** (1930).
- [41] J. C. Slater, **Phys. Rev.** **81**, **385** (1951), *ibid.* **82**, **538** (1951).
- [42] R. Gáspár, **Acta. Phys. Hung.** **3**, **263** (1954).
- [43] P. Hohenberg and W. Kohn, **Phys. Rev.** **136**, **B864** (1964).
- [44] M. Levy, Proc. Nat. **Acad. Sci. USA** **76**, **6062** (1979).
- [45] W. Kohn and L. J. Sham, **Phys. Rev.** **140**, **A1133** (1965).
- [46] J. P. Perdew, J. Tao, V. N. Staroverov, and G. E. Scuseria, J. **Chem. Phys.** **120**, **6898** (2004)
- [47] T. Kato, **Comm. Pure. Appl. Math.** **10**, **151**. The cusp condition applies to systems with Coulomb interactions, (1957).
- [48] E. H. Lieb and B. Simon, **Phys. Rev. Lett.** **31**, **681** (1973).
- [49] O. Gunnarsson and H. Hjelmberg, **Phys. Scr.** **11**, **97** (1975).
- [50] O. Gunnarsson and B. I. Lundqvist, **Phys. Rev. B** **13**, **4274** (1976).
- [51] M. Levy and J. P. Perdew, **Phys. Rev. A** **32**, **2010** (1985).
- [52] U. von Barth and L. Hedin, **J. Phys. C: Solid State Phys.** **5**, **1629** (1972).
- [53] E. H. Lieb, **Int. J. Quantum Chem.** **24**, **243** (1983).
- [54] K. Capelle and G. Vignale, **Phys. Rev. Lett.** **86**, **5546** (2000).
- [55] H. Eschrig and W. E. Pickett, **Solid State Commun.** **118**, **123** (2001).

- [56] W. Kohn, A. Savin, and C. A. Ullrich, *Int. J. Quantum Chem.* **100**, **20** (2004).
- [57] C. Filippi, C. J. Umrigar, and M. Taut, *J. Chem. Phys.* **100**, **1290** (1994).
- [58] A. D. Becke, *Phys. Rev. A* **33**, 3098 (1988).
- [59] C. Lee, W. Yang, and R. G. Parr, *Phys. Rev. B* **37**, **785** (1988).
- [60] B. G. Johnson, P. M. W. Gill, and J. A. Pople, *J. Chem. Phys.* **97**, **7846** (1992), *ibid.* **98**, **5612** (1993).
- [61] See, for example, A. D. Becke, *J. Chem. Phys.* **98**, **5648** (1998).
- [62] A. D. Boese and N. C. Handy, *J. Chem. Phys.* **114**, **5497** (2001).
- [63] J. P. Perdew, K. Burke, and M. Ernzerhof, *Phys. Rev. Lett.* **77**, **3865** (1996); *ibid.* **78**, **1386** (E) (1997).
- [64] M. Ernzerhof and G. E. Scuseria, *J. Chem. Phys.* **110**, **5029** (1999).
- [65] H. J. F. Jansen and A. J. Freeman, *Phys. Rev. B* **30**, **561**, (1984).
- [66] P. W. Teare, *Acta Cryst.* **12**, **294** (1959).
- [67] S. Kavesh and J. M. Schultz, *J. Polym. Sci. Part A-2*, **8**, **243** (1970).
- [68] B. Montanari, P. Ballone, and R. O. Jones, *J. Chem. Phys.* **108**, **6947** (1998).
- [69] This functional uses the Becke approximation for exchange and the correlation energy functional of J. P. Perdew, *Phys. Rev. B* **33**, **8822** (1986).
- [70] J. P. Perdew, S. Kurth, A. Zupan, and P. Blaha, *Phys. Rev. Lett.* **82**, **2544** (1999).
- [71] J. Tao, J. P. Perdew, V. N. Staroverov, and G. E. Scuseria, *Phys. Rev. Lett.* **91**, **146401** (2003).
- [72] <http://www.answers.com/topic/crystal-structure>.
- [73] http://www.sciencedaily.com/articles/c/crystal_structure.htm .

- [74] S.-K. Ma and K. A. Brueckner, **Phys. Rev.** **165**, 18 (1968). [75] http://www.en.wikipedia.org/wiki/Crystal_structure.
- [76] D.D. Koelling, B.N. Harmon, **J. Phys. C: Solid State Phys.** **10** **3107–3114** (1977).
- [77] A.H. MacDonald, W.E. Pickett, D.D. Koelling, **J. Phys. C: Solid State Phys.** **13**, 2675–2683(1980).
- [78] D.J. Singh, **Plane Waves, Pseudo-potential and the LAPW Method**, Kluwer Academic Publisher, Boston, Dordrecht, London, (1994).
- [79] <http://cst-www.nrl.navy.mil/lattice/>
- [80] K. Schwarz, P. Blaha, G.K.H. Madsen, **Comput. Phys. Commun.** **147**, 71–76, (2002).
- [81] J.C. Slater, **Phys. Rev.** **51**, 151–156 (1937).
- [82] O.K. Andersen, **Phys. Rev. B** **12**, 3060–3083(1975).
- [83] E. Sjöstedt, L. Nordström, D.J. Singh, **Solid State Comm.** **114**, 15–20(2000).
- [84] G. H. K. Madsen, P. Blaha, K. Schwarz, E. Sjöstedt, L. Nordström, **Phys. Rev. B** **64** (2001).
- [85] P. Blaha, K. Schwarz, G.K.H. Madsen, D. Kvasnicka, J. Luitz, **An augmented plane wave plus local orbitals program for calculating crystal properties**, Vienna University of Technology, Austria, ISBN 3-9501031-1-2(2001).
- [86] E. Wimmer, H. Krakauer, M. Weinert, A.J. Freeman, **Phys. Rev. B** **24**, 864–875, (1981).
- [87] M. Weinert, E. Wimmer, A.J. Freeman, **Phys. Rev. B** **26**, 4571–4578 (1982).
- [88] M. Iglesias, K. Schwarz, P. Blaha, D. Baldomir, **Phys. Chem. Minerals** **28**, 67–75(2001).
- [89] V. N. Strocov, R. Claessen, G. Nicolay, S. Hüfner, A. Kimura,

- A. Harasawa, S. Shin, A. Kakizaki, H.I. Starnberg, P.O. Nilsson, P. Blaha, **Phys. Rev. B** **63**, 205108-1-16 (2001).
- [90] S. Pillet, M. Souhassou, C. Lecomte, K. Schwarz, P. Blaha, M. Re´rat, A. Lichanot, P. Roversi, **Acta Cryst. A** **290**, 290–303(2001) .
- [91] <http://www.wien2k.at/>
- [92] Chan-Jeong Park, Sun-Ghil Lee, Young-Jo Ko, and K. J. Chang, **Phys. Re. B Vol. 59**, 1998.
- [93] Yingxiang Cai, Songtao Wu, Rui Xu, and Jie Yu. **Phys. Re. B73**,2006
- [94] Haozhe Liu, Ho-kwang Mao, Maddury Somayazulu, Yang Ding, Yue Meng, and Daniel Häusermann **Phys. Re. B70**, 094114, (2004).
- [95] Sukit Limpijumnong and Sirichok Jungthawan, **Physical Re. B 70**, 054104 (2004).
- [96] Gerward, L. J.: **Synchrotron. Rad. 2** ,233(1995)
- [97] D. J. Singh Kluwer **Academic Publisher, Boston, Dordrecht, London** (1994).
- [98] P. Blaha, K. Schwarz, P. Sorantin, and S. B. Trickey, **Comput. Phys. Commun.**, **59**, 399-415 (1990).
- [99] P. Blaha, K. Schwarz, G. K. H. Madsen, D. Kvasnicka, and J. Luitz, Vienna University of **Technology, Austria ISBN 3-9501031-1-2**(2001).

جامعة النجاح الوطنية
كلية الدراسات العليا

دراسة مركبي ZnO و BeO تحت ضغط مرتفع

إعداد

عمر محمود اسعد اسليم

إشراف

د. محمد أبو جعفر

قدمت هذه الأطروحة استكمالاً لمتطلبات درجة الماجستير في الفيزياء بكلية الدراسات العليا في جامعة النجاح الوطنية في نابلس، فلسطين.

2008

دراسة مركبي ZnO و BeO تحت تأثير ضغط مرتفع

إعداد

عمر محمود اسعد اسليم

إشراف

د. محمد أبو جعفر

الملخص

تتحدث هذه الأطروحة عن تحول بعض المركبات تحت تأثير ضغط مرتفع من تركيب إلى آخر، حيث أن دراسة أشباه الموصلات جذبت اهتمام الكثير من العلماء في الفترة الاخيره نظرا لأهميتها العملية والتطبيقية في المجال الصناعي والالكتروني . وحيث الدراسة العملية والتجريبية في هذا المجال مكلفه جدا من الناحية المالية والتقنية وتحتاج إلى جهد كبير وزمن طويل للحصول على نتائج فان ظهور وتطور الحاسبات الضخمة والسريعة أدى إلى ظهور وتطوير أساليب حسابيه تعتمد نظم المحاكاة مما أدى إلى تسهيل الدراسات وتوفير الجهد والمال والوقت في الحصول على نتائج جيدة في مجال التركيب الالكتروني ومعرفة طبيعة المواد التي نتعامل معها من ناحية معرفه التركيب الالكتروني لها وإعطاء أفرصه لتطوير الروابط بين المواد لإنتاج مواد مثاليه بصفات محده سابقا والتمكن من حساب مستويات الطاقة وتحديد طاقه الفجوة والتي تحدد طبيعة المركب إذا ما كان موصل أو شبه موصل أو عازل.

العديد من الأساليب ظهرت لمعالجه مثل هذه الحسابات والدراسات ولكن في هذه الأطروحة تم الاعتماد على أسلوب الجهد المزيد والتام ذو الموجات المستوية الخطية والذي يعمل تحت برنامج حاسوب يسمى (WIEN2K) والذي يعتمد بدوره على نظريه توزيع كثافة الشحنات داخل القذرات والتي يستخدم فيها أكثر من أسلوب تقريبي مثل (Wu-), (GGA), (LDA) , (Cohen). في دراسة مركب BeO تم حساب معادله ألكاله لكل التراكيب الممكنة مثل (ZB) ، wurtzite (W), rocksalt (RS) zincblende (ZB) وتم تحديد أبعاد أبلوره لكل تركيب وحساب الحجم والضغط الذي تتكون عنده كل بلوره ومن ثم تم حساب الضغط الانتقالي والذي يتحول عنده تركيب موجود إلى تركيب آخر مثل الانتقال من تركيب (W) إلى تركيب (RS) أو الانتقال من تركيب (ZB) إلى تركيب (RS) وتم أيضا حساب طاقه الفجوة لكل تركيب من

التراكيب المذكورة حيث وجد إن طاقه الفجوة تتراوح ما بين ($8\sim 6\text{eV}$) مما يعني أن هذا المركب هو عازل في جميع حالاته وتراكيبه.

بنفس الطريقة تم دراسة مركب ZnO ونفس الأسلوب تم استخدامه لتحديد الانتقال التركيبي وحساب الضغط الانتقالي من تركيب (W) إلى تركيب (RS) ومن تركيب (W) إلى تركيب (CsCl) ومن تركيب (ZB) إلى تركيب (RS) ومن تركيب (ZB) إلى تركيب (CsCl) وأخيرا من تركيب (RS) إلى تركيب (CsCl) ، وقد تم حساب معادله أحواله لكل من التراكيب السابقة وتم تحديد أبعاد أبلوره في كل حاله وحساب طاقه الفجوة لكل تركيب حيث تبين أن طاقه الفجوة لهذا المركب تتراوح من ($1.5\sim 0.3\text{eV}$) مما يعني أن هذا المركب هو شبه موصل في جميع تراكيبه.

من الدراسة السابقة استطعنا الحصول على النتائج التالية:

- ١- إن الحسابات التي حصلنا عليها تتطابق بشكل كبير مع الحسابات السابقة النظرية والتجريبية.
- ٢- إن الانتقال التركيبي من تركيب إلى آخر ممكن تحت ضغط مناسب ومعين.
- ٣- مركب BeO يسلك سلوك العوازل في جميع تراكيبه.
- ٤- تركيب (W) هو التركيب الأساسي والطبيعي لمركب BeO عن درجه حرارة الغرفة.
- ٥- ZnO له سلوك أشباه الموصلات في جميع تراكيبه إلا في حاله كلوريد السيزيوم فهو شبه معدن.

